Advances in Colloid and Interface Science 342 (2025) 103492

Contents lists available at ScienceDirect

Advances in Colloid and Interface Science

journal homepage: www.elsevier.com/locate/cis

A comprehensive review and trends in lubrication modelling

Suhaib Ardah [a,*], Francisco J. Profito [b], Daniele Dini [a]

[a] Department of Mechanical Engineering, Imperial College London, London SW7 2AZ, UK
[b] Department of Mechanical Engineering, Polytechnic School of the University of São Paulo, São Paulo, Brazil

ARTICLE INFO

Keywords:
Lubrication
Fluid-solid interactions
Multiscale modelling
Machine learning

ABSTRACT

Lubrication plays a pivotal role in modern society, given its significant economic and environmental implications, particularly in relation to friction, wear and the failure of moving mechanical systems. With recent breakthroughs in computational architectures, the development of advanced simulation frameworks has been greatly accelerated, facilitating the study of surfaces, lubricants and additives at unprecedented scales. However, the inherently multiscale nature of lubricated contacts necessitates a delicate balance between computationally efficient continuum descriptions and detailed atomistic accuracy for addressing the complex physiochemical phenomena spanning vastly different spatiotemporal scales. This review explores the dilemma of modelling inherently multiphysics tribological interactions, which drive the evolution of lubricated interfaces and shape tribosystem performances across the scales as accurately and simultaneously as efficiently as possible. It critically examines state-of-the-art modelling tools, their applications and limitations across spatiotemporal domains. Moreover, the capacity for machine learning to aggregate extensive datasets, address multi-physical complexities ranging from atomic dimensions to macroscopic scales and accelerate simulation workflows is explored, offering transformative perspectives for the future of lubrication modelling.

1. Introduction

In the ever-evolving landscape of research, the science of rubbing interfaces, encapsulated within the field of tribology, has witnessed numerous advancements and continues to evolve across a plethora of disciplines. The technological developments driven by the Industrial Revolution [1] have shed light on the impact of friction and wear on a myriad of engineering and natural systems, emphasising the importance of a comprehensive understanding of the physiochemical phenomena occurring at contacting interfaces. Tribological interactions play a critical role in everyday life and are ubiquitous in diverse systems [2], ranging from biological applications, such as dental care [3], cartilage rehydration [4] and blood circulation [5], to industrial applications, such as transportation [6], energy [7] and nanomaterials [8]. Fig. 1 illustrates the realm of applications featuring tribological interactions.

Conceptually, lubrication refers to the practice of controlling friction and wear between interacting surfaces that engage in continuous rubbing by interposing a substance that facilitates their separation and smooth movement. Although lubricants are commonly found in liquid state and composed of base oils (*e.g.* mineral and synthetic oils) and additives [22], they can also exist as gases (*e.g.* nitrogen and helium) mostly used in low load and high-speed contacts [23], and as solids (*e.g.* graphite and polytetrafluoroethylene) in applications where conventional fluid lubricants may not be as effective, such as in aerospace and nuclear radiation environments [24]. When a lubricant is introduced into the vicinity of sliding interfaces, it forms a thin, easily sheared film that inhibits direct contact between the surfaces, thus enforcing fluid friction in place of dry friction. This film also acts as a carrier, transporting interfacial heat and undesired substances such as wear debris and contaminants away from the contact region. The effectiveness of a lubricating film is dictated by its ability to control the multiphysical tribological interactions that occur in highly localised regions inside the contact [25,26] (see Fig. 2A). These interactions govern not only the evolution of the contacting surfaces but, ultimately, the performance and lifespan of tribosystems. However, in many practical applications, it is often impractical for a lubricant to ensure the complete separation of the contacting interfaces due to the severity of the operating conditions (*e.g.* high thermomechanical loads and low speed), the lubricant's constitutive behaviour governed by intermolecular forces, and the adhesive forces driven by contact topography. Therefore, various lubrication regimes can emerge, influenced by tribological interactions at the macro-, micro- or nano-scale, either independently or collectively. In

* Corresponding author.
E-mail address: s.ardah19@imperial.ac.uk (S. Ardah).

https://doi.org/10.1016/j.cis.2025.103492
Received in revised form 22 March 2025;
Available online 1 April 2025

this context, numerical simulations play a critical role in predicting the interplay between various multiscale and multiphysics phenomena, such as fluid flow and cavitation, complex rheology, heat transfer and thermal effects, asperity contact, surface wettability, adhesion and percolation, all of which occurring simultaneously across different length and time scales [25] (see Fig. 2A). Achieving a comprehensive understanding of the underlying mechanisms governing friction, wear, lubrication and failure at tribological interfaces can contribute to the tailoring of innovative surface engineering technologies and advanced materials and lubricants for more reliable and cost-effective tribosystems [27,28].

The conception of rigorous mathematical formulations [24,29–32] and the relatively low computational demand associated with approximating their solutions have catalysed the extensive utilisation of continuum mechanics-based models for simulating lubricated contacts over large spatiotemporal scales. Such simulation modelling has been implemented in academic codes using conventional discretisation schemes [33–35] (*e.g.* Finite Difference Method, Finite Element Method and Finite Volume Method) or in commercial and open-source software packages based on the Computational Fluid Dynamics (CFD) approach [36–39] (*e.g.* OpenFOAM, Ansys Fluent and COMSOL Multiphysics), through which the behaviour of lubricated contacts can be elucidated. Nevertheless, the breakdown of continuum theories at the micro- and nano-scale levels [40,41] limits the applicability of continuum-based predictions to long timescales and large length-scales. Consequently, phenomena governed by atomic and molecular interactions, such as complex rheology, wall-slip and tribofilm behaviour, microscale shock waves and fluid-solid interactions, cannot be accurately modelled using continuum-based modelling techniques. These limitations can be addressed by adopting atomic-scale simulations (*e.g.* molecular dynamics (MD), Monte Carlo (MC) and Density Functional Theory (DFT)) [42], which unravel the underlying atomistic and molecular interactions to provide insights into the molecular origins of the macroscale behaviour of tribosystems [8]. Atomic-scale modelling techniques, facilitated by open-source software packages such as the Large-scale Atomic/Molecular Massively Parallel Simulator (LAMMPS) [43], Vienna *Ab initio* Simulation Package (VASP) [44] and QUANTUM opEn Source Package for Research in Electronic Structure, Simulation, and Optimization (ESPRESSO) [45], elucidate the dynamics and interactions of molecular assemblies representative of nanoscale phenomena. For instance, MD simulations [46] can be employed to examine the constitutive behaviour of lubricant flow by tracking the trajectories of molecules confined within a system based on Newton's equations of motion and interatomic potentials. Despite these advantages, atomistic simulations require high computational demands and are limited to small length- and time-scales. Therefore, they are incapable of accounting for heterogeneous processes that occur in realistic, full-scale systems.

Fueled by the rapid growth in computational resources [47], multiscale modelling has emerged as a novel simulation strategy designed to overcome the limitations associated with single-scale simulation frameworks. Multiscale modelling is complementary in bridging the expansive spatiotemporal scales of complex engineering systems [48,49], thereby contributing to accelerating the development of friction reduction technologies for rubbing interfaces. This is achieved by simulating macroscopic continuum models based on information, such as surface roughness effects [50–53], film viscosity [54,55] and slip length [56,57], obtained from finer-scale computational models, rather than resorting on deterministic or empirical constitutive models [58].

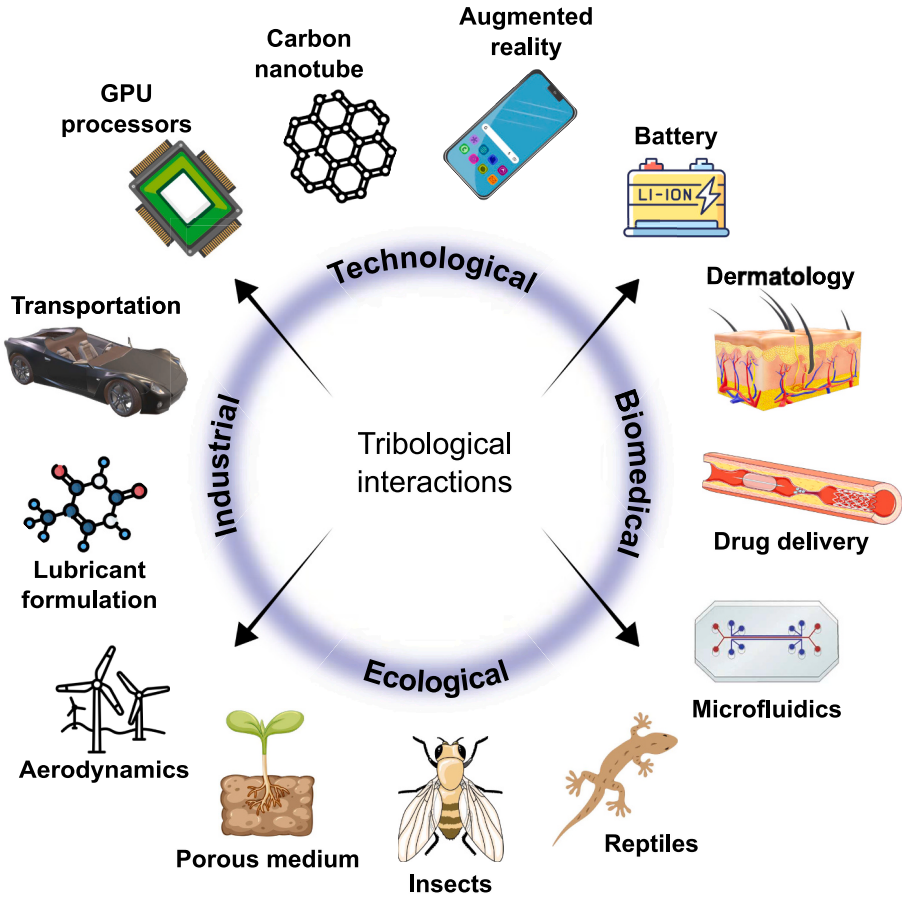

Fig. 1. A representative flavour of applications that feature tribological interactions evolving at contacting interfaces, including but not limited to, technological-, biomedical-, ecological- and industrial-based tribosystems. The reader is referred to [9–21], beginning with "*Augmented reality*" and moving clockwise through the references for an overview of the direct and indirect role of tribology in those applications.

However, robust bridging algorithms and appropriate boundary conditions [59] are fundamental to multiscale models as they govern the hierarchical coupling of various single-scale sub-models. These algorithms and boundary conditions collectively contribute to linking the gap between the various spatiotemporal phenomena in engineering systems. Recent studies in other scientific disciplines [60–62] have advocated for the synergistic integration of machine learning (ML) tools with scale-bridging multiscale models. This harmonious approach can facilitate automatic feedback between coarse- and fine-scale simulations, extract relevant parameters for known physics-based problems, expedite the solutions of ordinary and partial differential equations, and develop robust models to predict atomistic trajectories efficiently. Nevertheless, the success of ML models is intertwined with the quality, quantity and relevance of data, as well as the complexity of the simulated system. This reliance explains the relative scarcity of ML-integrated studies in the field of tribological simulations [63–65].

This paper aims to review the current mathematical and computational modelling and simulation tools used to predict the interactions that govern the tribological performance of lubricated interfaces across the different spatiotemporal scales. The primary focus is on computational approaches, and while various other factors contribute to tribological behaviour, an in-depth exploration of these aspects falls beyond the scope of this review. Instead, we highlight theoretical frameworks and numerical methodologies that underpin the modelling of tribosystems, providing a structured perspective on their predictive capabilities and limitations. Additionally, we offer prospective views on integrating machine learning models to address the challenges in modelling the multiphysics and multiscale behaviour of tribosystems. Accordingly, the remainder of the paper is structured as follows: a succinct background on lubrication regimes is provided in Section 2, followed by a review of state-of-the-art modelling techniques employed to uncover tribological mechanisms at the macro-, micro-, and nano-scale levels in Section 3 – Section 5, respectively. Building on this foundation, Section 6 discusses the coupling strategies employed in multiscale models, while Section 7 explores the integration of machine learning algorithms in tribological simulations. Finally, the paper concludes with concise remarks in Section 8.

2. Lubrication regimes

To introduce our overview of the mathematical and computational modelling of lubricated interfaces, it is essential to establish a comprehensive understanding of the correlation between lubrication regimes and operational and tribosystem conditions. The Stribeck curve, depicted in Fig. 3A, portrays the different lubrication regimes—boundary, mixed, and full-film lubrication—as a function of the dimensionless Hersey number $H = \eta U/W$ or film thickness ratio $\lambda = h_{\min}/\sigma$, where η is the lubricant dynamic viscosity, U the surface velocity, W the applied load, $h_{\min}$ the minimum lubricant film thickness, and σ the combined standard deviation of the surface roughness. The Stribeck curve is a fundamental tool for qualitatively understanding the lubrication regimes, the transition in frictional behaviour between them, and their dependence on the aforementioned operational and tribosystem parameters.

2.1. Boundary lubrication

In the boundary lubrication (BL) regime, the total applied load is carried by the surface asperities, and the friction behaviour is governed by the interactions between these asperities and the composition and kinetics of tribofilms attached to the surfaces [66,67]. Tribofilms are thin molecular layers formed as a result of complex tribo-mechanochemical interactions between lubricant molecules and surface materials and roughness. This regime generally results in higher friction forces compared to other lubrication regimes. Machine elements operating under boundary lubrication often function at high loads and/or low speeds, characterised by insufficient hydrodynamic film separation.

2.2. Mixed lubrication

As the lubricant film thickness increases, it begins to fill the valleys of the surface topographies, and the lubricant in these valleys can become pressurised, partially supporting the applied load. The contact between the asperity tips supports the remaining load, thus characterising the

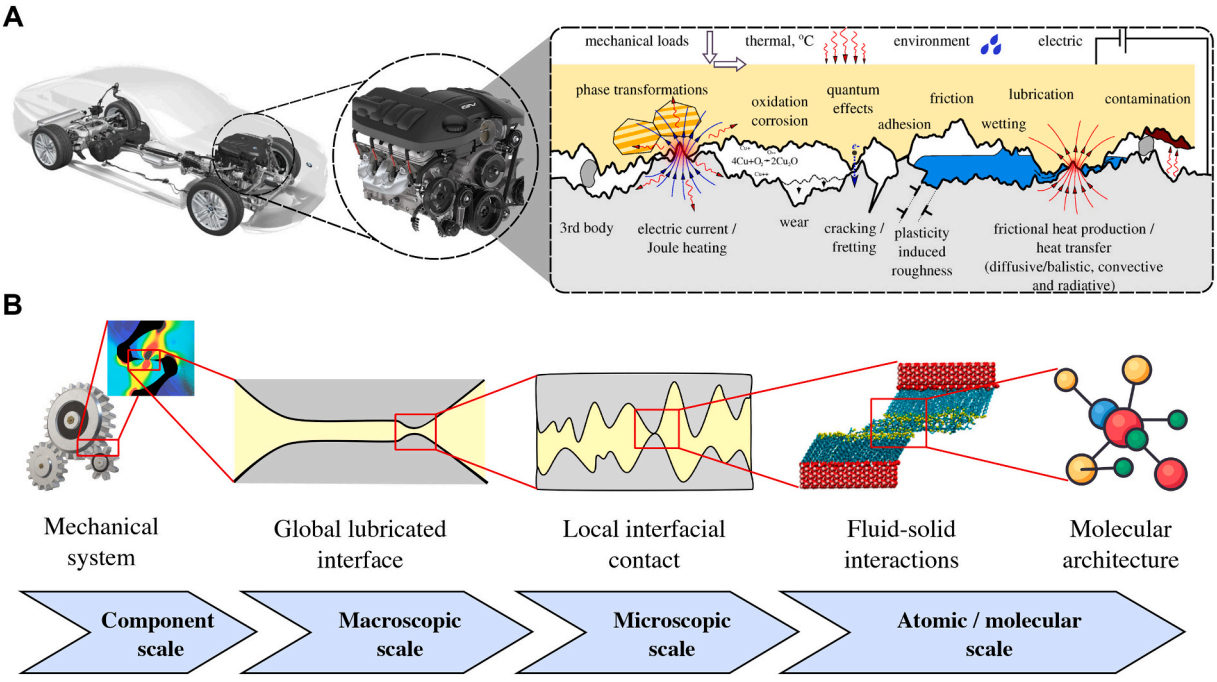

Fig. 2. Multiscale and multiphysics aspects of modelling tribosystems. (A) An overview of the physiochemical events that transpire at rubbing interfaces. The third figure is reprinted from [25], with permission from Elsevier. (B) The hierarchical nature of lubricated contacts spanning different spatiotemporal scales.

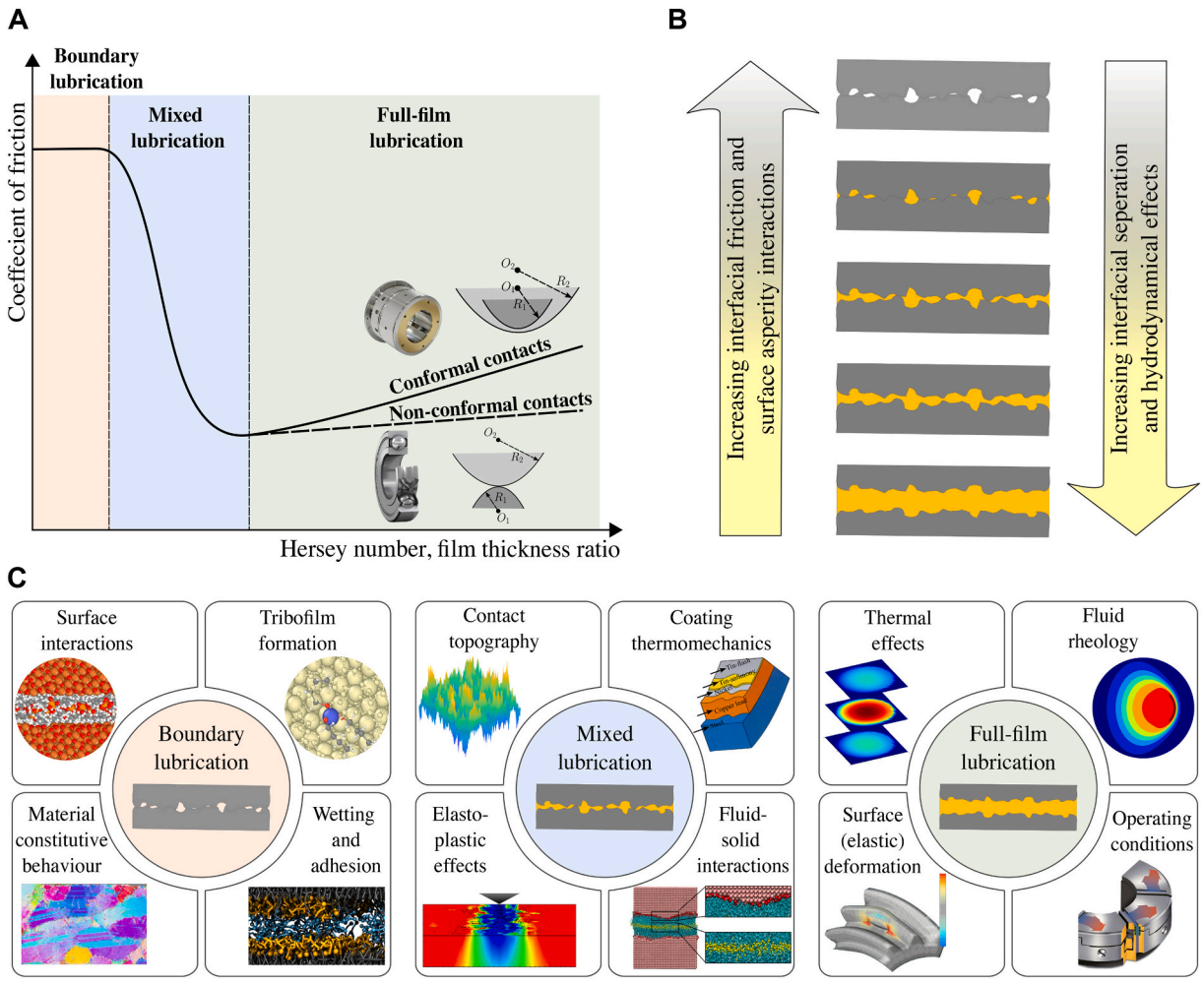

Fig. 3. Multiphysics and multiscale characteristics spanning the lubrication regimes. (A) A typical Stribeck curve illustrating the lubrication regimes and the relationship between the friction coefficient and the dimensionless Hersey number $H = \eta U/W$ or film thickness ratio $\lambda = h_{\min}/\sigma$, which combine operational parameters, lubricant properties and surface roughness information. (B) A pictorial overview illustrating the variations in the frictional, asperity and hydrodynamical effects of tribological interfaces with respect to the lubricant volume that inhibits the contact vicinity. (C) A schematic of the key factors that drive the evolution of contacting interfaces under boundary, mixed and full-film lubrication regimes. This diagram highlights the critical roles of surface roughness and materials, tribofilm composition and kinetics, lubricant rheology, contact geometry, surface deformations, applied load, surface velocities and thermal effects in determining the prevailing lubrication regime and the associated frictional behaviour.

mixed lubrication (ML) regime [68]. Mixed lubrication is more prevalent at moderate operating speeds and loads or when more viscous films are formed compared to boundary lubrication [69]. Friction forces in this regime are governed by the properties of both the tribofilms and the lubricant, and their magnitudes are lower than those of boundary lubrication.

2.3. *Full-film lubrication*

A further increase in the lubricant film thickness, driven by higher surface speeds and/or increased lubricant viscosity for a given load, leads to a greater proportion of the applied load being carried by the fluid film and a reduction in the load supported by the asperity contacts. A sufficiently thick lubricant film completely separates the contact bodies, resulting in a full-film lubrication regime subdivided into hydrodynamic or elastohydrodynamic regimes.

In hydrodynamic lubrication (HL), the hydrodynamic pressures are insufficient to cause significant elastic deformation of the bounding solids. This regime is commonly found in conformal contacts such as piston skirts and piston rings–cylinder liner contacts, sliding bearings, journal bearings, thrust bearings, and spherical bearings, among others. It is characterised by lower friction coefficients compared to the mixed lubrication regime, as portrayed in Fig. 3A. The film thickness and frictional losses in the HL regime are mainly influenced by the lubricant viscosity, contact geometry, surface velocities, and thermal effects imposed by the operating conditions [24].

Conversely, elastohydrodynamic lubrication (EHL) involves fluid pressures that are sufficiently high to induce significant elastic deformation of the contacting surfaces, establishing a strong coupling between hydrodynamic pressures and fluid film thickness. Depending on the contact geometry, load magnitude and mechanical properties of the contact surfaces, the EHL regime can be subdivided into *hard*-EHL and *soft*-EHL [31]. The *hard*-EHL regime is typically found in lubricated *counterformal* contacts, such as line and point contacts involving surfaces with *high* elastic modulus (*e.g.* metals). Examples of systems operating under *hard*-EHL include rolling element bearings, gear tooth contacts and cam-followers. In these cases, solid deformations occur mainly due to the *surface compression* induced by the elevated fluid pressures ($\sim$ 0.5 GPa to 5 GPa) developed in the contact. These high pressures also significantly influence lubricant rheology, particularly piezoviscous, density-pressure and shear thinning behaviours, and so must be considered for accurate predictions. In systems undergoing continuous rubbing and operating under *hard*-EHL conditions, the separating film thickness typically does not exceed 20 % of the average distortion of the

surfaces [70]. In *classical* EHL, the central and minimum lubricant film thicknesses are considered to be primarily governed by the lubricant *entrainment* speed and rheological properties at the low-pressure contact inlet. In contrast, friction is significantly affected by the lubricant *sliding* speed, rheology and thermal effects within the contact region. For a comprehensive assessment of *classical hard*-EHL, the reader is referred to the detailed reviews by [71–73].

Recent research based on the *quantitative* EHL approach has revealed that in real *hard*-EHL contacts, the minimum oil film thickness is governed not only by inlet lubricant rheology but also by the high-pressure viscosity response and glass transition pressure of the lubricant [74,75]. Conversely, it was confirmed that the inlet lubricant low-pressure viscosity predominantly influences the central film thickness; however, for accurate central film thickness predictions, the maximum lubricant pressure and the shear dependence of viscosity at the inlet should also be considered [76]. Furthermore, results from *quantitative* EHL studies have highlighted critical aspects affecting EHL friction. These include the significance of lubricant viscoelasticity on traction, the effect of thermal conductivity of coatings on EHL friction and the finding that the maximum traction coefficient is not always a limiting stress. Additionally, the assumed equivalence of a traction EHL curve to a flow curve and the initial linear region of a traction curve have been scrutinised [75].

The *soft*-EHL regime typically occurs in lubricated *conformal* contacts and/or in systems involving surfaces with relatively *low* elastic modulus (*e.g.* rubber, soft contacts). Even in conformal contacts with high elastic modulus under moderate loads, significant solid deformations can occur due to the *global flexibility or compliance* of the entire structure rather than surface compression. In these cases, the lower load magnitudes and, consequently, lower hydrodynamic pressures (< 0.5 GPa) make changes in the lubricant rheology (mainly piezoviscous effects) less prominent and sometimes negligible. More recently, the effect of viscosity on the deformation behaviour of soft contacts has also been incorporated in visco-elasto-hydrodynamic lubrication (VEHL) solvers [77,78]. Examples of lubrication systems operating under *soft*-EHL include journal bearings, thrust bearings, elastomers and biomechanics devices. In this regime, the lubricant film thickness and friction are governed by the surface velocities, lubricant viscosity and thermal effects throughout the lubricated domain.

Notably, even under severe EHL conditions, the contact surfaces can remain fully separated by a continuum lubricant film, with no asperity contact (full-film EHL). However, the mixed-EHL regime is established if asperity contact occurs under EHL conditions.

3. Full-film lubrication: Depicting the continuum behaviour

Simulation frameworks based either on the Navier-Stokes equations or lower-dimensional Reynolds-type equations have proven effective in providing satisfactory results of relevant physical phenomena occurring in lubricated interfaces at the basis of the continuum mechanics theory. However, the high computational cost and complexity of traditional computational fluid dynamics (CFD) solvers, typically used to solve the Navier-Stokes equations, have propelled the use of Reynolds-type solvers, which offer a more computationally efficient approach to evaluating thin film lubrication problems. This section presents the fundamentals of Reynolds-type solvers, including the mathematical models that describe the physics of lubricated contacts, as well as the coupling strategies commonly used in the solution processes to account for the interdependent interactions between lubricant film flow, structural deformation and interfacial heat transfer. Detailed derivations of the governing equations, along with descriptions of the numerical methods generally used to solve these equations, can be found in specialised textbooks [30–32,34,67,70,79–81]. A Cartesian coordinate system O*xyz* is adopted to represent the mathematical models, with O*x*, O*y* and O*z* axes corresponding to the longitudinal, transversal and vertical directions, respectively, as illustrated in Fig. 4.

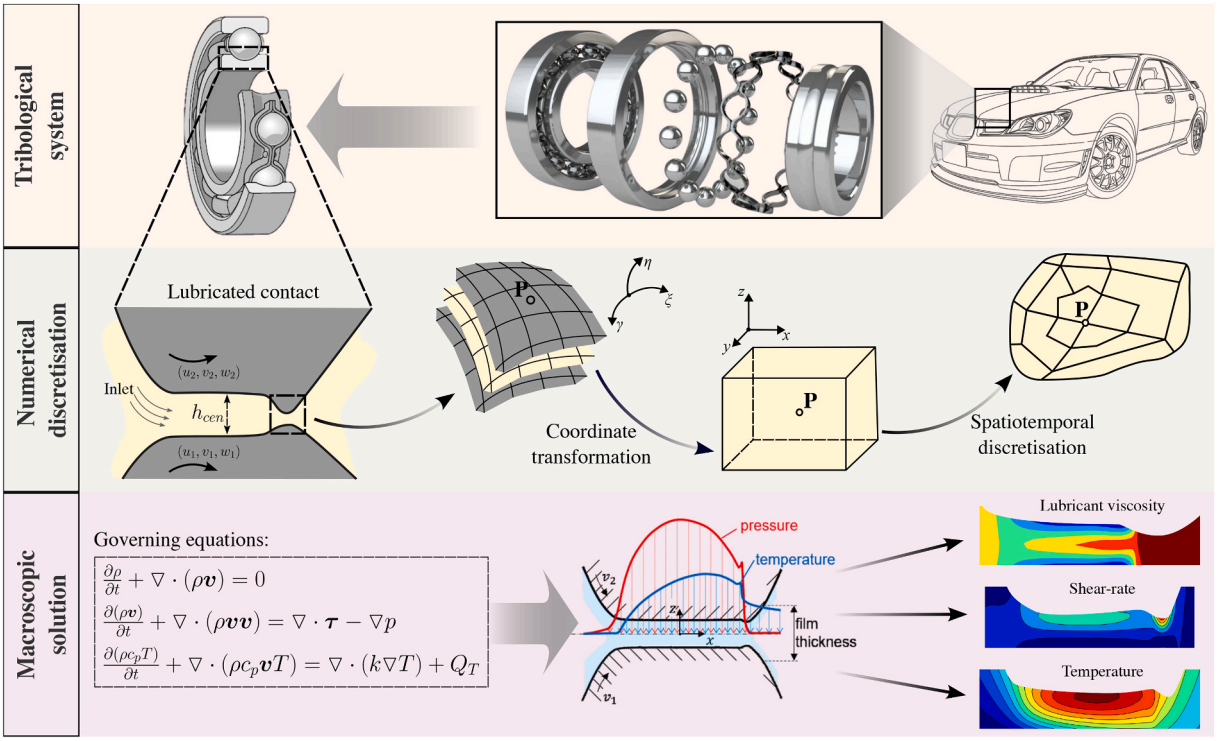

Fig. 4. Modelling the macroscopic (or continuum) behaviour of lubricated interfaces, such as in mechanical ball bearings of vehicles, using coordinate transformation, mesh generation techniques and discretisation methods to solve the governing equations numerically. These include, for example, the continuity and momentum equations for fluid flow, as well as the energy equation to account for thermal effects.

3.1. Lubricant film flow

The Reynolds lubrication equation is widely used to describe the lubricant flow behaviour between lubricated interfaces, mainly due to its lower computational cost and complexity compared to solving the full Navier-Stokes equations [36,82]. The Reynolds equation is a lower-dimensional, second-order partial differential equation that governs the pressure distribution within thin lubricant films. The *classical* Reynolds equation is derived from the Navier-Stokes momentum and continuity equations, based on the following simplifying assumptions of the lubrication theory [29–32,34,70,81]:

1. The fluid is assumed to be a continuum medium, and the Navier–Stokes equations are applicable.
2. The lubricant film is continuous and fully separates the contact surfaces.
3. The film thickness is much smaller than the other dimensions of the contact. This fundamental assumption of the lubrication theory results in negligible pressure gradients across the film thickness.
4. The lubricant flow is assumed to be free of edges, and inertia effects are negligible. This is due to the thin film characteristic of lubricated contacts, which generally results in laminar flows with very small Reynolds numbers, where slow viscous flow effects predominate.
5. Body forces are considered negligible.
6. No-slip condition is assumed at the fluid-solid interfaces.
7. The contact surfaces are considered perfectly smooth, without roughness.
8. The lubricant properties are assumed constant across the film thickness.

Given the surface contact kinematics $\mathbf{v_1}(x,y,t) = [u_1 \;\; v_1]^T$ and $\mathbf{v_2}(x,y,t) = [u_2 \;\; v_2]^T$ in the x- and y-directions, the lubricant film thickness $h(x,y,t)$, the lubricant dynamic viscosity $\eta(x,y,t)$ and density $\rho(x,y,t)$, the hydrodynamic pressure distribution within the lubricant film can be described by the *classical* Reynolds equation, which in its expanded and strong conservation forms is expressed as follows [30–32,70,81].

$$\frac{\partial}{\partial x}\left(\frac{\rho h^3}{12\eta}\frac{\partial p}{\partial x}\right)+\frac{\partial}{\partial y}\left(\frac{\rho h^3}{12\eta}\frac{\partial p}{\partial y}\right)=\frac{\partial}{\partial x}\left[\frac{\rho h(u_2+u_1)}{2}\right]+\frac{\partial}{\partial y}\left[\frac{\rho h(v_2+v_1)}{2}\right]+\frac{\partial(\rho h)}{\partial t}, \tag{1}$$

$$\underbrace{\nabla\cdot(\Gamma_{\mathbf{d}}\nabla p)}_{\substack{\text{Poiseuille Flow}\\ \text{Term}}} = \underbrace{\nabla\cdot(\Gamma_{\mathbf{c}}\mathbf{v_e})}_{\substack{\text{Couette Flow}\\ \text{Term}}} + \underbrace{\frac{\partial(\rho h)}{\partial t}}_{\substack{\text{Squeeze}\\ \text{Term}}}, \tag{2}$$

$$\Gamma_{\mathbf{d}} = \frac{\rho h^3}{12\eta}\begin{bmatrix}1 & 0\\ 0 & 1\end{bmatrix}, \quad \Gamma_{\mathbf{c}} = \rho h\begin{bmatrix}1 & 0\\ 0 & 1\end{bmatrix}, \quad \mathbf{v_e} = \begin{bmatrix}\frac{(u_2+u_1)}{2} & \frac{(v_2+v_1)}{2}\end{bmatrix}^T.$$

where $p(x,y,t)$ denotes the hydrodynamic pressure, $\nabla(\cdot) = \begin{bmatrix}\frac{\partial(\cdot)}{\partial x} & \frac{\partial(\cdot)}{\partial y}\end{bmatrix}^T$ represents the gradient operator, $\Gamma_{\mathbf{d}}$ and $\Gamma_{\mathbf{c}}$ are the diffusivity and convective matrices, respectively, and $\mathbf{v_e}$ is the average surface velocity vector.

Although the *classical* Reynolds equation (Eq. 2) effectively describes the lubricant flow behaviour through narrow gaps, it does not properly account for variations in the lubricant properties across the film thickness. Nevertheless, these limitations have been addressed to extend the applicability of Reynolds-based models to a broader range of lubrication problems. The so-called *generalised* Reynolds equation (GRE) [83] extends the lubrication theory by incorporating thermohydrodynamic effects, allowing for variations in the lubricant properties, such as viscosity and density, across the film thickness. Accordingly, the *generalised* Reynolds equation can be expressed using the aforementioned variables as follows [30,34,83,84]:

$$\underbrace{\nabla\cdot(\Gamma_{\mathbf{d}}\nabla p)}_{\substack{\text{Poiseuille Flow}\\ \text{Term}}} = \underbrace{\nabla\cdot(\Gamma_{\mathbf{c}}\mathbf{v_e}+\Gamma_{\mathbf{c1}}\mathbf{v_1})}_{\substack{\text{Couette Flow}\\ \text{Term}}} + \underbrace{\frac{\partial\rho_e}{\partial t}}_{\substack{\text{Squeeze}\\ \text{Term}}}, \tag{3}$$

$$\Gamma_{\mathbf{d}} = \varepsilon\begin{bmatrix}1 & 0\\ 0 & 1\end{bmatrix}, \quad \Gamma_{\mathbf{c}} = \rho_e^*\begin{bmatrix}1 & 0\\ 0 & 1\end{bmatrix}, \quad \Gamma_{\mathbf{c1}} = \rho_1^*\begin{bmatrix}1 & 0\\ 0 & 1\end{bmatrix},$$

$$\varepsilon = \frac{\eta_e}{\eta_e'}\rho' - \rho'', \quad \rho_e^* = 2\eta_e\rho', \quad \rho_1^* = \rho_e - \rho_e^*,$$

$$\frac{1}{\eta_e} = \int_{z_1}^{z_2}\frac{dz}{\eta}, \quad \frac{1}{\eta_e'} = \int_{z_1}^{z_2}\frac{z\;dz}{\eta}, \quad \rho_e = \int_{z_1}^{z_2}\rho\;dz,$$

$$\rho' = \int_{z_1}^{z_2}\rho\left(\int_{z_1}^{z}\frac{dz'}{\eta}\right)dz, \quad \rho'' = \int_{z_1}^{z_2}\rho\left(\int_{z_1}^{z}\frac{z'dz'}{\eta}\right)dz.$$

The reader is referred to [85–87] for a thorough derivation of the generalised Reynolds equation for non-Newtonian thermal elastohydrodynamic lubrication, which explicitly incorporates lubricant's rheological law into the formulation. Additionally, for a comprehensive discussion on the derivations, validity and limitations of Reynolds-based models, the reader is referred to [88–90].

3.2. Fluid-film cavitation

Cavitation is a critical phenomenon in fluid-film lubrication, characterised by the rupture of the lubricant film when the hydrodynamic pressure falls below the saturation pressure of dissolved gases or vapour pressure of the lubricant [91,92]. Fluids generally cannot sustain the tensile stresses associated with sub-ambient pressures, particularly in lubrication systems where intense shear stresses and viscous dissipation prevail. When pressure drops below the saturation limit of dissolved gases (gaseous cavitation) or the vapour pressure of the lubricant (vapour cavitation), the lubricant film breaks down, forming cavities filled with a biphasic mixture of liquid and gas/vapour [93–95]. Cavitation is initiated when tensile stresses exceed the fluid's tensile strength, resulting in nucleation of gas or vapour bubbles. These bubbles can expand rapidly under continued low pressures and collapse violently when local pressure is restored. This bubble collapse releases significant localised energy, which can lead to high-impact micro-jets and shock waves [94]. This phenomenon is more prevalent in fast transient tribodynamic lubricated systems and can compromise the structural integrity of contacting surfaces, leading to localised erosion, material pitting and fatigue wear over time [96,97].

In tribological systems, cavitation can also occur under starved lubrication conditions, where the available lubricant is insufficient to maintain adequate surface separation, resulting in increased asperity contact and wear [67]. This deficiency in lubrication intensifies friction and wear and can promote surface damage due to the repeated collapse of cavitation bubbles near the surfaces [98]. Furthermore, the presence of cavitation alters the effective viscosity and density of the lubricant and, consequently, the overall tribological performance of the system. Beyond surface degradation, cavitation critically impacts the efficiency and durability of lubricated machine components such as bearings, seals and gears. Uncontrolled cavitation can accelerate wear and shorten service life, often leading to premature failure. Therefore, accurately predicting cavitation behaviour, including the evolution, size and spatial distribution of cavitated zones, is vital. Mathematical models based on mass conservation, coupled with advanced numerical methods, are essential for simulating this phenomenon and gaining a more precise understanding of the cavitation process [99]. This understanding is essential for optimising tribosystem performances and designing surfaces to mitigate cavitation's detrimental effects.

Before examining the mathematical models developed to address hydrodynamic cavitation, it is important to recognise that fluid-film cavitation can manifest in various forms, depending on the

composition of the biphasic mixture within the cavities and the specific conditions leading to the formation of ruptured zones [95,100]. In lubrication systems, three main types of fluid-film cavitation are typically identified [95]:

1. Gaseous cavitation: Characterised by the presence of one or more gas species dispersed within the biphasic mixture formed in the cavitated regions. This biphasic mixture (gas bubble) develops mainly due to the diffusion of gases previously dissolved in the liquid lubricant when the fluid pressure drops below the saturation pressure of each gas species. In some cases, gases from the atmospheric environment may also contribute to forming the cavitation zone, a phenomenon known as air entrainment or inlet suction [101,102]).
2. Pseudo-cavitation: This is a particular form of gaseous cavitation that occurs when the biphasic mixture (gas bubble) expands due to surrounding depressurisation without additional gas mass diffusion from the liquid into the gas phase. In other words, the expansion happens without increased mass within the cavitation zones.
3. Vapour cavitation: This occurs due to thermodynamic non-equilibrium effects when film pressure falls below the vapour pressure of the lubricant at a given temperature. It is most likely to occur in systems subject to fast transient conditions, leading to superficial damage due to the high-frequency growth and collapse of cavitation bubbles.

As previously discussed, predicting hydrodynamic cavitation poses significant challenges in the numerical solution of lubrication problems due to the rupture of the lubricant film, which makes the conventional Reynolds equation inadequate for capturing the cavitation zones. The limitations of the Reynolds solution are evident in Sommerfeld's model [103], which permits the calculation of sub-ambient pressures and fails to account for film rupture within the lubricated domain. This issue was later addressed by Gümbel's model [104] (also known as the half-Sommerfeld model), which only considers pressures equal to or greater than a specified limit defined as cavitation pressure p_{cav}. The cavitation pressure p_{cav} represents either the saturation pressure of the gases dissolved in the lubricant (in the case of gaseous cavitation) or the vapour pressure of the lubricant (in the case of vapour cavitation). While Gümbel's approach effectively eliminates non-physical negative pressures by setting them equal to p_{cav}, it does not enforce mass conservation at the cavitation boundaries.

Subsequently, the Swift-Stieber model [105,106] was introduced and has since been extensively used to address cavitation in lubrication problems. The Swift-Stieber (or Reynolds) model assumes that pressure gradients are zero at the cavitation boundaries, specifically at the reformation $\mathfrak{C}^-$ and rupture $\mathfrak{C}^+$ boundaries. Within the cavitation regions $\mathfrak{D}^0$, pressures are considered constant and equal to the cavitation pressure limit p_{cav}. These conditions can be mathematically expressed as follows:

$$\begin{cases} p = p_{cav} & \text{in } \mathfrak{D}^0, \\ \dfrac{\partial p}{\partial \boldsymbol{n}} = 0 & \text{on } \mathfrak{C}^- \text{ and } \mathfrak{C}^+, \end{cases} \tag{4}$$

where $\boldsymbol{n}$ denotes the unit vector normal to the cavitation boundaries. Although the Swift-Stieber conditions provide more accurate predictions for cavitation, they ensure mass conservation only at the rupture boundaries [107]. This limitation significantly affects the accuracy of performance predictions in lubrication problems with textured surfaces [108].

Jakobsson, Floberg, and Olsson (JFO) introduced a set of complementary boundary conditions for cavitation that ensures mass conservation of lubricant flow throughout the entire lubricated domain, including at both rupture and reformation cavitation boundaries [109–111]. Since its introduction, the JFO cavitation model has been widely adopted in lubrication modelling. The key assumptions made by the authors are outlined as follows:

1. Within the cavitation regions, the pressure of the biphasic mixture remains constant and equal to the cavitation pressure limit (p_{cav}) corresponding to the type of cavitation (gaseous or vapour cavitation) being considered.
2. Within the cavitation regions, the liquid phase (lubricant) of the biphasic mixture is transported in-between gas/vapour fingers that extend across the entire film thickness.
3. At the cavitation boundaries, mass conservation is enforced by imposing complementary boundary conditions, which must be applied in conjunction with the solution of the Reynolds equation. These complementary mass conservation conditions can be mathematically expressed as [30]:

$$\rho h(\theta - 1)\left(\frac{U_n}{2} - W_n\right) + \frac{\rho h^3}{12\eta}\frac{\partial p}{\partial \boldsymbol{n}} = 0, \tag{5}$$

where h denotes the film thickness, θ represents the film fraction, which corresponds to the ratio of liquid lubricant volume over the cavitation regions, and $\boldsymbol{n}$ is the unit vector normal to the cavitation boundaries. Additionally, U_n and W_n are the sliding and moving boundary velocities in the normal direction $\boldsymbol{n}$, respectively. Based on Eq. 5, when the fluid film is broken down, the negative pressure gradient near the ruptured boundaries ($\mathfrak{C}^+$) must be zero, indicating that θ is equal to one. Conversely, when the film is reformed, the surrounding pressure gradient is positive, leading to an expected discontinuity in both θ and the pressure gradient.

Nonetheless, implementing the JFO model encounters several practical limitations, including the high computational cost, convergence issues and challenges in maintaining the numerical solution stability. Additionally, predicting the locations of film rupture and reformation is particularly difficult, as the cavitation boundaries are unknown *a priori*, given the moving boundary problem characteristic of such a phenomenon. Various cavitation models and algorithms have been developed to address these challenges, aiming to integrate the JFO boundary conditions with the Reynolds equation solution. One of the most widely used models is the Elrod-Adams $p-\theta$ cavitation model [112–114]. This model introduces an auxiliary variable, the film fraction θ, to account for the ratio of liquid lubricant within the biphasic mixture formed by cavitation. In this formulation, θ is defined as $\theta = \rho/\rho_c$, where ρ_c represents the density of the liquid lubricant at cavitation pressure. A modified Reynolds equation can thus be expressed as follows:

$$\underbrace{\nabla\cdot(\Gamma_{\mathbf{d}}\nabla p)}_{\substack{\text{Poiseuille}\\ \text{Term}}} = \underbrace{\nabla\cdot[\theta(\Gamma_{\mathbf{c}}\mathbf{v_e} + \Gamma_{\mathbf{c1}}\mathbf{v_1})]}_{\substack{\text{Couette}\\ \text{Term}}} + \underbrace{\frac{\partial(\theta\rho_e)}{\partial t}}_{\substack{\text{Squeeze}\\ \text{Term}}}, \tag{6}$$

with the complementarity boundary conditions for cavitation:

$$\{p - p_{cav})(1-\theta) = 0 \rightarrow \begin{pmatrix} p > p_{cav} & \rightarrow & \theta = 1 & & \text{in } \mathfrak{D}^+, \\ p = p_{cav} & \rightarrow & 0 \leq & \theta < 1 & \text{in } \mathfrak{D}^{\mathbf{0}}, \end{pmatrix} \tag{7}$$

where $\mathfrak{D}^+$ denotes the pressured regions within the lubricated domain, while $0 \leq \theta < 1$ indicates the breakdown of the lubricant film inside the cavitated regions $\mathfrak{D}^0$, signifying the presence of a homogeneous mixture of liquid and gases/vapours in those regions. A fully developed lubricant film is achieved when $\theta = 1$. For a more detailed analysis of the application and numerical implementation of the $p-\theta$ Elrod-Adams cavitation algorithm in conjunction with the solution of the (generalised) Reynolds equation for lubrication problems involving both conformal and counterformal contacts, readers are referred to [33,108,115].

Several other mass-conserving numerical algorithms have been developed using finite difference methods [116,117], finite element methods [118,119] and boundary element methods [120]. Vijayaraghavan and Keith Jr. [121,122] revamped the computational efficiency of the Elrod algorithm [114] for implementing the JFO boundary conditions by utilising the principle of constant bulk modulus compressibility. Sahlin et al. [123] derived a modified Reynolds equation that

accommodates arbitrary compressibility relations and cavitation, while Bayada et al. [124] proposed a continuous complementarity formulation using a two-scale approach. Giacopini et al. [125] introduced the discretised linear complementarity problem (LCP) formulation, and Almqvist et al. [126] developed an open-source algorithm for solving the cavitation LCP formulation using Lemke's pivoting algorithm [127] to determine a solution in a finite number of iterative steps. Bayada [128] also proposed two algorithms to solve a new cavitation model based on a compressible Reynolds equation, where a barometric-isentropic assumption is applied to derive the pressure-density relation. Woloszynski et al. [129] later introduced the Fischer-Burmeister-Newton-Schur (FBNS) algorithm, which reformulates the complementarity problem into an unconstrained system of equations for enhanced computational efficiency. Additionally, Brunetière [130] presented a finite element solution to a general formulation of the Reynolds equation for both liquid and gas lubrication, while Ransegnola et al. [131] proposed a modification of the Elrod-Adams cavitation algorithm to efficiently solve fluid film bearings, considering both gaseous and vapour cavitation, without the need of a switch function.

3.3. Deformation of the contact surfaces

Addressing the fluid-structure interaction between hydrodynamic pressures and solid deformations is indispensable for understanding the tribological behaviour of lubricated contacts, especially in tribosystems operating within the EHL regime. This interaction requires accurately assessing the elastic deformations of the contacting surfaces induced by the fluid pressures. As previously discussed, these displacements result in significant variations in lubricant film thickness, thereby influencing the overall lubrication performance of the system. Typically, the solid deformation problem is modelled using approaches based on either the half-space theory or finite element analysis, depending on the size of the contact region relative to the dimensions of the contacting bodies and the complexity of the geometric features and materials defining the lubricating interfaces.

3.3.1. Elastic half-space solution

The *Hertzian* theory [132] can be regarded as the foundation of practical contact mechanics, providing reliable predictions of deformation and stress distributions within and at the interface of counterformal contacting solids [40,133]. The theory is based on a particular solution to the general elastic half-space formulation, which assumes a semi-ellipsoidal distribution of the interfacial pressure over an elliptic contact area. Before exploring the classical solutions for interfacial displacements in a general elastic half-space subjected to normal loads, it is important to outline the following key assumptions of the *Hertzian* theory [40,70]:

1. The materials in contact are homogeneous, isotropic and non-conforming.
2. The contacting bodies are elastic and exhibit small strains; hence, the theory of elasticity [134] may be applicable.
3. The bodies in contact are assumed to be semi-infinite elastic half-spaces, *i.e.* the contact area and the extent of deformation are significantly smaller than the geometrical dimensions of the contacting bodies.
4. Contact stress is caused by a load that is normal to the contact tangent plane, implying the absence of any tangential forces between the solids.
5. The surfaces are frictionless and have negligible roughness.

Accordingly, solutions based on the aforementioned Hertzian assumptions within the framework of the elastic half-space theory are commonly used to evaluate the normal surface displacements induced by interfacial pressure distributions in elastic bodies. One example of such a pressure-displacement relationship in three-dimensional elastic half-space problems is given by the Boussinesq convolution integral (also referred to as the Boussinesq-Cerruti potential function) [135], expressed as follows:

$$\delta(x,y) = \frac{(1-\nu^2)}{\pi E}\iint_{\Omega}\frac{p(x',y')}{\sqrt{(x-x')^2+(y-y')^2}}\,dx'dy', \tag{8}$$

where ν and E are the Poisson's ratio and Young's modulus of the half-space material, respectively. The Boussinesq equation (Eq. 8) governs the normal elastic displacement $\delta(x,y)$ at the surface point (x,y) due to the pressure distribution $p(x',y')$ over the area Ω. Although this equation primarily describes the displacement field in a three-dimensional elastic half-space, as in point contacts, the Boussinesq convolution integral can also be utilised to approximate the interfacial displacements in two-dimensional line contacts by considering changes in contact geometry and loading conditions [70]. The Flamant solution [136] is used to calculate the normal elastic displacement $\delta(x)$ at the interface in line contacts, where a pressure profile $p(x')$ is applied over a line domain Ω'. With respect to a reference point, x_r, the Flamant equation is expressed as follows:

$$\delta(x) = -\frac{2(1-\nu^2)}{\pi E}\int_{\Omega'}\ln\left|\frac{x-x'}{x-x_r}\right|p(x')\,dx'. \tag{9}$$

In addition to the Boussinesq and Flamant solutions, several other formulations have been developed within elasticity theory to address the deformation of elastic half-space bodies under various loading conditions. These include Mindlin's solution [137], which accounts for subsurface loads in a half-space; Kelvin's solution [138], applicable for concentrated forces in infinite space; and the Papkovich–Neuber general solution [139–141], which formulates the elasticity problem in terms of harmonic functions.

Numerically evaluating the surface displacements by integrating the previously mentioned pressure-displacement relationships (Eq. 8 and Eq. 9) over the entire contact domain can be both computationally demanding and time-consuming, especially when fine mesh grids are used to discretize the contacting geometries. The direct summation (DS) method is often employed to reduce this computational burden. In this approach, nodal surface displacements are computed by multiplying a matrix of influence coefficients (ICs) with the pressure distribution vector or matrix for two-dimensional line and three-dimensional point contact problems, respectively [142]. The influence coefficients, which are derived from Green's function for elastic half-space bodies, characterise the surface displacement, stress and strain responses to a unit load applied at a specific surface point. The accuracy of the IC matrix approach is influenced by the mesh topology and the interpolation method used to approximate the pressure distribution within each mesh element. For instance, in EHL problems, depending on the required accuracy [67,143], the hydrodynamic pressure can be interpolated using constant (or zero-order polynomial) [144], piecewise bilinear (or first-order polynomial) [145] or piecewise biquadratic (or second-order polynomial) approximations [146].

In addition to the computationally intensive DS method, several alternative numerical techniques have been proposed to efficiently calculate surface elastic displacements, many of which are conceived by exploiting the convolution properties of Eq. 8 and Eq. 9, especially in densely discretised computational domains. These methods include the multi-level multi-integration (MLMI) method [147], the differential deflection method [148,149], the moving grid method (MGM) [150], the conjugate gradient method (CGM) [151,152], the fast Fourier transform (FFT) approach [153], discrete convolution and fast Fourier transform (DC-FFT) [154], continuous convolution and Fourier transform (CC-FT) [155], mixed discrete-continuous convolution with duplicated padding and FFT (DCD-FFT) [156], discrete convolution, continuous convolution, and FFT (DC-CC-FFT) [157] and the discrete-continuous convolution with IC summation and FFT (DCS-FFT) [158], among others. For detailed reviews on the performance of FFT-based algorithms in solving contact mechanics problems involving pressure-

displacement convolution integrals, readers are referred to [67,142,155,159].

Alternatively, pressure-induced elastic deformations can be evaluated by solving the classical linear elasticity equations. These equations provide a complete description of continuous linear elastic isotropic materials based on the generalised Hooke's constitutive law without relying on the simplifying assumptions of half-space theory [34]. These equations are given as follows [134]:

$$\nabla\cdot\boldsymbol{\sigma} = 0, \qquad \boldsymbol{\sigma} = \boldsymbol{C}\cdot\boldsymbol{\varepsilon}(\boldsymbol{U}), \qquad \boldsymbol{U} = \begin{bmatrix}\delta_x & \delta_y & \delta_z\end{bmatrix}, \tag{10}$$

where $\boldsymbol{\sigma}$ represents the stress tensor, which describes the distribution of internal forces within the deformed material. The constitutive tensor $\boldsymbol{C}$ relates stresses to strains in the material, incorporating constitutive properties such as Young's modulus and Poisson's ratio, which are essential for determining the material's response to applied loads. The strain tensor $\boldsymbol{\varepsilon}$ characterises the material's deformation in terms of relative displacement, while $\boldsymbol{U}$ denotes the spatial displacement vector, with its components δ_x, δ_y, and δ_z corresponding to displacements in the x, y and z directions, respectively.

3.3.2. Finite element solution

Despite their widespread application in contact mechanics, elastic half-space solutions are generally limited to interfacial problems where the dimensions of the contact area are small compared to the overall size of the contacting bodies. Consequently, these solutions become inadequate for assessing the structural deformations in lubricated conformal contact bearings (*e.g.* journal and thrust bearings), where the entire geometry of the system significantly influences the response. Furthermore, non-linear and rate-dependent material properties can also play a critical role in compliant systems, such as in elastomers and biomechanical devices.

In practical applications, non-linear behaviour in solids can arise from material or geometric non-linearity. Material non-linearity is observed when the stress-strain relationship is not proportional, as in hyper-elastic materials. More complex scenarios include rate-dependent materials, such as viscoelastic materials, where the response depends on the magnitude of applied stress and the rate at which it is applied. On the other hand, geometric non-linearity occurs when a solid undergoes large deformations, causing a significant difference between its undeformed and deformed configurations. Under such conditions, using the undeformed geometry for expressing or solving the linear strain-displacement or equilibrium equations is no longer appropriate, requiring more advanced methodologies to account for the altered geometry and resulting stresses.

The structural problem associated with tribocontacts can be effectively addressed using the Finite Element Method (FEM). In this approach, the problem is reformulated into a system of simultaneous algebraic equations, and a variational method is applied to approximate the solution, following the principle of energy minimization [160]. This enables the analysis of components with complex geometries, material behaviours and boundary conditions in both static and dynamic scenarios. For linear materials, the numerical solution of the mathematical problem is accomplished by solving the following system of ordinary differential equations (ODEs), which arises from the FEM discretisation of the governing equations [161]:

$$[\mathbf{M}]\{\ddot{\boldsymbol{u}}\} + [\mathbf{B}]\{\dot{\boldsymbol{u}}\} + [\mathbf{K}]\{\boldsymbol{u}\} = \{\boldsymbol{f}\}, \tag{11}$$

where $[\mathbf{M}]$, $[\mathbf{B}]$ and $[\mathbf{K}]$ are the mass, damping and stiffness matrices of the full FEM model of the bearing structure, respectively. The vectors $\{\ddot{\boldsymbol{u}}\}$, $\{\dot{\boldsymbol{u}}\}$ and $\{\boldsymbol{u}\}$ are the nodal accelerations, velocities and displacements, respectively, while $\{\boldsymbol{f}\}$ represents the applied nodal forces. These vector quantities encompass all the three-dimensional degrees of freedom (DOFs) for each node of the entire FEM model.

In elastohydrodynamic lubrication analysis, only the displacements at the contact surfaces are needed to evaluate the tribological performance of the interface. Consequently, to minimise computational cost, substructure (or super-element/condensation) techniques [162] are commonly employed to *reduce* the full FEM model to an equivalent system that *retains* only the degrees of freedom associated with the nodes on the bearing surfaces. The *reduced* form of Eq. 11 can be expressed as:

$$[\mathbf{M_r}]\left\{\ddot{\boldsymbol{u}}_\mathbf{r}\right\} + [\mathbf{B_r}]\left\{\dot{\boldsymbol{u}}_\mathbf{r}\right\} + [\mathbf{K_r}]\{\boldsymbol{u}_\mathbf{r}\} = \{\boldsymbol{f}_\mathbf{r}\}, \tag{12}$$

where the subscript r denotes quantities corresponding to the reduced system. It is important to notice that, unlike the sparse matrices of the full FEM model, the matrices of the reduced system are fully populated due to the inherent coupling of all degrees of freedom in substructure systems (super-elements) [163]. Additionally, any boundary conditions defined for the full FEM model are automatically incorporated and enforced in the condensed model.

The substructure matrices can be generated as a pre-processing step in commercial software packages, such as Abaqus, Ansys or COMSOL. The nodal force vector of the reduced model can then be expressed in terms of the hydrodynamic pressure distribution acting on the bearing surface as follows:

$$\{\boldsymbol{f}_\mathbf{r}\} = [\mathbf{A}]\{\boldsymbol{p}\}, \tag{13}$$

where $[\mathbf{A}]$ is the total area matrix and $\{\boldsymbol{p}\}$ is the vector of the nodal hydrodynamic pressures acting on the bearing surface. Substituting Eq. 13 into Eq. 12, one obtains:

$$[\mathbf{M_r}]\left\{\ddot{\boldsymbol{u}}_\mathbf{r}\right\} + [\mathbf{B_r}]\left\{\dot{\boldsymbol{u}}_\mathbf{r}\right\} + [\mathbf{K_r}]\{\boldsymbol{u}_\mathbf{r}\} = [\mathbf{A}]\{\boldsymbol{p}\}. \tag{14}$$

The kinematic quantities in Eq. 14 are originally calculated with respect to the global coordinate system of the full FEM model. However, to correct the lubricant film thickness, such quantities have to be determined relative to the local tribocontact reference system where the fluid film geometry is described.

In bearing analysis, Eq. 14 represents a linear structural vibration problem, with external loads resulting from the hydrodynamic pressure distribution applied to the bearing surface. When both the gross rigid body motion and the vibrational response of the bearing are coupled, the floating frame of reference formulation (FFRF) for flexible multibody dynamic systems (FMDS) is often used to describe the mechanical behaviour of the system. In many applications, mechanical boundary conditions in the FEM model are not clearly defined, and so the structure is often treated as an unconstrained body. This introduces challenges in the solution process due to the singularity of the stiffness matrix in free-free systems. To address this issue, Component Mode Synthesis (CMS) procedures, such as the Craig-Bampton method, are widely employed for model order reduction, effectively eliminating the rigid body modes from the FEM model [164–166].

3.4. Energy equation for the lubricant film

The dissipation of friction-induced energy as interfacial heat plays a critical role in the tribological performance of systems, as thermal effects significantly influence both lubricant chemistry and the thermo-mechanical behaviour of contacting surfaces. As temperatures exceed ambient levels, the average molecular motion and intermolecular distances in fluids tend to increase, resulting in greater molecular momentum and a reduction in intermolecular forces [42,167,168]. Consequently, fluid viscosity tends to decrease with increasing temperatures, leading to a thinning of the lubricant film and an increased risk of seizure within the clearance.

The temperature distribution within the lubricant film is governed by the three-dimensional energy equation for compressible viscous fluids, which in its strong conservation form can be expressed as follows [30,32,34,79,169]:

$$\frac{\partial(\rho c_p T)}{\partial t} + \nabla\cdot(\rho c_p \boldsymbol{v} T) = \nabla\cdot(k\nabla T) + Q_T, \tag{15}$$

$$Q_T = Q_p + Q_{cp} + Q_\Phi + \dot{q}_v,$$

$$Q_p = \underbrace{\beta T\left(\frac{\partial p}{\partial t} + \boldsymbol{v}\cdot\nabla p\right)}_{\substack{\text{Compressive}\\ \text{Heating/Cooling}}}, \quad Q_{cp} = \underbrace{\rho T\left(\frac{\partial c_p}{\partial t} + \boldsymbol{v}\cdot\nabla c_p\right)}_{\substack{\text{Enthalpic}\\ \text{Heating/Cooling}}}, \quad Q_\Phi$$

$$= \underbrace{\eta\left[\left(\frac{\partial u}{\partial z}\right)^2 + \left(\frac{\partial v}{\partial z}\right)^2\right]}_{\substack{\text{Shear}\\ \text{Heating}}}.$$

In this equation, $T(x,y,z,t)$ represents the lubricant temperature, while $\rho(x,y,z,t)$, $c_p(x,y,z,t)$, $k(x,y,z,t)$, $\beta(x,y,z,t)$ and $\eta(x,y,z,t)$ denote the lubricant density, thermal heat capacity, thermal conductivity, thermal compressibility and dynamic viscosity, respectively. Additionally, $\boldsymbol{v}(x,y,z,t) = u(x,y,z,t)\hat{\mathbf{i}} + v(x,y,z,t)\hat{\mathbf{j}} + w(x,y,z,t)\hat{\mathbf{k}}$ represents the fluid velocity vector field, and $\dot{q}_v$ corresponds to the rate of internal heat generation within the lubricant film, resulting from various factors, including viscous dissipation and interactions between surface asperities.

In full three-dimensional thermohydrodynamic lubrication (THL) problems, the fluid energy equation must be solved in conjunction with the *generalised* Reynolds equation (Eq. 3). This approach accounts for how temperature variations across the film thickness influence the lubricant density and viscosity along that direction and, consequently, the hydrodynamic pressure generation and viscous friction throughout the contact.

3.5. Interfacial heat transfer

Incorporating accurate thermal boundary conditions is essential for accurately modelling complex, real-world lubrication systems, particularly for predicting the longevity of lubricated surfaces. The thermal management efficiency of the lubricated system is governed by the thermophysical properties of the contact interface, which dictate the extent to which the frictional heat can be dissipated from the contact region. In evaluating the thermal behaviour of tribosystems, numerical solutions commonly rely on either fluid-solid interaction (FSI)-based conjugate heat transfer models or the classical heat source method, derived from the Carslaw-Jaeger integral formulation. In the following analysis, subscripts s denote the lower ($s = 1$) and upper ($s = 2$) surfaces of the lubricated system.

3.5.1. Conjugate heat transfer model

Conjugate heat transfer (CHT) [170,171] refers to the simultaneous heat transfer between a fluid and its surrounding solid, involving the interaction of heat transfer processes in both mediums. This coupling of conduction within the solid and convection within the fluid makes accurate prediction of CHT essential for engineering applications where these mechanisms are interdependent and vital to system performance. Examples include heat exchangers, semiconductor cooling, automotive thermal management and many other systems where heat exchange between fluid and solid components directly impacts efficiency and safety [172]. In lubrication modelling, computational CHT analysis ensures the continuity of temperature and heat flow at the fluid-solid interface. CHT addresses both fluid and solid heat transfer challenges by facilitating the exchange of thermal boundary conditions based on the thermal solutions computed within each domain, ensuring a more comprehensive thermal analysis of the lubricated system [173,174].

Analogous to the thermal analysis of the entraining fluid described in Eq. 15, the thermal behaviour of the bounding solids is assessed by omitting the numerical terms related to heat generation within the solids. This simplification focuses on the conduction process, assuming that heat generation is negligible. As a result, the temperature distribution within the solid bodies is computed using the following equation:

$$\frac{\partial(\rho_s c_{p_s} T_s)}{\partial t} + \nabla\cdot(\rho_s c_{p_s} \boldsymbol{v_s} T_s) = \nabla\cdot(k_s \nabla T_s), \tag{16}$$

where ρ_s, c_{p_s} and k_s represent the density, specific thermal capacity and thermal conductivity of the contacting body (s), respectively. The term $\boldsymbol{v_s}$ denotes the velocity vector of the solid's surface, defined as $\boldsymbol{v_s} = [u_s \quad v_s \quad w_s]^T$. This velocity matrix captures the spatial motion of the solid surface in the coordinate directions.

A key factor influencing the accuracy of conjugate heat transfer solutions is the choice of coupling algorithm utilised to capture the thermal interaction between the fluid and structural solvers. This algorithm ensures temperature and heat flux continuity at the fluid-solid domain interfaces, which is critical for an accurate thermal prediction [175]. Numerically, this can be achieved using one of two primary approaches: monolithic or partitioned techniques. In the monolithic approach, the fluid and solid equations are solved simultaneously within a single, unified computational framework. This strongly coupled method ensures a direct and fully integrated solution for the entire system, hence improving consistency at the fluid-solid interface but often increasing computational complexity. Alternatively, partitioned techniques tackle the fluid and solid thermal problems separately, with the coupling enforced at the interface through direct iterative schemes. In this approach, the solvers pertaining to the fluid and solid domains are run independently, and the solutions are exchanged iteratively at the interface until convergence is achieved [175,176]. Although this method allows for greater flexibility in handling complex systems and leveraging specialised solvers for each domain, it may require more computational effort to ensure accurate coupling across the interface.

3.5.2. Heat source integration solution

The surface heat source integral equation developed by Carslaw and Jaeger [177,178] is commonly employed in lubrication modelling for estimating the temperature distribution across the contacting surfaces. Originally formulated to address problems involving infinite half-space bodies, the Carslaw and Jaeger theory predicts the surface temperature of the solid (s) at nodal position (x,y) due to a surface heat source located at a different position (x',y') [179]. Under transient conditions, the temperature distribution can be evaluated as follows [67]:

$$T_s(x,y,t) = T_{b_s} + \frac{1}{4\rho_s c_{p_s}\sqrt{(\pi\alpha_s)^3}}\int_0^t\int\int_\Omega \frac{q_s(x',y',t')}{\sqrt{(t-t')^3}} \times \exp\left(-\frac{R^2}{4\alpha_s(t-t')}\right) dx'\,dy'\,dt', \tag{17}$$

where $R = \sqrt{[x-x'-u_s(t-t')]^2 + [y-y'-v_s(t-t')]^2}$ represents the distance between the moving heat source point (x',y'), convected at velocity, $\boldsymbol{v_s}(x,y,t) = (u_s, v_s)$ and the response point (x,y), T_{b_s} is the body bulk temperature, $\alpha_s = k_s(\rho_s c_{p_s})^{-1}$ is the thermal diffusivity of the solid material and q_s quantifies the heat flux generated by the source at (x',y') at time t',. This formulation is analogous to Eq. 8, which is used to predict surface elastic deformation under applied loads. Similarly, calculating the temperature distribution using Eq. 17 can be computationally expensive, particularly when employing denser computational grids, as the integral needs to be evaluated for each node across the surface. To address this computational challenge, a variety of numerical techniques have been developed to improve the efficiency of temperature rise calculations. Readers are referred to [180–183] for an overview of the advanced numerical methods, such as the multi-level multi-integration (MLMI) and the fast Fourier transform (FFT)-based methods.

Furthermore, one-dimensional temperature solutions, mostly prev-

alent for line contact problems, can be analysed using the one-dimensional form of the transient Carslaw and Jaeger integration model. This approach incorporates the same surface properties described earlier and is expressed as:

$$T_s(x,t) = T_{b_s} + \frac{1}{\sqrt{4\pi\alpha_s}} \int_0^t \int_\Omega \frac{q_s(x',t')}{\sqrt{t-t'}} \times \exp\left(-\frac{[x-x'-u_s(t-t')]^2}{4\alpha_s(t-t')} \right) dx'\,dt'. \tag{18}$$

It is worth mentioning that Eq. 18 assumes heat is transferred perpendicularly into the surface interfaces. Therefore, its application is limited to systems characterised by a high Peclet number ($Pe > 5$), where the heat transfer perpendicular to the velocity of the heat source dominates, and the lateral heat diffusion is negligible [67]. In other words, under such conditions, heat only diffuses a short distance into the solid during the time it takes for the surface to move through the heated zone [36]. Therefore, for a given case where either surface is stationary, the transient heat transfer solution may not apply, and instead, Johnson's steady-state model [40] is often employed. This model accounts for the contribution of the heat flux from the fluid domain to a specific surface element. The steady-state discretised form of the temperature distribution can be expressed as follows [35]:

$$T_s(x_m) = T_{b_s} + \sum_{all\ n} q_{n_s} S_{m,n}, \tag{19}$$

where q_{s_n} is the heat flux from the fluid to the solid at a surface point n, acting on an elementary area $dx_n\,dy_n$. Furthermore, $S_{m,n}$ denotes the influence coefficient matrix representing the effect of the heat flux at point n, with coordinates (x_n, y_n), on the nodal position m, with coordinates (x_m, y_m) [36]. The influence coefficient $S_{m,n}$ is evaluated as:

$$S_{m,n} = \frac{1}{2\pi k_s} \int \int_\Omega \frac{dx'\,dy'}{\sqrt{(x_n - x')^2 + (y_n - y')^2}}, \tag{20}$$

using the numerical techniques discussed earlier in subsubsection 3.3.1 to capture the effects of the heat distribution across the surface.

3.5.3. Lubricant rheology

The utilisation of accurate constitutive laws to capture the continuum behaviour of lubricants is crucial for predicting the performance of tribological systems, as the rheological properties of lubricants (*e.g.* viscosity and density) are highly sensitive to the temperature, pressure and shear rate conditions within the contact zone. For example, Newtonian behaviour, which is characterised by a linear relationship between shear stress and shear rate, is typically valid at relatively low shear rates. For pure mineral oils, this relationship holds for shear rates up to approximately 10^6 s^{-1}. However, this linear relationship breaks down under high shear rates, especially in elastohydrodynamic lubrication regimes, and the lubricant begins to exhibit non-Newtonian behaviour. One of the most commonly observed non-Newtonian behaviours in lubricant oils is *shear-thinning*, where lubricant's viscosity decreases as the shear rate increases. This phenomenon occurs as the internal structure of the lubricant, such as fluid particles or molecular chains, undergoes reorganisation or "thinning" under stress, reducing resistance to flow [22]. In lubricants that contain dissolved polymers, such as multigrade oils commonly used in internal combustion engines, high shear conditions cause the long, randomly oriented polymer chains to align with the flow. This alignment reduces the internal resistance to flow and consequently lowers the bulk viscosity of the lubricant. This effect is particularly pronounced in oils formulated with viscosity index (VI) improvers—polymeric additives designed to stabilise the oil's viscosity across a wide temperature range [184–186]. These polymers play a key role in enabling multigrade oils to perform effectively under cold-start and high-temperature conditions by stabilising viscosity fluctuations. However, the polymers' susceptibility to shear-thinning can reduce the lubricant film thickness, particularly under heavy load conditions. This thinning of the lubricant film may compromise its ability to protect against wear and surface damage, reducing the effectiveness of the lubricant in preventing direct contact between surfaces.

Breakthroughs in experimental protocols [187,188] as well as computing power [46,189] have been paramount in the development and understanding of the EHL theory by deriving constitutive models aimed at explicating the lubricant behaviour in elastohydrodynamic (EHD) contacts. Molecular simulations have become a vital tool for providing insights into the complex interactions of lubricant and additive molecules that influence the macroscopic performance of tribological systems, as discussed later in Section 5. Classical EHL theory laid the foundation for understanding thin film behaviour under high pressure and shear, particularly in load-carrying capacity, friction and thermal stability [190]. It also provides empirical tools [188,191–193], such as pressure-viscosity relationships and film thickness equations, to predict tribological performance without requiring extensive numerical simulations. However, classical EHL has limitations in accurately representing piezoviscous behaviour and complex lubricants [194], particularly with phenomena such as the super-Arrhenius pressure response [195]. These issues stem from assumptions such as the Newtonian inlet and Eyring non-Newtonian behaviour, which oversimplify the system [196]. To overcome these limitations, the quantitative EHL approach has emerged, incorporating advanced computational methods and experimental data, such as viscosity-pressure measurements from high-pressure viscometers [194,195,197]. This allows for more accurate rheological models and performance predictions [75], accounting for complex contact conditions like shear stress, thermal effects and surface topography.

The extreme and complex conditions within EHD contacts make it challenging to study lubricant behaviour, as experimental and computational resources are often limited. Additionally, the complex composition of lubricating fluids presents further challenges in fully understanding lubrication performance. Glass transition [198] is an important phenomenon which refers to the transition that a lubricant undergoes from a fluid-like state to a more solid-like, glassy state triggered under the extreme pressures and temperatures of EHL regimes. Unlike conventional phase changes such as melting or freezing, which entail a distinct change in state, the glass transition is gradual and reversible, leading to a significant increase in viscosity [199,200]. As a result, the lubricant behaves more like an elastic solid than a viscous fluid [201], thus influencing its load-carrying capacity [202]. At the molecular level, the high pressure during glass transition reduces the mobility of lubricant molecules, decreasing their kinetic energy and resulting in increased viscosity [203]. As the glass transition approaches, the concept of "*lubricant fragility*" becomes important, as it measures how quickly the viscosity increases with changes in temperature and pressure [204,205]. A lubricant becomes more fragile as it nears the glass transition, causing it to be more likely to undergo this transition at the high pressures typical of EHL environments. In EHL applications, understanding lubricant fragility is critical for designing lubricants and additives that can perform under the severe conditions present in these systems [205–207].

It is worth noting that, in addition to experimental data and physics-based insights, machine learning (ML) techniques are garnering significant attention in advancing rheological studies within the context of EHL. Machine learning offers several advantages in addressing intricate problems, handling large datasets and providing valuable insights into lubricant performance across various operating conditions [208]. By deploying ML tools in tribological applications [209–211], researchers can conduct detailed analyses of complex rheological behaviours, such as viscoelasticity and thixotropy, which may be difficult to capture with conventional methods. Moreover, ML can accelerate the development of new lubricants by streamlining experimental processes, enabling faster identification of optimal formulations and automating the entire rheological evaluation pipeline—from data acquisition and analysis to

hypothesis validation and model creation. As discussed in more detail in Section 7, ML has the potential to revolutionise the way rheological properties are studied, enhancing both the efficiency and accuracy of lubricant performance predictions under diverse conditions.

3.6. Multiphysics coupling

The inherent non-linearity of the governing equations, combined with the interdependence of multiple physical phenomena governing lubricated contacts, as shown in Fig. 5, entails the use of robust fluid-solid interaction (FSI) coupling methods, which are the crux of any continuum-based framework for accurately modelling the complex interactions within tribosystems. In the mathematical modelling of lubrication problems, FSI methods can be classified into two main categories, namely monolithic and partitioned approaches.

Monolithic (or full-system) approaches involve solving the flow and structural equations simultaneously within a single coupling iteration, often utilising implicit Newton-Raphson schemes. These methods have been shown to offer excellent numerical stability and rapid convergence rates, as demonstrated in several studies [212–215]. The strong coupling in monolithic models ensures that information is consistently exchanged between the fluid and structural domains, hence preventing the localised loss of information when handling the hydrodynamic and structural aspects separately [34]. Although such robust integration improves the accuracy of the coupled solution, particularly in complex lubrication scenarios, one of the main challenges of the monolithic approach is the high computational cost associated with solving the system of equations, primarily when tackling severe loading conditions. This is mainly due to the need to invert a full (dense) Jacobian matrix, which grows in size and complexity with the number of variables in the problem. For large-scale or highly non-linear problems, this matrix inversion process can become computationally expensive and resource-intensive, potentially limiting the practical application of monolithic methods in cases where real-time or large-scale simulations are required.

Unlike monolithic coupling techniques, partitioned (or sequential) coupling methods solve the hydrodynamic and structural problems separately, *i.e.* there is no *a priori* explicit coupling between the fluid and structure sub-models as in monolithic schemes. Instead, partitioned methods require a coupling algorithm to link the fluid and structural solvers, ergo ensuring that each subsystem is informed of the overall behaviour of the coupled system. For example, inspired by FSI problems beyond the tribological arena [216,217], the performances of Fixed Point Gauss-Seidel Method (PGMF) and Point Gauss-Seidel Method with Aitken Acceleration (PGMA) were assessed in [35] for solving heavily-loaded EHL problems. These methods, as well as the Interface Quasi-Newton Method with Inverse Jacobian from Least-Squares approximation (IQN-ILS), were also applied in [218] for simulating connecting-rod bearings operating in mixed-EHL regimes. One of the key advantages of partitioned methods is their ability to integrate specialised solvers for the fluid and solid domains, enabling the integration of dedicated codes within the coupling framework to address each subsystem independently as "*black-box*" solvers. This can simplify the complexity of fluid-structure interaction problems that involve a wide range of multiphysics phenomena and reduce the computational cost of coupling iterations by enhancing the convergence rates while maintaining solution accuracy. Nevertheless, partitioned methods can suffer from slower convergence compared to monolithic coupling schemes, particularly if the interaction between the fluid and solid domains is strong. The readers are referred to [216,217,219] for detailed analysis of these coupling algorithms and their application in FSI problems. Additionally, Table 1 reports a non-exhaustive list of numerical modelling techniques employing partitioned FSI coupling to assess lubrication problems.

4. Mixed lubrication: The smaller-scale details that matter

Numerous (bio)mechanical components subject to severe contact conditions—such as rolling bearings, gears, cam-followers, piston rings, sliding bearings, seals and human joints—operate fully or partially within the mixed lubrication regime. Reiterating on what was briefly discussed in Section 2, the mixed lubrication regime is particularly prevalent in systems operating under heavy loads, low speeds, elevated temperatures, intense vibrations, or lubricated with low-viscosity fluids.

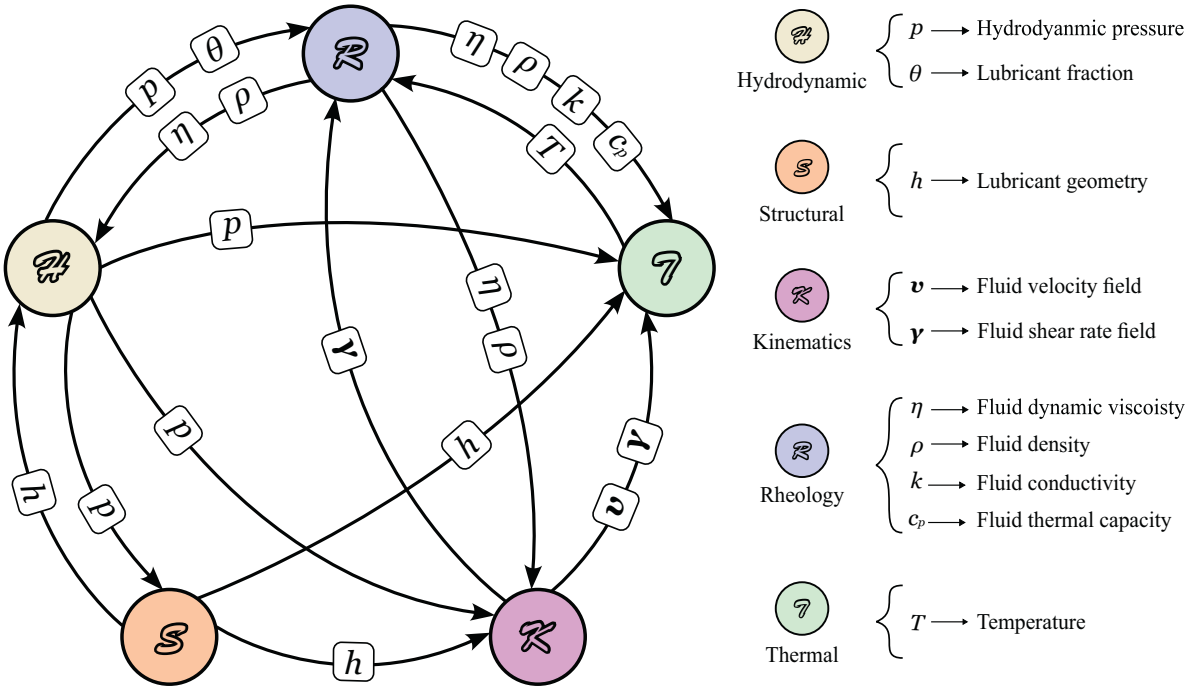

Fig. 5. Architecture of the coupling framework for simulating the macroscopic, multiphysical fluid-solid interactions in lubricated contacts. The schematic illustrates the interconnections between the hydrodynamic, structural, kinematic, rheology and thermal solvers (depicted as circles), with the required inputs and calculated outputs for each solver shown as rounded rectangles, highlighting their interdependence.

Table 1
A selective list of modelling algorithms that adopt partitioned and monolithic FSI coupling strategies for simulating the continuum behaviour of lubricated tribosystems.

Category	Sub-model	Key features	Reference
Partitioned	Straightforward	Utilises Gauss-Seidel relaxation for the iterative solution of the Reynolds equation to compute hydrodynamic pressures based on a fixed film thickness distribution	[220]
	Inverse	Film thickness is computed inversely by solving the Reynolds equation, and the resulting pressures are obtained using a cubic approximation	[221]
	Coupled differential deflection	The coupling of the FSI problem is achieved using a differential form of the deformation equation, derived from half-space theory	[222]
	Multigrid	Numerical solutions are attained using computational domains with varying mesh densities, improving convergence rates by targeting error wavelength decay	[223]
	Line relaxation	A hybrid relaxation method often integrated into multigrid solvers, alternating between Jacobi and Gauss-Seidel based on local flow conditions and addressing multiple points along a grid line simultaneously	[224]
	Progressive mesh densification	Mesh densities are progressively refined from coarse to fine, starting with initial guesses on a coarse grid that are used to improve solution accuracy on finer grids	[225]
	Semi-system	Diagonal dominance in the coefficient matrix is achieved by treating the film thickness in Couette flow term as a function of unknown nodal pressures and influence coefficient matrix	[146]
	Interface Quasi-Newton	Accelerates convergence using a quasi-Newton method with a least-squares approximation of the inverse Jacobian	[218]
	Aitken relaxation	Dynamically varies the under-relaxation parameter in a coupling iteration according to the results of the previous iterations	[218]
Monolithic	Full-system	Coupling between hydrodynamic and structural effects is achieved by solving the system of equations within a single framework	[226]
	Homotopy	Adopts the "*continuation*" process, whereby one problem is deformed into another by the continuous variation of a single parameter for generating a convergent series solution for nonlinear systems	[227]

In mixed lubrication, the lubricant film thickness is insufficient to completely separate the surface asperities, often resulting in the coexistence of confined lubricant films and direct asperity contacts, which together support the applied load, as per Fig. 6. Given that in this regime the average lubricant film thickness is comparable to the surface roughness, it is crucial to consider the influence of surface topography on assessing the tribological performance, integrity and longevity of the contact interfaces. Consequently, an in-depth comprehension of the mechanisms that govern mixed lubrication is paramount for achieving efficient, reliable and optimised engineering components.

The interaction between lubricant hydrodynamic action and asperity contact in modelling mixed lubrication regime presents challenges due to the increased geometric complexity introduced by surface topography. This added complexity significantly raises the computational effort required to resolve small-scale surface features accurately. Moreover, capturing such intricate geometric details using the aforementioned modelling and solution approaches is often impractical in most engineering applications, as their underlying smooth surface assumption limits their applicability to full-film lubrication regimes. In recent decades, significant progress has been made in developing mathematical models and numerical methods for predicting the mixed lubrication behaviour between rough surfaces. The following sections briefly survey the most commonly used modelling approaches for assessing mixed lubrication in tribosystems. While a comprehensive review of specific topics is beyond the scope of this work, readers are encouraged to consult the following references for a thorough overview of rough contact mechanics [26,158,229–232], mixed lubrication [233–235] and numerical methods for handling rough and textured surfaces [236,237]. Broadly, the most common approaches used for modelling fluid flow and rough contact in mixed lubrication include statistical or stochastic methods that account for the randomness of surface roughness, multiscale techniques such as averaging and homogenisation methods that capture phenomena across different scales, and deterministic approaches that provide precise predictions from the microscale. The timeline in Fig. 7 depicts the various models developed over the past 60 years to address mixed lubrication problems.

4.1. Statistical and multiscale modelling

The following sections outline the statistical and averaging/homogenisation methods often employed to model hydrodynamic and rough contact effects in mixed lubrication.

4.1.1. Lubricant film flow between rough surfaces

In mixed lubrication, the influence of the microscopic roughness scale on lubrication is often incorporated into the macroscopic governing equations through specific coefficients. These coefficients, commonly referred to as flow factors or homogenisation coefficients, translate the microscopic effects of lubricant flow into macroscopic models. The determination of these coefficients and the specific formulation of the macroscopic governing equations depend on the chosen modelling approach.

Early studies on the effect of surface roughness on hydrodynamic flow [241–243,299,300] applied stochastic process theory to lubrication problems, treating lubricant film thickness in the presence of roughness as a stochastic process. This approach led to the derivation of a stochastic Reynolds equation for the mean (or expected) film pressure. Subsequently, Patir and Cheng [50,51] introduced a pioneering average flow model widely recognised for its capacity to account for realistic three-dimensional surface topographies in lubrication analysis. This model locally averages lubricant flow at the microscopic roughness scale, yielding an averaged Reynolds equation expressed in terms of *flow factors*, which correct pressure- and shear-driven flows to incorporate the influence of roughness on the macroscopic scale. These flow factors are calculated *a priori* by deterministically solving the mixed lubrication problem at the microscale on a statistical ensemble of rough surface cells for specific roughness patterns. In their original work, Patir and Cheng provided expressions for the pressure and shear flow factors for surfaces with Gaussian distribution, which have since been widely applied in mixed lubrication analysis. Their model provides reasonably accurate average pressure distributions for isotropic and orthotropic surface topographies. However, limitations in tackling crossflow in anisotropic surfaces were later addressed by subsequent studies [113,301], which proposed an extended generalised tensorial form of the average flow model. Other averaging methods, such as the volume averaging method, which combines spatial and temporal averaging, have been devised to account for unlubricated contact areas and more accurate boundary conditions in flow factor calculations [302]. Further refinements to the average flow model have included cavitation effects [264], surface contact [303,304] and the combined influence of elastic deformation, inter-asperity cavitation and thermal effects [305].

Applying homogenisation theory to modelling fluid flow between

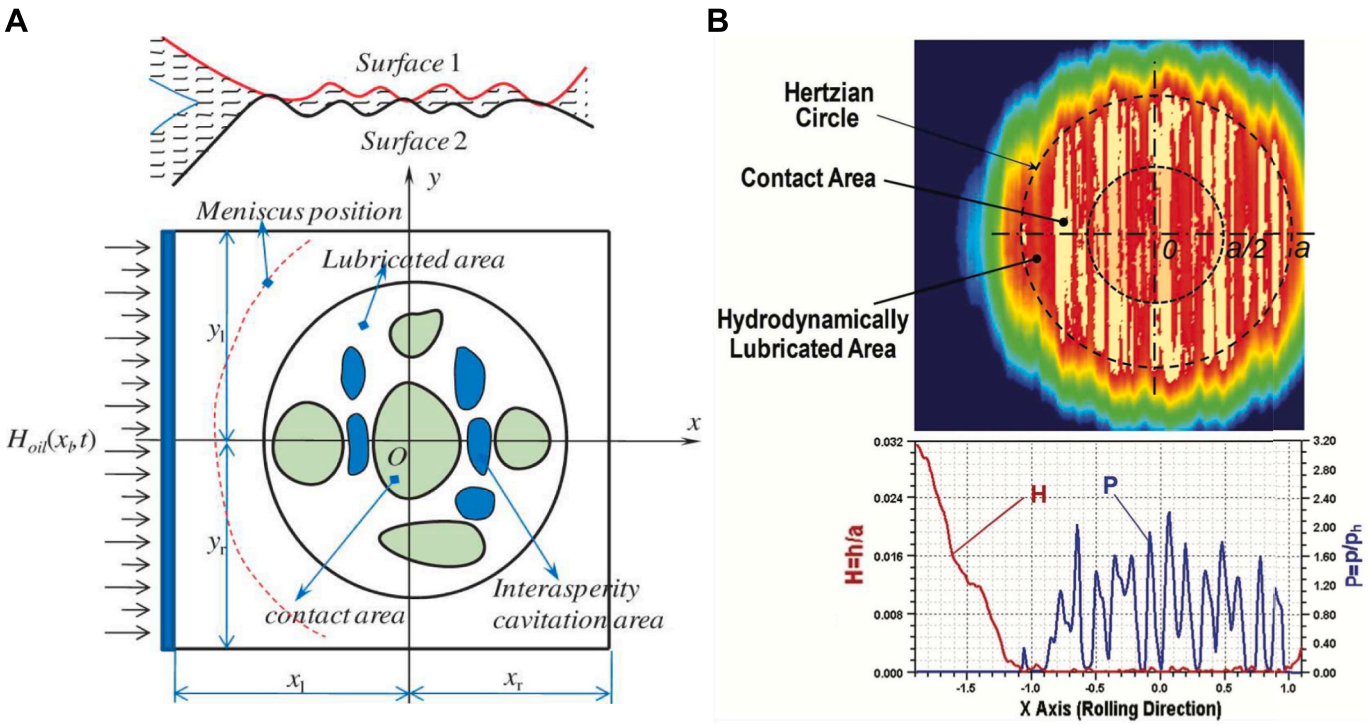

Fig. 6. Contact of lubricated rough surfaces. (A) Schematic diagram of mixed lubrication regime in circular point contact [67]. (B) Deterministic mixed lubrication solution for a circular point contact, illustrating the hydrodynamically lubricated and asperity contact areas. Reprinted from [228], with permission from Sage Publications.

rough surfaces has proven effective in deriving homogenised Reynolds equations within a rigorous mathematical framework, thus providing more accurate predictions for surfaces with arbitrary roughness. This approach has been deployed by various studies, including those by Bayada et al. [251,252,306], Buscaglia et al. [261] and Almqvist et al. [53,272,307], each of which has derived a different form of the homogenised Reynolds equation depending on the topography (smooth or rough) and kinematic conditions (stationary or non-stationary) of the contacting surfaces. Based on mathematical principles for evaluating partial differential equations with rapidly oscillating coefficients [308], homogenisation methods applied to lubrication problems commonly adopt a two-scale description of the confined film geometry. Short-length and time-scale effects induced by surface roughness are evaluated at the local microscale, while the homogenised Reynolds equation governs the global macroscale behaviour. In addition to providing a rigorous mathematical framework for deriving the homogenised Reynolds equation, homogenisation methods establish more appropriate boundary conditions for solving the microscopic problem, ensuring a more accurate determination of homogenisation coefficients for arbitrary roughness patterns [309]. This eliminates the empirical characteristics of local flow corrections in Patir and Cheng's model, making homogenisation methods a valuable tool for enhancing the accuracy of mixed lubrication analysis and providing a robust framework for assessing fluid flow in lubricated interfaces.

Rom et al. [310] conducted a comprehensive comparison between the homogenisation method and Patir and Cheng's average flow model, two of the most commonly used approaches for modelling the lubricant flow in mixed lubrication. The study revealed that the inaccurate boundary conditions used in Patir and Cheng's model for solving the microscale problem led to significant deviations in averaged pressure distributions for non-symmetric surface patterns, whereas results for symmetric patterns closely matched those obtained using the homogenisation method. The authors also emphasised a key advantage of the homogenisation technique—its ability to upscale average pressure solutions to retrieve microscale information—resulting in more accurate predictions of performance parameters such as peak pressure and friction for both symmetric and non-symmetric patterns. Additionally, the study noted that the homogenisation approach is not limited to periodic roughness and can be extended using *reiterated homogenisation* [273,311], offering a computationally efficient strategy for evaluating rough and textured surfaces. Given these advantages and minimal additional computational effort and complexity, the homogenisation method is recommended as the preferred approach for handling surface topographies with arbitrary patterns. An important development in this field has been the contribution provided by Persson and co-workers, who have used Persson's contact mechanics theory [258] and the 2D Bruggeman effective medium theory to derive analytical expressions for the fluid flow factors describing the fluid flow, and for the frictional shear stress factors to compute frictional shear stress at asperities [312]. The proposed homogenisation theory was shown to describe the transition from the hydrodynamic lubrication to the boundary lubrication regime occurring in soft contacts [313], enabling the consistent calculation of both asperity–asperity and asperity–fluid interactions and their effects on the average fluid flow and solid contact mechanics at the interface, also in the presence of surface anisotropy.

Moreover, Fourt and Arghir [279] conducted a comparative analysis of the homogenisation approach and a multiscale method inspired by studies on pressure-driven flow in porous media with irregular permeability [314,315]. To evaluate the solution of the compressible Reynolds equation, the authors extended the multiscale method to incorporate the Couette flow term (or wedge-term), hence enabling the implicit modelling of all length scales (*i.e.* full contact and roughness scales) without relying on the periodicity assumption required by the homogenisation approach for short-length scales (*i.e.* roughness pattern). Despite both approaches exhibiting comparable numerical accuracy and computational efficiency, the authors suggested that the proposed multiscale model may be particularly effective for integrating additional nonlinear effects, such as sporadic asperity contacts or the presence of temperature fields.

More recently, Pattnayak and Arghir [316] introduced a set of

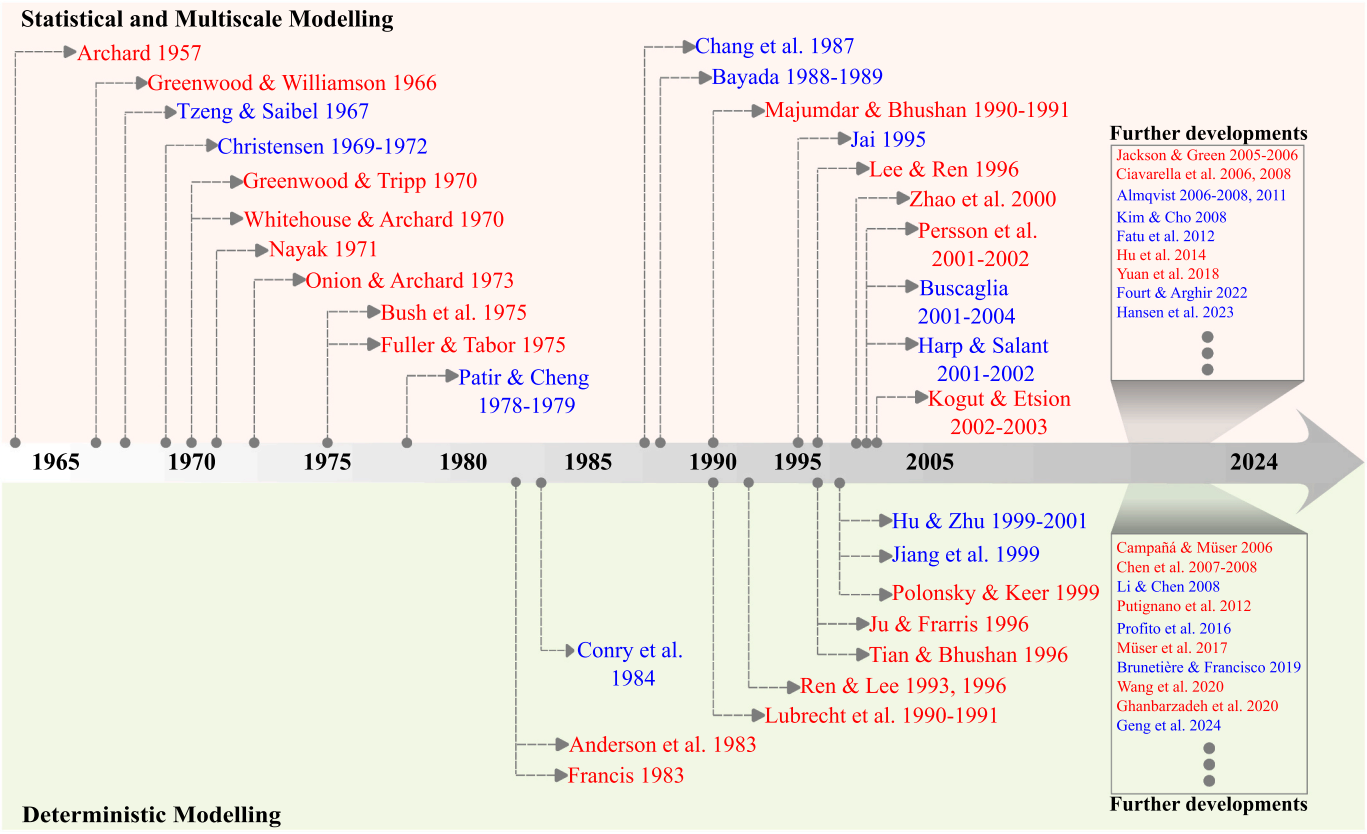

Fig. 7. A timeline depicting the seminal key advances in tackling mixed lubrication regimes using statistical, multiscale and deterministic modelling approaches. For statistical models, the following hydrodynamic and asperity contact modelling approaches are listed, denoted in blue and red, respectively: Archard [238], Greenwood & Williamson [239], Tzeng & Saibel [240], Christensen [241–243], Greenwoood & Tripp [244], Whitehouse & Archard [245], Nayak [246], Onion & Archard [247], Bush et al. [248], Fuller & Tabor [249], Patir & Cheng [50,51], Chang et al. [250], Bayada [251,252], Majumdar & Bhushan [253,254], Jai [255], Lee & Ren [256], Zhao et al. [257], Persson et al. [258–260], Buscaglia [261,262,263], Harp & Salant [264,265], Kogut & Etsion [266,267], Jackson & Green [268,269], Ciavarella et al. [270,271], Almqvist [53,272,273,274], Kim & Cho [275], Fatu et al. [276], Hu et al. [277], Yuan et al. [278], Fourt & Arghir [279], Hansen et al. [280]. For deterministic modes, the following coupled mixed lubrication and asperity contact modelling approaches are listed, denoted in blue and red, respectively: Anderson et al. [281], Francis [282], Conry et al. [283], Lubrecht et al. [284], Ren & Lee [150,256], Ju & Farris [153], Tian & Bhushan [285], Hu & Zhu [286–288], Jiang et al. [289], Polonsky & Keer [152], Campañá & Müser [290], Chen et al. [156,291], Li & Chen [292,293], Putignano et al. [294], Profito et al. [295], Müser et al. [26], Brunetière & Francisco [296], Wang et al. [158], Ghanbarzadeh et al. [297], Geng et al. [298].

normalised homogenisation coefficients, analogous to Patir and Cheng's flow factors, for modelling mixed and full-film lubrication regimes for rough and running-in flat surfaces. A modified Greenwood and Williamson rough contact model was employed to account for inter-asperity interactions. Artificial Gaussian isotropic and non-isotropic rough surfaces were characterised using a height distribution function (HDF) and a Gaussian auto-correlation function (ACF) [317], while running-in surfaces were modelled with a Weibull HDF and an exponential ACF [318] to better replicate real surface engineering properties. Through numerical tests on various surface types, the authors demonstrated the effectiveness of the proposed normalised coefficients compared to the originally proposed Patir and Cheng's flow factors. Based on these findings, they proposed curve-fitted equations to efficiently incorporate Gaussian roughness effects into the solution of the global homogenised Reynolds equation.

Since the applied load in the mixed lubrication regime is supported by both the lubricant film and surface asperities, statistical rough contact models or stiffness contact curves derived from deterministic calculations are often employed to estimate the corresponding average asperity contact pressures. This is particularly true when either averaging/homogenisation or multiscale methods are used to compute the average hydrodynamic pressures, as will be subsequently reviewed.

4.1.2. *Contact between rough surfaces*

Modelling the contact mechanics of rough surfaces presents significant challenges due to the presence of microscopic irregularities in surface topographies. The renowned statistical modelling framework proposed by Greenwood and Williamson (GW) [239] characterises surface roughness as an ensemble of spherical asperities with equal radii of curvature and randomly distributed heights. This approach extends the classical elastic Hertzian theory for an individual asperity to a statistical aggregation of asperities with a prescribed height distribution; however, at least in its original form, it does not correctly describe contact mechanics because of the neglect of the long-range elastic coupling between the asperity contact regions. Over the years, several refinements have been made to the elastic asperity-based GW model [244–249,270,271,319–321]. Among these, the Greenwood and Tripp (GT) model offers an improved approach by considering paraboloidal asperities and accounting for non-aligned interactions between asperities. Furthermore, various statistical models have been developed to account for elastoplastic deformation in dry rough contacts. Notable models include the Chang-Etsion-Bogy (CEB) model [250], which integrates plastic deformation into the GW framework based on volume conservation, and the Zhao-Maietta-Chang (ZMC) model [257], which provides an analytical formulation describing the transition between elastic and plastic asperity deformations. Additionally, the Kogut-Etsion (KE) [266,267] and the Jackson-Green (JG) models [268,269] utilise

finite element analysis to develop elastoplastic models for individual asperities and subsequently extend them to an ensemble of statistically distributed asperities following the GW framework. As mentioned above, alternative methods based on the Persson's theory [258] can be adopted to obtain an accurate representation of interactions of asperities across the scales, which also overcome some of original GW limitations. Readers are referred to [229,230,232,322,323] for extensive reviews of rough contact modelling approaches applied to stochastically distributed asperities in modelling mixed lubrication regimes.

Most of the statistical and multiscale models outlined above primarily capture the overall influence of local hydrodynamic and asperity contact effects. This compromises the accuracy of resolving localised flow and asperity contact interactions, vital for evaluating lubrication breakdown and surface failures in complex engineering topographies. Nevertheless, statistical and multiscale models offer a computationally efficient and time-effective framework for analysing lubricated rough surfaces.

4.2. Deterministic modelling

Although averaging and homogenisation methods can effectively capture the influence of surface topography on the macroscopic behaviour of rough lubricated surfaces by predicting the average hydrodynamic and asperity contact pressure distributions, they often fail to provide detailed insights into local variations in critical quantities. These include high localised fluid and contact pressures, stress fields, minimum film thickness and flash temperatures, which are vital for predicting and precluding lubrication breakdown and failure mechanisms. In recent decades, advancements in computational power and numerical techniques have enabled the development of deterministic methods for modelling mixed lubrication problems. These methods incorporate a full-scale representation of the microscopic geometry of surface topography into the governing equations, therefore offering a detailed analysis of lubrication and microcontact phenomena by simultaneously solving the hydrodynamic and asperity contact problems within a unified framework. However, this modelling approach demands significantly higher computational effort due to the fine mesh resolution needed to represent microscale features accurately.

It is important to note that averaging or homogenisation models rely on separate deterministic models to compute the flow factors or homogenisation coefficients for specific surface topographies. Therefore, deterministic mixed lubrication models are essential for accurate mixed lubrication analysis. They provide a detailed understanding of the microscopic interactions and flow characteristics that averaging or homogenisation models alone cannot capture. This underscores the critical role of deterministic models in improving the accuracy and reliability of mixed lubrication performance predictions in engineering applications.

4.2.1. Full deterministic Mixed lubrication modelling

Prior to the rapid advancements in computational power, early deterministic solutions primarily focused on steady-state conditions, addressing artificially generated surface irregularities such as dimples, semicircular bumps and sinusoidal waviness [324–328]. These methods were later expanded to include analyses of measured surface topographies [329,330]. Jiang et al. [289] introduced a pioneering deterministic transient mixed lubrication model for point contact applied with actual engineering surfaces. Their approach employed a partitioned solution strategy in which hydrodynamic and asperity contact pressures were calculated separately and updated in a sequential iterative process. The Reynolds equation governing fluid pressure was solved using a multigrid method, while an FFT-based procedure was used to evaluate asperity contact pressures in contact areas [158]. Building upon this work, Hu and Zhu [286–288] developed a fully coupled unified framework that improved convergence and stability by simultaneously solving lubricated and asperity contact regions within a single system of equations. This unified model enabled the simulation of the transitions from full-film and mixed lubrication to boundary lubrication and dry contact under various roughness patterns and operating parameters. Fig. 6B illustrates the results obtained using this framework for a circular contact, distinguishing between hydrodynamically lubricated and asperity contact areas. Subsequent extensions of Hu and Zhu's model incorporated additional phenomena, such as thermal effects, elastoplasticity, inter-asperity cavitation and starvation [67]. Moreover, numerical and computational enhancements, including discrete convolution and FFT (DC-FFT) [142], differential strategy [331] and progressive mesh densification techniques [332], further improved the model's efficiency and accuracy. While initial concerns were raised regarding the numerical implementation and accuracy of the unified framework, these issues were adequately addressed, reinforcing its robustness and applicability in mixed lubrication analysis [225].

Deterministic mixed lubrication simulations have also been used to investigate the hydrodynamic pressure generation between parallel rough surfaces, a phenomenon not fully explained by classical lubrication theory based on the Reynolds equation but observed experimentally for many years. Inspired by Li and Chen's [292,293] scaling-based methodology for efficiently incorporating deterministic simulation results into full-cycle engine simulations of piston ring–cylinder liner conjunctions, Profito et al. [295] developed a deterministic mixed lubrication model for Twin Land Oil Control Rings (TLOCRs). This model is based on quasi-static simultaneous solutions of the microscale hydrodynamic and asperity contact problems, accounting for inter-asperity cavitation using mass-conserving models. The outer lands of the TLOCR were assumed flat and sliding parallel to measured cylinder liner surfaces, both before and after wear. The model predicted significant hydrodynamic load capacity due to fluid pressure build-up around asperities and honing grooves. Results indicated that, under mixed lubrication conditions, worn surfaces generated higher average hydrodynamic load capacity and reduced asperity contact compared to unworn surfaces. This was attributed to the smoothing of plateau regions and reduced asperity curvature from wear, which facilitated lubricant flow across the surface.

More recently, Brunetière and Francisco [296] utilised a mixed lubrication model based on an asperity-based contact model for investigating the hydrodynamic pressure build-up between parallel rough surfaces in mechanical seals. They identified the transverse pumping mechanism as the source of the fluid pressure build-up, resulting from the combined effect of local lateral lubricant flow induced by surface roughness, which must be counterbalanced by additional pressure flows to maintain mass flow conservation of the lubricant at the interface. Their study underscores the critical role of surface roughness in influencing lubricant flow and pressure generation in mechanical seals.

Wang et al. [333] later developed a deterministic model for parallel rough surfaces, building on Hu and Zhu's unified approach, which incorporated effects not considered in Brunetière and Francisco's model. Their model incorporated the asperity interactions and the influence of fluid pressure on asperity deformation (micro-EHL effect). The study demonstrated that the micro-EHL effect at the roughness scale is a crucial mechanism influencing fluid pressure build-up between parallel rough surfaces. This development highlights the importance of considering the interaction between asperities and fluid pressures to model and understand lubrication phenomena at the roughness scale accurately.

Furthermore, Geng et al. [298] proposed a deterministic mixed lubrication framework incorporating a mass-conserving cavitation model for simulating rough, parallel surfaces. The model employs a trained neural network for predicting contact pressure solutions and a modified form of Archard's equation for capturing the wear evolution of surfaces operating under running-in conditions. The model's accuracy was validated against experimental results for various wear conditions, while the contact pressure predictions showcased the robustness of the trained neural network. The study also highlighted the importance of considering the elastic deformation of rough surfaces when modelling heavily loaded contacts using computationally efficient algorithms.

4.2.2. Deterministic asperity contact modelling

While deterministically coupled models enable detailed simulations of boundary and mixed lubrication regimes, the development of *ad-hoc* algorithms for complex contact mechanics problems provides the flexibility to integrate different models for hydrodynamic and asperity contact calculations using robust numerical schemes. Such an approach can leverage the strengths of both statistical and deterministic methods, offering a more comprehensive understanding of tribological phenomena. Deterministic simulations facilitate the assessment of localised effects associated with microscopic surface features, while statistical and multiscale models capture the macroscopic influence of surface roughness on lubrication behaviour. An example is the interactive deterministic-statistical modelling approach [334–336], which combines macroscale average lubrication analysis with microscale deterministic asperity contact simulations. Due to this scale integration, it is often referred to as the macro-micro approach [67]. The following provides a flavour of key deterministic approaches used in modelling the contact mechanics of rough surfaces and their applications in tribosystem studies.

Deterministic solutions based on the half-space theory can be adopted to evaluate rough surface displacements and stresses under traction forces. Assuming small deformations and large contact radii relative to contact size, the half-space theory [40] utilises influence functions to model displacement as a convolution of traction and corresponding influence functions (or Green's functions) [337]. Classical pressure-displacement relations include the Boussinesq-Cerruti [135] and Flamant solutions [136] for plane stress/strain conditions, while other models such as the Tripp [338] and Westergaard [339] solutions tackle periodic continuum problems. Advances in computational performances have catalysed the development of a plethora of numerical methods that efficiently handle such convolutions. In addition to Francis' [282], Lai and Cheng's [340] as well as Webster and Sayles' [341] models, Ren and Lee [150,256] proposed a moving grid method (MGM) that reduces memory usage by exploiting grid uniformity and symmetry. Brandt and Lubrecht [284] introduced the multi-level multi-integration (MLMI) method for simulating realistic rough surfaces while lowering the computational complexity from $\mathcal{O}(N^2)$ down to $\mathcal{O}(N\ln N)$ by leveraging kernel decay, where N denotes the number of computational mesh points. Tian and Bhushan [285] proposed the conjugate gradient method (CGM) for simulating rough surface contacts using quadratic programming, and was later enhanced by Fast Fourier Transform (FFT) methods such as those proposed by Nogi and Kato [151] in addition to Polonsky and Keer [152]. FFT-based algorithms have since gained popularity in tribology for efficiently solving convolution integrals by transforming the equations from the spatial to the frequency domain [67]. Furthermore, Liu et al. [154] addressed the FFT periodicity errors with the Discrete Convolution and Fast Fourier Transform (DC-FFT) method by zero-padding of the domain in order to avoid periodicity artifacts. Wang et al. [142] deduced in a comparative study that the DC-FFT method is approximately five times faster than the MLMI technique and much faster than the DS method for evaluating surface elastic deformation. The readers are referred to [67,155,158] for further details on FFT-based algorithms for analysing tribological interactions.

The boundary element method (BEM) [342,343], which transforms governing differential equations into boundary integral equations over the surface or boundary of a domain, significantly improves the computational efficiency of contact problems as displacement and stress approximations are limited to the boundaries of the domain rather than the bulk of the contacting bodies. The application of BEM in studying contact problems was outlined by Anderson et al. [281] for assessing smooth contacting bodies and was later followed by numerous investigations which focused on the contact of rough surfaces [337,343,344]. Putignano et al. [294] developed a BEM-based numerical model based on a non-uniform adaptive meshing scheme for evaluating the elastic contact solution between rough surfaces, whereby mesh refinement was carried out in regions characterised by high magnitudes of stress and strain gradients for enhancing the computational efficiency and accuracy. The developed model was subsequently employed to investigate the influence of roughness properties on contacting behaviour. A linear relationship was observed between the real contact area and pressure for low squeezing pressures, with a proportionality coefficient of "2" falling between the predictions of Persson's and BGT models [345]. These linear relationships were lost when asperities with large curvatures were brought into contact under high loads. The authors also demonstrated that, while the ratio of true contact area to dimensionless pressure varied for different Hurst exponents, the RMS gradient, and not the Hurst exponent, influenced the proportionality coefficient. In a later study [346], a similar effect for the cut-off wavelength was obtained, *i.e.* the influence of the cut-off wave-vector on the contact area ratio was indeed through the RMS gradient. Moreover, the same conclusion was held true in the non-linear range of contact area evolution. The authors suggested that discrepancies in other studies [347,348] could stem from insufficient mesh refinement at the contact boundaries or an inadequate number of mesh points per contact area (in uniform grids), therefore raising questions regarding the convergence of the solutions in those cases. The readers are referred to [25,231,337] for an extensive review of BEM and its utilisation for tackling contact mechanics problems.

The geometric flexibility offered by the finite element method (FEM) [349–352] has catapulted its implementation for examining contact problems, whereby materials constitutive behaviour can be described using infinitesimal or finite strain formulations. In FEM, an explicit relation between the strain and the stress can be prescribed, either within infinitesimal or finite strain formulations, thus allowing for arbitrary constitutive material models to be considered, starting from simple linear elasticity up to complex crystal plasticity. The application of FEM to tribological problems involves the discretisation of the volumes of contacting bodies and an appropriate treatment of their contact interactions [25]. The arbitrariness of material models, as well as the geometries of contacting solids and their heterogeneity that can be attained in the treatment of contact interfaces, makes this method a multipurpose engineering tool. For example, Hyun et al. [347] applied FEM to analyse frictionless, non-adhesive contacts between self-affine fractal surfaces with roughness incorporated down to the discretisation scale. A wide range of parameters, such as the roughness amplitude, the roughness exponent and the Poisson's ratio, were examined, and the average load carried by the rough surfaces was investigated. Furthermore, FEM was also utilised in tackling rough contact problems pertaining to viscoelastic materials. Wriggers and Reinelt [353] proposed a finite element model in which a rough surface was decomposed into a limited number of harmonic functions with different wavelengths and amplitudes. The effects of hysteresis and adhesion were considered, and a fair agreement was obtained compared with experiments. However, the authors were able to capture only a small range of roughness due to the extremely high computational efforts involved. Despite the recognition that the FEM has gained as a result of its diverse application and accuracy in exploring various material behaviours [354], FEM requires significant storage space and suffers from instabilities in the convergence of the iterative solution.

The Green's function molecular dynamics (GFMD) [26,355] is a widely used approach for tackling contact mechanics problems through molecular dynamics. Campañá and Müser [290] proposed the GFMD, replacing a semi-infinite, harmonic solid with a single layer of atom for computational efficiency. By simulating real surfaces and artificially generated surfaces, the results revealed Gaussian-tailed stress distributions for random surfaces and exponential-tailed ones for experimental surfaces [356]. However, the true contact area was largely unaffected by this difference, with a proportionality coefficient (κ) of around 2, lying between Persson's and BGT's models. Almqvist et al. [357] further investigated GFMD, showing that the real contact area was proportional to the squeezing pressure at low loads, while interfacial separation

depended logarithmically on applied force. Three numerical methods, namely BEM, GFMD and smart-block classical MD, were employed in the study. Despite the good agreement that was achieved in comparison with Persson's prediction for high loads, the rather small size system used in the computations yielded *finite size effect* for large separations. This was also investigated by Pastewka et al. [358] using GFMD to study contact stiffness, finding it linear with squeezing pressure over a large range of loading conditions, contrary to the power law trend presented by Pohrt and Popov [359]. Furthermore, Prodanov et al. [360] systematically studied the influence of thermodynamic, fractal and continuum corrections on the relative contact area and mean gap using GFMD, finding the continuum and fractal corrections to be most significant vis-à-vis the contact area. To achieve convergence in the solution, fine discretisation and a smaller wavelength range were required for small and large Hurst exponents, respectively. Nonetheless, finite size and discretisation had minimal effects for large Hurst exponents and low pressure, while systems characterised by small Hurst exponents required much finer grids under high pressure. In addition, the authors suggested incorporating the RMS gradient into the dimensionless pressure representation, a practice that was adopted in other studies [361,362].

Recently, an interesting multi-scale coupling method has been proposed by Bonari and co-workers [363,364], which integrates the FEM at the macroscale and the BEM at the microscale to accurately solve contact mechanics problems. This approach leverages FEM for modelling the overall macroscopic geometry while using BEM for incorporating the mechanical response governed by rough surfaces at the microscopic scale. This procedure overcomes the classical limitations of applying FEM and BEM separately while allowing alternative macroscale contact mechanics formulations to be as well invoked, *e.g.* mortar methods.

4.3. Interfacial boundary slippage

One of the key assumptions underlying the Generalised Equations of the Mechanics of Viscous Thin Films (*i.e.* Reynolds equation) [30] is the well-known no-slip boundary condition, which assumes that the wall and the adhering fluid are both travelling at the same velocity. In other words, the fluid layer is stationary relative to the surface motion. Although being a universally accepted approximation for modelling macroscopic engineering problems, there exist circumstances in which the no-slip condition may portray implausible interpretations of the microscopic lubricant behaviour. Intermolecular forces, such as van der Waals, electrostatic and steric interactions, can significantly influence fluid dynamics at the microscale, particularly in lubrication regimes where molecular-level effects become pronounced. These factors can alter the lubricant film thickness, the boundary slip behaviour and the stability of thin lubricant layers, notably in the presence of flexible or deformable interfaces. Although a detailed discussion of these effects is beyond the scope of this review, they are recognised as important factors in the lubrication modelling of confined systems. For example, numerous experimental [365–368] and theoretical [56,57,369] studies have highlighted the inherent limitations of the no-slip condition for predicting the overall lubrication system behaviour, especially for hydro (oleo)phobic surfaces [370]. In such scenarios, intermolecular forces reduce fluid-wall adhesion, thus enhancing boundary slippage and altering the effective viscosity near the solid interfaces. Their impact is further influenced by surface texture [371], liquid molecule polarity [372], wettability [373] and contact angle [374]. Furthermore, these forces can contribute to interface deformation in flexible and soft interfaces, influencing load-carrying capacity and tribological performances. While these effects may be negligible in some macroscopic lubrication models, their role in micro- and nano-scale lubrication is critical and warrants considerations in specific applications.

Increasing attention has been devoted towards addressing the impacts of interfacial slippage effects on tribosystem performances through robust and universal algorithms. An example is the Navier slip length model [375–377], which assumes a linear relationship between the slip velocity of the fluid layer adjacent to the surface and the tangential shear rate, expressed as:

$$v_i = -\lambda\sigma, \tag{21}$$

where $\sigma = \eta(\partial v/\partial z)$ is the surface shear stress and $\lambda = b/\eta$, with b being the Navier slip length coefficient. This coefficient indicates a hypothetical distance below the fluid-solid interface at which the no-slip condition holds. Despite advances in refining the slip length relationship [378,379], the Navier model lacks a predictive framework for the slip length based on system parameters [380] and assumes slippage occurs in an unpredictive manner [381].

Alternatively, the Tresca slip model [382,383] (or critical shear stress model), akin to the critical shear stress model in solid mechanics [384], entails the initiation of interfacial slip only when the surface shear stress σ reaches a critical value σ_{max} [385]. Hence, this restricts the materialisation of slippage throughout the domain, as opposed to the aforementioned Navier slip condition. The Tresca model is mathematically expressed as [385]:

$$\begin{cases} |\sigma| < \sigma_{max} \rightarrow & v = 0 \quad \text{(no slip occurs)}, \\ |\sigma| = \sigma_{max} \rightarrow & v = -\lambda\sigma \quad \text{(slip occurs)}, \end{cases} \tag{22}$$

with $\lambda \geq 0$. To overcome the drawbacks of the Navier slip model, Spikes and Granick [386] proposed the double parameter slip (DPS) model by incorporating the critical shear stress criterion into the Navier slip model. This was later applied in [387] for analysing one-dimensional bearings using a mass-conserving cavitation model. The DPS model defines interfacial velocity as follows [385]:

$$\begin{cases} |\sigma| < \sigma_{max} & \rightarrow \quad v = 0, \\ \sigma \geq \sigma_{max} & \rightarrow \quad v = -\lambda(\sigma - \sigma_{max}), \\ \sigma \leq -\sigma_{max} & \rightarrow \quad v = -\lambda(\sigma + \sigma_{max}). \end{cases} \tag{23}$$

5. Learning from the smaller Scales

Since the introduction of the hard-sphere model for liquid dynamics [388,389], and with advancements in computational resources, molecular simulations have been instrumental in revealing the nanoscale physiochemical mechanisms driving processes across various scientific disciplines. These simulations play a vital role in modelling tribosystems, enabling the assessment of transport-related physical quantities that impact both macroscopic and microscopic interfacial behaviours. Two foundational techniques in molecular simulations are the Monte Carlo (MC) [390] and Molecular Dynamics (MD) [42] methods, employing statistical and deterministic modelling approaches, respectively. However, MD is widely employed for simulating tribological interactions induced by fluid flow behaviour [42,391]. MD simulations solve atomic trajectories by applying Newton's equations of motion to atom ensembles over a series of short time steps using finite difference methods [391], thus providing critical dynamic information such as molecular positions, velocities, and accelerations. The accuracy of MD simulations heavily depends on the force fields [392], which define the intermolecular and intramolecular interactions between atoms, as well as the thermostat method [393], which regulates heat dissipation near contact interfaces during shear processes [59]. This section explores how MD simulations can be leveraged to enhance the precision of continuum lubrication models by incorporating data from smaller spatio-temporal scales. Additionally, it highlights how MD can address continuum breakdown at the atomic level to revamp the macro- and micro-scale modelling of lubricated contacts. The readers are referred to [42,59,394–396] for further insights into MD simulations and their applications.

5.1. From molecular outputs to continuum inputs

Predicting lubricant behaviour under extreme conditions, such as those in EHL regimes, remains a contentious challenge in tribology. While continuum models offer powerful computational tools for simulating the frictional behaviour in tribological contacts, they are constrained by assumptions related to lubricant rheology and flow boundary conditions. The difficulty in validating these assumptions arises from the extreme pressure and shear rate conditions within lubricated contacts, or "*buried interfaces*", which are difficult to investigate experimentally. Over the past decade, MD simulations have become increasingly valuable for elucidating the atomistic and molecular mechanisms at play under such severe conditions, providing essential insights for scaling up to larger models. Recent MD simulations have demonstrated strong quantitative agreement with experimental friction and viscosity measurements, highlighting their potential to inform and complement macroscale models, either on their own or through multiscale coupling approaches [46,391,397]. This capability is particularly valuable for conditions relevant to machine components, where replicating the exact contact conditions in experiments is often infeasible due to uncontrollable factors such as shear heating and interfacial slip.

Expanding on the precise modelling of lubricant rheological behaviour, MD simulations have recently offered key insights into the relationships between applied pressure, shear rates, and lubricant responses, encompassing both the fluid's structural and phase behaviour as well as its interactions with surfaces. These findings have also been closely tied to relevant molecular structures. Precise viscosity measurements under high-pressure conditions are essential for predicting macroscale phenomena, EHL film thickness and friction [188,197,398]. In the inlet region, where pressures range from 10 to 100 MPa, viscosity is a key determinant of film thickness, whereas viscous effects govern EHL friction in the contact centre, where pressures exceed 1 GPa. Advances in computational power, the development of highly parallelized simulation software and improvements in force field accuracy have positioned non-equilibrium molecular dynamics (NEMD) simulations as powerful tools for predicting the high-pressure viscosity of lubricant molecules [391]. Over the past two decades, bulk NEMD simulations have been extensively employed to study fluids operating under high pressure and shear conditions. For instance, McCabe et al. [399] and Liu et al. [400] used NEMD simulations to examine the pressure-dependent viscosity of 9-octylheptadecane and 1-decene trimer. While the Newtonian viscosity was underestimated due to the united atoms (UA) force fields, the pressure-viscosity coefficient (α) showed strong agreement with experimental data. The accuracy of any MD simulation is highly contingent on the force field applied, making the selection and rigorous testing of force fields critical prior to conducting production simulations [401]. Predicting viscosity index (VI) and α values for new molecules is a valuable application of NEMD, as these properties are crucial for enhancing EHL performances [402].

Non-equilibrium molecular dynamics simulations have also been employed to examine the validity of the Eyring [403] and Carreau [404] shear thinning models, both of which are frequently applied in EHL predictions. Bair and colleagues [405] compared NEMD simulations with the high-pressure viscosity of a molecular lubricant (squalane) obtained from a rheometer. Although the experimental and simulation data spanned several orders of magnitude in shear rate, they converged onto a single time-temperature superposition master curve, which was successfully fitted using the power-law Carreau model [404]. Similarly, Liu and co-workers [400] utilised the Carreau model to describe the shear thinning behaviour of squalane and various poly-alpha-olefin (PAO) molecules, correlating shear thinning with molecular conformational changes, quantified through the radius of gyration. Recent bulk NEMD simulations by Jadhao and Robbins [406] revealed that the Carreau model more accurately describes viscosity-shear rate behaviour at lower pressures, whereas the Eyring model offers a better fit at higher pressures. Furthermore, the "*incremental viscosity*" described by the Eyring model, measured for Lennard-Jones fluids using a 'shear-kick' NEMD method, has been identified as a special case of the Carreau model [407].

A key assumption in bulk NEMD simulations is that the fluid develops a linear velocity profile between sliding surfaces. However, deviations from this Couette flow behaviour often occur under nanoconfinement, where phase transitions such as vitrification or crystallization, along with significant viscosity increases, can cause shear to localise at the confining surfaces or within the fluid itself [408]. Robbins and Smith [409] suggested that high pressures may trigger phase transitions similar to those observed in relatively thicker EHL films ($\approx$ 100 nm) [188]. For more than half a century, nonlinear flow has been invoked to explain experimental findings on EHL regimes [410,411], though direct experimental evidence has been elusive for realistic lubricants. Confined NEMD simulations, however, have captured this behaviour with increasing complexity. Comprehensive NEMD studies of atomic fluids under EHL conditions have revealed a transition from Couette flow to various forms of shear localisation with rising pressures [412–414]. These include central localisation (CL), where the outer regions of the fluid move with the confining surfaces while the central region undergoes shear, and plug slip (PS), where the outer layers shear and the central region remains unsheared. More recently, NEMD simulations of molecular systems have demonstrated similar behaviours [415–417].

The EHL friction coefficients obtained from these NEMD simulations closely aligned with extrapolations at lower shear rates [415,417], as illustrated in Fig. 3.3 from [59]. This figure illustrates the variation in friction with logarithmic shear rate for two molecular fluids: 2,6,10,15,19,23-hexamethyl-tetracosane (squalane) and 2,3-dimethyl-2-[(3-methylbicyclo[2.2.1]hept-2-yl)methyl]bicyclo[2.2.1]heptane (DM2H). Squalane, which is a linear C_{24} alkane with six methyl branches, is frequently used as a model lubricant designed to minimise friction, whereas DM2H is a rigid bicyclic molecule engineered to produce high friction, particularly in traction drives [418]. In Fig. 3.3a-i, the friction coefficient of squalane rises logarithmically with shear rate and also increases with pressure [415], a behaviour commonly seen in both experimental studies and NEMD simulations under EHL conditions [188]. Notably, the slope of the friction coefficient with logarithmic shear rate decreases as pressure increases, similar to observations in NEMD simulations of binary atomic Lennard-Jones fluids [413]. At very high shear rates, the friction coefficient of squalane at 0.5 GPa surpasses that at 2.0 GPa, a phenomenon also reported in studies on Lennard-Jones fluids [414].

Molecular dynamics and non-equilibrium molecular dynamics simulations have been instrumental not only in understanding fluid properties but also in elucidating the behaviour of solid materials under extreme conditions [8,25,41,419,420]. This is particularly important for tribological systems, where a deep understanding of wear, surface deformation and fluid-solid interface interactions is crucial for addressing lubrication challenges. These simulations bridge the gap between atomic-scale mechanisms and macroscopic tribosystem performances by providing vital insights into the mechanical response of the contacting surfaces, such as elasticity, hardness and adhesion, mainly due to applied stresses, contact pressures and shearing forces. For example, Pastewka and Robbins [421] highlighted the importance of atomic-scale roughness effects in analysing friction and adhesion, thus influencing the macroscopic contact behaviour of heavily loaded contacts. Furthermore, various studies such as those conducted by Mo et al. [422], Aghababaei et al. [423], Eder and co-workers [424,425] and Sha et al. [426] have provided key fundamental understanding of how nanoscale friction, adhesive wear mechanisms and hardness properties at the atomic scale influence friction and wear. These insights are invaluable for improving the performance and durability of materials in lubrication systems, where atomic interactions play a pivotal role.

The study of phase transformations in materials under lubrication conditions [46,413,415,427] has been pivotal to understanding how atomic-level changes impact the performances of lubrication systems. Molecular dynamics, in particular, have provided valuable insights into how stresses, temperature fluctuations, and contact pressures influence material properties and lubrication efficiency under high-pressure and high-shear environments. For example, Vandenhaute et al. [428] employed large-scale MD simulations to investigate phase transitions in metal-organic frameworks (MOFs) under mechanical stress, revealing that structural phase changes in confined systems like porous materials significantly impact their tribological performance and durability under cyclic loading. Additionally, MD simulations have demonstrated the critical role of temperature-induced phase transitions in lubricants, such as in phase change materials (PCMs) [427] like paraffin waxes, which undergo solid-liquid transitions as they absorb or release heat, and can accordingly help regulate temperature but can also influence lubricant performances under high temperatures. Furthermore, MD simulations are also advancing nanotribology, aiding in the development of next-generation lubricants that offer greater durability, reduced wear and improved energy efficiency [429,430]. Berman et al. [431] used MD simulations to show that graphene nanoscrolls, when paired with diamond-like carbon, achieved macroscale superlubricity by forming incommensurate contact. Similarly, Li et al. [432] explored cooperative lubrication in graphene-water systems, showing that graphene helps relieve lateral stress while enhancing the rolling behaviour of water molecules, leading to improved lubrication performances. These studies underscore the indispensable role of atomic-scale simulations in understanding phase transformations and their effects on tribological properties, thus driving innovations in lubricant design and enhanced mechanical performance.

Incorporating atomic-scale insights from MD and NEMD simulations into continuum-based models enhances the predictive accuracy of lubrication performances, particularly in systems governed by interfacial behaviour, such as in thin film or boundary lubrication regimes. These simulations reveal detailed atomic-level interactions, such as fluid structuring, layering and slip behaviour, which are difficult to capture relying solely on continuum methods [59,433]. For example, Thompson and Robbins [408] employed MD models to examine the slip behaviour and fluid dynamics at the fluid-solid interface under shear, revealing how slip length can vary with shear rate and interaction strength, thus providing critical data for refining high-pressure lubrication models. Additionally, Wang et al. [434] investigated the impact of surface wettability and roughness on lubrication performance through MD simulations, demonstrating the influence of fluid layering and interfacial slip behaviour on frictional forces. More recently, Zheng et al. [435] explored the merits of nanoparticle lubricant additives in improving surface separation and promoting friction reduction through the interactions that transpire between the nanoparticles, lubricant film and contacting surfaces.

5.2. *Capturing chemical and physical phenomena via first-principle and MD models*

Deploying first-principle methods in conjunction with MD simulations provides a highly detailed perspective on the chemical and physical mechanisms underpinning lubrication performances. First-principle approaches rooted in quantum mechanics [436,437], such as density functional theory (DFT), offer comprehensive insights into the electronic structures and chemical interactions occurring between lubricant molecules and surfaces, which are crucial for predicting material behaviour under a range of operational conditions. By complementing these methods, MD simulations capture the dynamic behaviour of molecules over time, thus allowing for real-time observations of key tribological phenomena, such as friction, wear and lubrication performances at the molecular level. Integrating these two approaches–DFT for precise chemical bonding analysis and MD for modelling physical dynamics–facilitates bridging the gap between atomic-scale interactions and macroscopic tribological outcomes. In addition to advancing our understanding of tribological interactions, such consolidation plays a pivotal role in guiding the development of next-generation lubricants with optimised performances tailored to specific operational demands.

Integrating first-principle methods (*e.g.* DFT) with MD simulations provides a powerful framework for understanding the adsorption and dissociation of lubricant additives on solid surfaces. For example, Loehlé and Righi [438] used DFT calculations to investigate the tribochemistry of organophosphorus additives, revealing how the formation of iron phosphide tribofilms can significantly reduce friction and enhance wear protection. Moreover, the complementary role of MD models in explicating the dynamic behaviour of additives was explored by Hu et al. [439] in examining the role of nanoparticles in improving the load-carrying capacity of lubricant through the formation of protective layers on surfaces, ergo extending the lifespan of lubricated components.

Another arena where first-principle methods and MD simulations excel is providing a detailed understanding of the tensile forces acting on molecular bonds under compression and shear in lubrication systems. DFT offers a quantum-level perspective on the behaviour of molecular bonds by leveraging the precise electron distribution, especially in additives like zinc dialkyldithiophosphate (ZDDP) [440,441]. Zhang et al. [442] explored the significance of electron migration mechanisms on bismuthyl bromide (BiOBr) surfaces, demonstrating through DFT modelling how this affects the material's photocatalytic efficiency and the generation of reactive species like hydroxyl radicals. In addition, the study revealed how effective electron migration towards oxygen molecules can result in more electrons being diffused into electron-rich sites *via* electron density differences. On the other hand, MD simulations elucidate the mechanical behaviour of molecules under dynamic conditions like shear and compression. For example, Wei et al. [443] applied MD simulations in studying the impact of grain boundary defects on the tribological properties of molybdenum disulfide (MoS_2) during scratching processes. Their findings revealed that the combined pushing and interlocking actions between the diamond tip and MoS_2 atoms result in a lower critical breaking load for grain boundary defect-containing MoS_2 compared to the indentation process. This combination of DFT for electron dynamics and MD for mechanical behaviour offers a deep multiscale understanding of how additives and materials perform under extreme lubrication conditions, bridging the gap between atomic-scale phenomena and macroscopic tribological performance.

6. Spatiotemporal data extraction

Thus far, it is clear that a wide range of physicochemical interactions across multiple spatiotemporal scales shapes the intricate and hierarchical nature of lubrication problems. As previously noted, the relatively low computational cost and high efficiency of continuum models hinge on the constitutive laws governing fluid behaviour and the boundary conditions representing the physical constraints of lubrication systems. Conversely, atomistic modelling faces challenges despite its capacity to capture detailed atomic configurations and molecular trajectories due to its high computational demands and limitations in accessible time and length scales. Multiscale modelling, particularly in the context of lubricated interfaces, addresses these challenges by bridging multiple single-scale models to unify the characterisation of phenomena spanning vast length- and time scales. However, developing and deploying multiscale and multiphysics models remains complex, requiring interdisciplinary expertise and a deep understanding of key factors, such as the identification of relevant spatiotemporal scales, the selection of appropriate sub-models for each scale and the integration of these sub-models into a coherent multiscale framework [444]. At the heart of this integration is the implementation of robust coupling methods that could facilitate the exchange of information across multiple scales. These multiscale models can be broadly categorised into concurrent or hierarchical schemes, each offering distinct strategies for addressing the

multiscale response of lubrication systems.

Domain decomposition is a widely used concurrent molecular-continuum coupling technique [445–447], particularly effective in solving multiphysics problems across large computational domains [448–451]. This method partitions the global domain into multiple sub-domains [452], where discrete molecular-scale and continuum-scale problems are solved simultaneously. The communication between these sub-domains occurs through the exchange of information *via* an overlap or "*defect*" region, which acts as a communication layer for ensuring the on-the-fly data exchange. In fluid dynamics, for instance, the defect region serves as an interface between flow regimes where continuum assumptions break down, such as at the solid-liquid or liquid-vapour interfaces, or a moving shock wave between fast and slow moving fluid [59]. Although advancements have enabled domain decomposition to overcome the challenges related to inaccessible scales, its application at smaller scales often requires short time steps [46]. Achieving robust coupling between MD and CFD sub-solvers is particularly challenging as it entails balancing the behaviour of continuum region with the accurate evolution of the interfaces [453]. Therefore, selecting the appropriate boundary conditions, averaging methods, constraint algorithms, domain termination and particle insertion is critical for developing accurate concurrently coupled models [454]. Readers can refer to [447,455–457] for an in-depth overview of the application of domain decomposition and the associated challenges and remedies.

Unlike domain decomposition, hierarchical (or sequential) coupling methods offer an alternative approach in multiscale modelling by eliminating the need for directly coupling solvers or overlapping various sub-domains. Instead, hierarchical coupling relies on the sequential simulation of molecular and continuum models [458], whereby molecular-scale information, critical for describing physiochemical properties, is firstly evaluated "*offline*" and subsequently integrated into continuum models that portray component-scale phenomena. For example, complex boundary conditions, such as slip conditions, can be derived and utilised in continuum-based models (*e.g.* Reynolds equation) by parameterising macroscopic models using microscopic data [55,455]. Another approach based on the sequential coupling technique is embedded (or heterogeneous) coupling, whereby the macroscopic solver operates over the entire simulation domain, while microscopic solvers are strategically employed in specific regions to provide local enhancements where more detail is required. This overcomes the limitations of parameterisation, especially for vast parameter spaces or in scenarios where tabulating data is impractical [59,455]. While hierarchical multiscale simulations offer computational efficiency by embedding fine-scale models within coarse-scale frameworks, they may still encounter information loss when transferring data between scales [459]. Readers are encouraged to consult comprehensive reviews such as [455,457] for detailed information on hierarchical coupling methods.

7. Application of machine learning in lubrication

The yearning desire for powerful and cost-efficient computational tools, driven by the exponential rise in data, has accelerated the development of novel techniques broadly encapsulated under the term "*artificial intelligence*". These tools process vast amounts of data by leveraging computational and experimental (stochastic) frameworks [460]. Analogous to data mining and data binning techniques, machine learning (ML) algorithms identify and exploit low-dimensional feature spaces within large datasets to predict, classify and extract valuable, interpretable information [208,461], whereby their integration has been transformative across a wide range of scientific disciplines [62,462–467]. The training process of ML models can be categorised into supervised learning [468], unsupervised learning [469], semi-supervised learning [470] and reinforcement learning [471]. The readers are referred to [472,473] for an in-depth analysis of the aforementioned learning techniques. In the field of lubrication modelling, ML techniques have emerged as critical tools for analysing, predicting and optimising tribosystem performance, facilitating the development of more efficient and cost-effective lubricant formulations and surface materials [63–65].

Synonymous with how biological neurons function in the human brain [474,475], Artificial Neural Networks (ANNs) [476] are a class of deep learning algorithms consisting of interconnected nodes (hidden layers) that process and relay input signals through weighted connections. These weights are adjusted to minimise prediction errors and enhance model accuracy. The predictive power of ANN models, particularly in tribological applications [477,478], is governed by the underlying data analysis and network architecture, which can be refined using specialised training algorithms [479,480]. A recent advancement in the field is the introduction of Physics-Informed Neural Networks (PINNs) [481–483], which have garnered significant attention for embedding physics-based conservation laws directly into neural networks. Unlike traditional discretisation methods, PINNs can solve complex nonlinear partial differential equations (PDEs) by utilising automatic differentiation [484], enabling accurate computation of derivative terms essential for engineering applications [485–488]. Moreover, PINNs provide a mesh-free approach to solving PDEs by incorporating equations and constraints into the network's loss function, making them particularly useful for problems pertaining to lubrication systems, where conservation laws such as the Reynolds equation are critical [489]. Beyond ANNs and PINNs, a variety of machine learning models have been applied in tribological solutions, such as Convolutional Neural Networks (CNNs) [490], Support Vector Machines (SVMs) [491], and K-Nearest Neighbor (KNN) [492], along with numerous ensemble models [64,65,209]. The integration of machine learning within multiphysics simulations has led to the emergence of "*intelligent models*" that are capable of addressing ill-posed problems and leveraging the underlying physics expressed by partial differential equations, as portrayed in Fig. 8. These intelligent models hold significant promise for advancing the development of more efficient solutions in tribological systems.

Despite the promising advantages of ML models, their uptake in lubrication modelling–especially at the atomistic scale–has been gradual [64,65,494]. This is largely due to the complex physiochemical interactions evolving within contacting interfaces, which traditional regression models may struggle to capture accurately. Furthermore, integrating ML models presents several challenges, mainly involving the need for large-scale, high-quality datasets derived from MD computations and experiments, which are vital for the effective training of ML models, yet can be resource-intensive to generate. Moreover, ensuring the interpretability of ML models is essential, as the "*black-box*" nature of some approaches may hinder their application for diagnosing lubrication failures. Nevertheless, the development of synergies between ML and MD provides major prospects for advancing tribosystem modelling, such as evaluating MD trajectories [495], accelerating DFT calculations [496] and improving force-field computations [464], and ultimately building extensive databases for wear predictions [497], as well as enhancing nonlinear phenomena for creating scale-bridging frameworks [496,498,499]. Hybrid models that integrate data-driven ML approaches along with physics-based models can blend the predictive capabilities of ML with the reliability of fundamental physics, such as conservation laws and thermodynamic constraints, substantially revamping the interpretability of ML projections.

Furthermore, interdisciplinary collaborations can play a key role in realising the full potential of ML in tribological applications. The effective integration of such tools into atomistic-scale simulations through collaborative efforts of researchers from tribology, materials science and computer science can accelerate the development and application of the aforementioned "*intelligent models*" to address the lubrication-related challenges linked with wear prediction, lubricant performance and failure mechanism. For instance, ML algorithms can progressively replace the traditional trial-and-error approaches in the

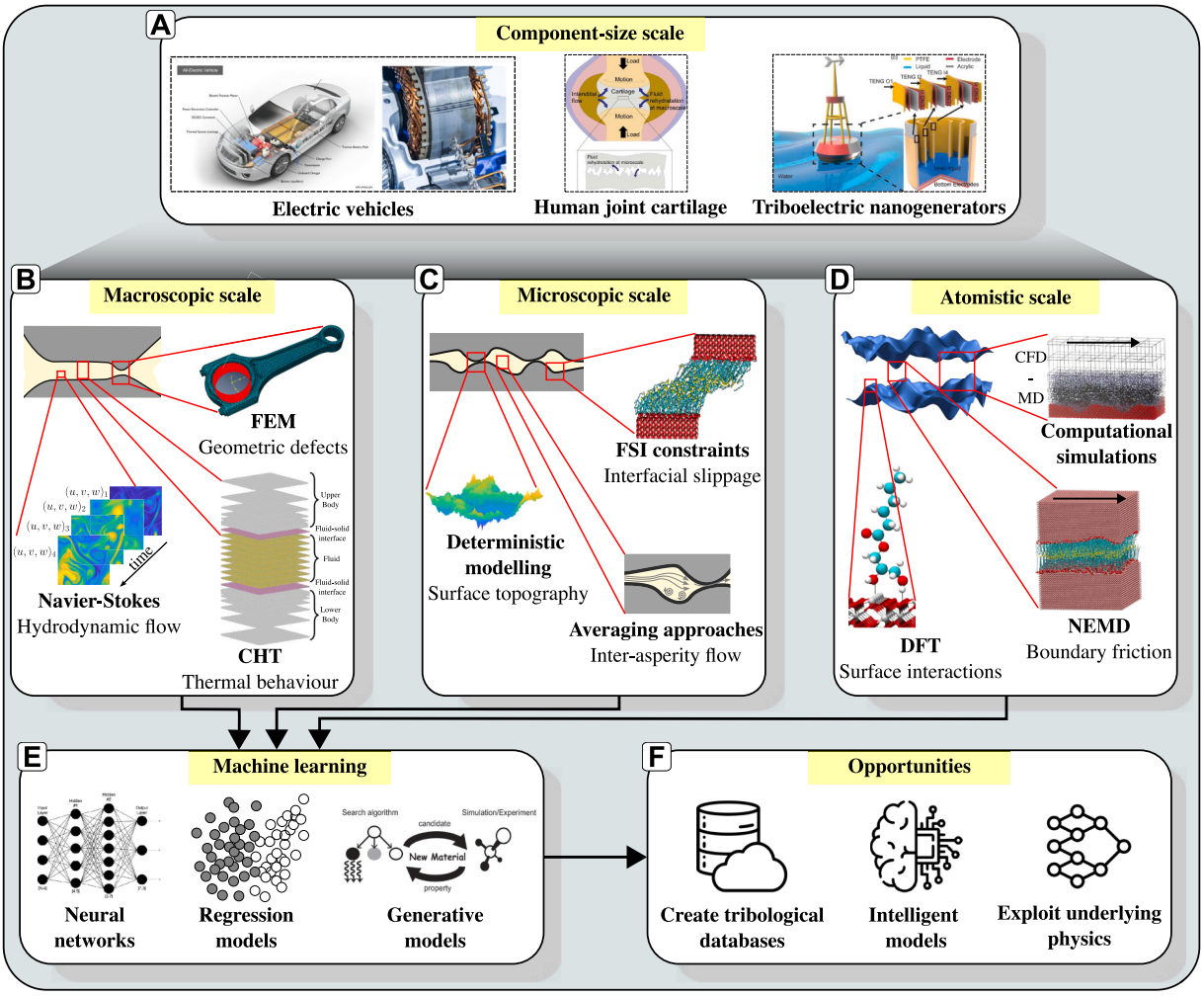

Fig. 8. Multiscale evaluation of tribological system performance using multiphysics approaches and machine learning models. (A) Examples of tribosystems with fluid-solid interactions spanning multiple spatiotemporal scales. (B—D) Schematics illustrate conventional computational techniques used to model tribological interactions at macro,- micro-, and nano-scales, driving the evolution of contact interfaces and overall tribological performance. (E) The integration of machine learning models—such as neural networks, regression and generative models—across these scales; the latter is adapted from Kajita et al. [493] under the terms of the associated CC-BY 4.0 license. (F) Highlights the advantages of incorporating machine learning models, such as developing intelligent surrogate models for bridging spatiotemporal scales, incorporating physics-based models, accelerating traditional computational methods, and creating knowledge databases for enhanced predictive capabilities.

prediction and formation of new combinations of base oils, additives and nanoparticles [62,211,461,500–502]. Kajita et al. [493] autonomously examined a wide range of molecular configurations in lubricant oils by combining MD calculations with Monte Carlo Tree Search (MCTS), a decision-making technique applied in areas such as game theory and artificial intelligence [503,504]. The integration of MCTS with rapid evaluations acquired through MD simulations enables a rigorous assessment of the potential stability and functionality of newly designed molecules, hence facilitating the autonomous discovery of optimal molecular structures and properties as well as extensive molecular design spaces. As a consequence of this interdisciplinary synergy, an iterative feedback loop can be created involving modellers contributing atomistic simulation data while experimentalists validate these predictions through real-world testing. This approach has already yielded advanced lubricants, such as nanoparticle-enhanced and bio-based formulations, that offer enhanced wear resistance, reduced friction and improved sustainability [505–509], ergo driving the development of eco-friendly solutions for lubrication systems.

8. Future perspectives

This paper comprehensively reviews the current state of the art in lubrication modelling across various scales and applications. Based on this assessment, several emerging trends can be identified and summarised below.

Significant progress has been made over the past decades in developing simulation frameworks for modelling the different lubrication regimes. However, a consistent need remains for computationally efficient deterministic mixed lubrication models that incorporate various multiphysics and synergistic microscale phenomena within a unified simulation framework. These phenomena include micro-TEHL, inter-asperity cavitation, thermal effects, wall-slip, tribochemistry and tribofilm kinetics, wear, inhomogeneous and nonlinear material behaviour, triboelectric effects, and percolation, among others. Such a framework would serve multiple purposes: (1) enhancing the understanding of the underlying interfacial multiphysics interactions, (2) calculating homogenisation coefficients for different surface topographies and interfacial conditions, and (3) bridging molecular/atomic and continuum-scale phenomena. Making this framework accessible online would further facilitate collaborations within the tribology community.

The adoption of advanced tribological models as a design tool integrated into standard engineering practice can be achieved by coupling lubrication and contact mechanics simulation frameworks with multiphysics software, such as COMSOL Multiphysics, ANSYS, Abaqus, OpenFOAM, MOOSE, and other commercial and open-source platforms. This integration is essential for accurately accounting for tribological phenomena in complex multibody and multiphysics engineering systems. It enables the assessment of specific design elements (*e.g.* complex geometric features, unusual structural materials, and surface finishes) and more realistic boundary and operational conditions (*e.g.* constraint characteristics, transient and vibrational effects, and intricate heat transfer behaviour) that influence tribosystem performance. Developing fast and stable partitioned coupling techniques is an effective strategy for integrating optimised codes, treating each physical phenomenon separately as a *"black-box"* solver, which is ideal for creating modular coupled schemes.

Furthermore, using multiscale methods should be facilitated through shared platforms and the development of modular packages and libraries. These methods should also be extended to account for the influence of surface roughness and other topographic features at the meso- and macro-scopic scales. For instance, the effects of surface microtextures could be considered in an averaged manner using flow factors or homogenisation coefficients, allowing for the investigation of textured surface performance in large lubricated domains without the need for high mesh resolutions to discretize textures. Homogenisation and other multiscale methods could also be employed to capture the influence of additional microscopic tribological phenomena, such as thermal effects, triboelectricity, and tribofilm evolution, on the macroscopic scale. This methodology would enhance the predictive accuracy of tribosystem models, enabling the design and optimisation of more efficient and reliable engineering systems.

Integrating multiscale modelling with artificial intelligence (AI) methods, such as Physics-Informed Neural Networks (PINNs), is essential for understanding and optimising tribological systems in complex engineering applications. This approach involves the development of simulation frameworks that efficiently couple multiphysics models across different scales, including hybrid strategies that merge molecular dynamics with continuum-scale modelling. These frameworks provide a powerful tool for analysing the influence of atomic, molecular and microscopic interfacial phenomena on macroscopic systems, thereby enhancing predictive accuracy and design optimisation. Moreover, data-driven techniques can play a significant role in developing reduced-order lubrication and contact mechanics models that efficiently incorporate tribological phenomena into the simulation of larger multibody engineering systems. This integration not only reduces computational costs but also supports system performance and reliability optimisation.

Addressing the inherent uncertainties in tribological systems and improving performance predictions requires the application of uncertainty quantification methods and the development of lubrication, contact mechanics and wear models based on governing equations with spatiotemporal stochastic parameters. These models can account for uncertainties in design parameters (*e.g.* gross geometry, clearances, tolerances, surface waviness and roughness), material and lubricant properties (*e.g.* structural compliance, surface hardness, elastic modulus, viscosity and tribofilm behaviour), boundary conditions and operating conditions (*e.g.* applied loads and kinematics). Such models can be particularly relevant for analysing lubricated systems subjected to stochastic excitations, such as the main bearings and gearbox bearings of wind turbines, where the randomness of wind conditions influences loads and kinematics. Furthermore, uncertainty quantification methods and stochastic models can be employed to assess the evolution of tribological performance of engineering systems over time, considering factors such as lubricant degradation and surface wear.

Hybrid modelling approaches offer a promising strategy for improving the accuracy and computational efficiency of tribological simulations. Due to the high accuracy required for predicting surface interactions in modern engineering systems, traditional single-scale computational methods often underperform in capturing the intricate behaviour of rough surfaces without incurring prohibitive computational costs. Hybrid models combine the computational speed of asperity-based models with the detailed accuracy of half-space/BEM and FEM techniques, enabling large-scale simulations of rough surface interactions while capturing complex stress distributions, deformation patterns, and nonlinear material behaviours through localised FEM or reduced-order models. These approaches are particularly advantageous for applications such as wear prediction, mixed lubrication, and rolling/sliding contacts, leading to more accurate and computationally efficient tribological simulations. This hybrid framework provides a promising direction for developing advanced simulation tools that balance computational cost with high precision, fostering innovations in the design and optimisation of engineering components in industries such as automotive and aerospace.

Despite the increasing prominence of simulation tools in modern engineering system design and optimisation, a multidisciplinary approach that integrates various advanced methodologies is essential for addressing the complexities of real-world systems. Combining physics-based models, AI algorithms, and experimental data can create more robust, reliable, and adaptive frameworks. Leveraging the precision of physics-based models for stress, deformation and material interactions, alongside the computational efficiency and predictive capabilities of AI, will enable real-time predictive maintenance and failure analysis. Such hybrid models, continuously refined and validated through experimental data, are expected to advance areas such as wear prediction, lubrication optimisation, and system failure diagnostics. This multidisciplinary approach will significantly benefit automotive, aerospace, and manufacturing industries by enhancing mechanical system performance, reducing unplanned downtime, and promoting sustainability through more efficient resource utilisation.

Determining critical parameters for improving the predictive capabilities of lubrication models, such as friction coefficients, wear rates, and surface roughness, remains a challenge due to the complexity of tribological systems and the large-scale interactions occurring at interfaces. Inverse problem modelling techniques offer a promising solution by enabling more accurate and efficient parameter estimation based on real-world experimental data. As real-time experimental data from advanced sensors and testing equipment become increasingly available, inverse modelling techniques will facilitate continuous updates and refinements to tribological models, thereby improving predictions related to wear, lubrication film behaviour, and surface interactions.

In addition to mechanical systems, lubrication-based modelling techniques can be revamped, tailored, and deployed to address the unique challenges confronted across various industries to optimise lubrication, wear, and surface interactions in other engineering systems. For instance, modelling the interactions in hydrogen-rich environments, such as hydrogen fuel cell systems, using MD simulations and FEM can provide insights into how lubricants and tribofilms behave under the influence of hydrogen. As hydrogen diffusion into metal surfaces leads to hydrogen embrittlement and negative impacts on the solid mechanical properties, the developed modelling tools can improve the material selection and lubricant formulation to prevent wear and failure. Another arena that can be explored is the energy sector, particularly wind turbines that operate in high-load and low-speed conditions where bearing and gearbox wear are major concerns. Elastohydrodynamic and mixed lubrication models can simulate asperity contact effects and lubricant film formation, thus extending turbine life and improving reliability under extreme operational conditions through optimal lubrication strategies. Referring to the trends above, advanced inverse problem modelling techniques can be employed to estimate key tribological parameters based on operational data, enabling real-time optimisation of lubrication protocols. Another research domain that can be analysed using the developed tools is the transportation sector, specifically electric and hybrid vehicles (EVs). High-speed transmissions require precise

modelling of lubricant rheology under extreme shear rates and temperatures, while nanofluid-enhanced lubricants—which incorporate nanoparticles like graphene or molybdenum disulfide (MoS_2)—are gaining traction for their ability to reduce wear and improve thermal management. Further challenges pertaining to electrical environments can be introduced, such as electromigration and electrical discharge, which are responsible for the degradation of lubricants and surfaces. As a result, multiscale simulations can help predict how these factors affect lubricant performance, while machine learning models can aid in engineering lubricant formulations for such specific conditions. Finally, yet importantly, synovial fluid is vital as a lubricant in biomedical applications, notably in developing biojoints and soft-contact systems. The unique behaviour exhibited by synovial fluid (*i.e.* both viscoelastic and shear-thinning) requires accurate modelling to replicate the mechanics of natural joints. Accordingly, finite element analysis and multiscale biomechanical models can be implemented to predict wear on joint implants, assess the longevity of bio-compatible coatings and evaluate interactions between soft tissues and implant surfaces under various loading conditions. This approach can accelerate the development of implants for reducing friction, preventing wear and extending the lifespan of artificial joints.

CRediT authorship contribution statement

Suhaib Ardah: Writing – review & editing, Writing – original draft, Methodology, Investigation, Data curation, Conceptualization. **Francisco J. Profito:** Writing – review & editing, Supervision, Methodology, Conceptualization. **Daniele Dini:** Writing – review & editing, Supervision, Resources, Project administration, Methodology, Conceptualization.

Declaration of competing interest

Suhaib Ardah reports financial support was provided by Engineering and Physical Sciences Research Council. Francisco J. Profito reports financial support was provided by State of Sao Paulo Research Foundation. Daniele Dini reports financial support was provided by Engineering and Physical Sciences Research Council. Daniele Dini reports financial support was provided by Royal Academy of Engineering. If there are other authors, they declare that they have no known competing financial interests or personal relationships that could have appeared to influence the work reported in this paper.

Acknowledgments

S. Ardah and D. Dini would like to acknowledge the support received from the Engineering and Physical Sciences Research Council, United Kingdom (EPSRC) *via* the InFUSE Prosperity Partnership EP/V038044/1. F.J. Profito would like to acknowledge the funding received from the São Paulo Research Foundation (FAPESP) *via* grant #2022/03110-0. D. Dini would also like to acknowledge the funding received from the Engineering and Physical Sciences Research Council, United Kingdom (EPSRC) *via* grant EP/N025954/1, as well as the support provided by the Shell/RAEng Research Chair in Complex Engineering Interfaces (RCSRF2122-14-143).

Availability of data and materials

The data that support the findings of this study are available from the corresponding author upon reasonable request or at tribology@imperial.ac.uk.

References

[1] Ciulli E. Tribology and industry: from the origins to 4.0. Front Mech Eng 2019;5:469821. https://doi.org/10.3389/fmech.2019.00055.
[2] Dowson D. A tribological day. Proc Inst Mech Eng J J Eng Tribol 2009;223(3):261–73. https://doi.org/10.1243/13506501JET557.
[3] Descartes S, Courtieux L, Berthier Y, Peditto F. Tribological study of oral care silica. Tribol Int 2015;82:551–60. https://doi.org/10.1016/j.triboint.2014.02.023.
[4] Putignano C, Burris D, Moore A, Dini D. Cartilage rehydration: the sliding-induced hydrodynamic triggering mechanism. Acta Biomater 2021;125:90–9. https://doi.org/10.1016/j.actbio.2021.02.040.
[5] Secomb TW. Tribological phenomena in blood vessels. In: Encyclopedia of tribology. Boston, MA, Boston, MA, USA: Springer; 2013. p. 3806–10. https://doi.org/10.1007/978-0-387-92897-5_1271.
[6] Tung SC, McMillan ML. Automotive tribology overview of current advances and challenges for the future. Tribol Int 2004;37(7):517–36. https://doi.org/10.1016/j.triboint.2004.01.013.
[7] Holmberg K, Erdemir A. Influence of tribology on global energy consumption, costs and emissions. Friction 2017;5(3):263–84. https://doi.org/10.1007/s40544-017-0183-5.
[8] Bhushan B, Israelachvili JN, Landman U. Nanotribology: friction, wear and lubrication at the atomic scale. Nature 1995;374(6523):607–16. https://doi.org/10.1038/374607a0.
[9] Ayyildiz M, Scaraggi M, Sirin O, Basdogan C, Persson BNJ. Contact mechanics between the human finger and a touchscreen under electroadhesion. Proc Natl Acad Sci U S A 2018;115(50):12668–73. https://doi.org/10.1073/pnas.1811750115.
[10] Sun C, Chen F, Tang X, Zhang D, Zheng K, Zhu G, et al. Simultaneous interfacial interaction and built-in electric field regulation of gaznon@ng for high-performance lithium-ion storage. Nano Energy 2022;99:107369. https://doi.org/10.1016/j.nanoen.2022.107369.
[11] Derler S, Gerhardt L-C. Tribology of skin: review and analysis of experimental results for the friction coefficient of human skin. Tribol Lett 2012;45(1):1–27. https://doi.org/10.1007/s11249-011-9854-y.
[12] Li J, Mooney DJ. Designing hydrogels for controlled drug delivery. Nat Rev Mater 2016;1(16,071):1–17. https://doi.org/10.1038/natrevmats.2016.71.
[13] Bhatia SN, Ingber DE. Microfluidic organs-on-chips. Nat Biotechnol 2014;32(8):760–72. https://doi.org/10.1038/nbt.2989.
[14] Zhou M, Pesika N, Zeng H, Tian Y, Israelachvili J. Recent advances in gecko adhesion and friction mechanisms and development of gecko-inspired dry adhesive surfaces. Friction 2013;1(2):114–29. https://doi.org/10.1007/s40544-013-0011-5.
[15] Song Y, Dai Z, Wang Z, Ji A, Gorb SN. The synergy between the insect-inspired claws and adhesive pads increases the attachment ability on various rough surfaces. Sci Rep 2016;6(26,219):1–9. https://doi.org/10.1038/srep26219.
[16] Zhang H, Liu S, Xiao H. Tribological properties of sliding quartz sand particle and shale rock contact under water and guar gum aqueous solution in hydraulic fracturing. Tribol Int 2019;129:416–26. https://doi.org/10.1016/j.triboint.2018.08.043.
[17] Dhanola A, Garg HC. Tribological challenges and advancements in wind turbine bearings: a review. Eng Fail Anal 2020;118:104885. https://doi.org/10.1016/j.engfailanal.2020.104885.
[18] Jason YJJ, How HG, Teoh YH, Chuah HG. A study on the tribological performance of nanolubricants. Processes 2020;8(11):1372. https://doi.org/10.3390/pr8111372.
[19] Holmberg K, Andersson P, Erdemir A. Global energy consumption due to friction in passenger cars. Tribol Int 2012;47:221–34. https://doi.org/10.1016/j.triboint.2011.11.022.
[20] Wu X, Wang H, Wang Z, Xu J, Wu Y, Xue R, et al. Highly conductive thermal interface materials with vertically aligned graphite-nanoplatelet filler towards: high power density electronic device cooling. Carbon 2021;182:445–53. https://doi.org/10.1016/j.carbon.2021.06.048.
[21] Servantie J, Gaspard P. Translational dynamics and friction in double-walled carbon nanotubes. Phys Rev B 2006;73(12):125428. https://doi.org/10.1103/PhysRevB.73.125428.
[22] Stachowiak GW, Batchelor AW. Engineering tribology, Butterworth-Heinemann, Oxford, England. UK 2014. https://doi.org/10.1016/C2011-0-07515-4.
[23] Miyoshi K. Solid lubrication fundamentals and applications, Taylor & Francis, Andover, England. UK 2019. https://doi.org/10.1201/9780429134333.
[24] Khonsari MM, Booser ER. Applied tribology: Bearing design and lubrication (tribology in practice series). Chichester, England, UK: Wiley; 2017.
[25] Vakis AI, Yastrebov VA, Scheibert J, Nicola L, Dini D, Minfray C, et al. Modeling and simulation in tribology across scales: an overview. Tribol Int 2018;125:169–99. https://doi.org/10.1016/j.triboint.2018.02.005.
[26] Müser MH, Dapp WB, Bugnicourt R, Sainsot P, Lesaffre N, Lubrecht TA, et al. Meeting the contact-mechanics challenge. Tribol Lett 2017;65(4):118. https://doi.org/10.1007/s11249-017-0900-2.
[27] Jost HP. Lubrication (tribology). Education and Research Report: Her Majesty's Stationary Office, London, UK; 1966.
[28] Holmberg K, Erdemir A. The impact of tribology on energy use and co2 emission globally and in combustion engine and electric cars. Tribol Int 2019;135:389–96. https://doi.org/10.1016/j.triboint.2019.03.024.
[29] Reynolds O. On the theory of lubrication and its application to mr. beauchamp tower's experiments, including an experimental determination of the viscosity of olive oil. Philos Transact R Soc Lond 1886;40:157–234.
[30] Frene J, Nicolas D, Degueurce B, Berthe D, Godet M. Hydrodynamic lubrication: Bearings and thrust bearings (tribology and Interface engineering)Vol. 33. Oxford, England, UK: Elsevier Science; 1997.

[31] Hamrock BJ, Schmid SR, Jacobson BO. Fundamentals of fluid film lubrication. 2nd ed. Boca Raton, FL, USA: CRC Press; 2004.
[32] Szeri AZ. Fluid film lubrication. Cambridge, England, UK: Cambridge University Press; 2010. https://doi.org/10.1017/CBO9780511782022.
[33] Profito FJ, Giacopini M, Zachariadis DC, Dini D. A general finite volume method for the solution of the Reynolds lubrication equation with a mass-conserving cavitation model. Tribol Lett 2015;60(1):18–21. https://doi.org/10.1007/s11249-015-0588-0.
[34] Habchi W. Finite element modeling of Elastohydrodynamic lubrication problems. Hoboken, NJ, USA: Wiley; 2018.
[35] Ardah S, Profito FJ, Dini D. An integrated finite volume framework for thermal elasto-hydrodynamic lubrication. Tribol Int 2023;177:107935. https://doi.org/10.1016/j.triboint.2022.107935.
[36] Hartinger M, Dumont M-L, Ioannides S, Gosman D, Spikes H. Cfd modeling of a thermal and shear-thinning elastohydrodynamic line contact. J Tribol 2008;130 (4). https://doi.org/10.1115/1.2958077.
[37] Tošić M, Larsson R, Jovanović J, Lohner T, Björling M, Stahl K. A computational fluid dynamics study on shearing mechanisms in thermal elastohydrodynamic line contacts. Lubricants 2019;7(8):69. https://doi.org/10.3390/lubricants7080069.
[38] Lohner T, Ziegltrum A, Stemplinger J-P, Stahl K. Engineering software solution for thermal elastohydrodynamic lubrication using multiphysics software. Adv Tribol 2016;2016(1):6507203. https://doi.org/10.1155/2016/6507203.
[39] Sadeghi F, Arya U, Aamer S, Meinel A. A review of computational fluid dynamics approaches used to investigate lubrication of rolling element bearings. J Tribol 2024;146(10). https://doi.org/10.1115/1.4065663.
[40] Johnson KL. Contact mechanics. Cambridge, England, UK: Cambridge University Press; 1985. https://doi.org/10.1017/CBO9781139171731.
[41] Luan B, Robbins MO. The breakdown of continuum models for mechanical contacts. Nature 2005;435(7044):929–32. https://doi.org/10.1038/nature03700.
[42] Allen MP, Tildesley DJ. Computer simulation of liquids. 2nd ed. Oxford, England, UK: Oxford University Press; 2017.
[43] Plimpton S. Fast parallel algorithms for short-range molecular dynamics. J Comput Phys 1995;117(1):1–19. https://doi.org/10.1006/jcph.1995.1039.
[44] Kresse G, Hafner J. *Ab initio* molecular dynamics for liquid metals. Phys Rev B 1993;47(1):558–561(R). https://doi.org/10.1103/PhysRevB.47.558.
[45] Giannozzi P, Baroni S, Bonini N, Calandra M, Car R, Cavazzoni C, et al. Quantum espresso: a modular and open-source software project for quantumsimulations of materials. J Phys Condens Matter 2009;21(39):395502. https://doi.org/10.1088/0953-8984/21/39/395502.
[46] Ewen JP, Spikes HA, Dini D. Contributions of molecular dynamics simulations to elastohydrodynamic lubrication. Tribol Lett 2021;69(1):1–15. https://doi.org/10.1007/s11249-021-01399-w.
[47] Groen D, Knap J, Neumann P, Suleimenova D, Veen L, Leiter K. Mastering the scales: a survey on the benefits of multiscale computing software. Phil Trans R Soc A 2019;377(2142). https://doi.org/10.1098/rsta.2018.0147.
[48] Li J, Zhang J, Ge W, Liu X. Multi-scale methodology for complex systems. Chem Eng Sci 2004;59(8):1687–700. https://doi.org/10.1016/j.ces.2004.01.025.
[49] Hoekstra A, Chopard B, Coveney P. Multiscale modelling and simulation: a position paper. Philos Trans Royal Soc A 2014;372(2021):20130377. https://doi.org/10.1098/rsta.2013.0377.
[50] Patir N, Cheng HS. An average flow model for determining effects of three-dimensional roughness on partial hydrodynamic lubrication. J Lubr Technol 1978;100(1):12–7. https://doi.org/10.1115/1.3453103.
[51] Patir N, Cheng HS. Application of average flow model to lubrication between rough sliding surfaces. J Lubr Technol 1979;101(2):220–9. https://doi.org/10.1115/1.3453329.
[52] Bayada G, Cid B, Vázquez C. Two-scale homogenization study of a Reynolds-rod elastohydrodynamic model. Math Models Methods Appl Sci 2003;13(02):259–93. https://doi.org/10.1142/S0218202503002489.
[53] Almqvist A, Dasht J. The homogenization process of the Reynolds equation describing compressible liquid flow. Tribol Int 2006;39(9):994–1002. https://doi.org/10.1016/j.triboint.2005.09.036.
[54] Martini A, Liu Y, Snurr RQ, Wang QJ. Molecular dynamics characterization of thin film viscosity for ehl simulation. Tribol Lett 2006;21(3):217–25. https://doi.org/10.1007/s11249-006-9023-x.
[55] Holland DM, Lockerby DA, Borg MK, Nicholls WD, Reese JM. Molecular dynamics pre-simulations for nanoscale computational fluid dynamics. Microfluid Nanofluid 2015;18(3):461–74. https://doi.org/10.1007/s10404-014-1443-6.
[56] Fillot N, Berro H, Vergne P. From continuous to molecular scale in modelling elastohydrodynamic lubrication: nanoscale surface slip effects on film thickness and friction. Tribol Lett 2011;43(3):257–66. https://doi.org/10.1007/s11249-011-9804-8.
[57] Savio D, Fillot N, Vergne P, Hetzler H, Seemann W, Morales Espejel GE. A multiscale study on the wall slip effect in a ceramic–steel contact with nanometer-thick lubricant film by a nano-to-elastohydrodynamic lubrication approach. J Tribol 2015;137(3). https://doi.org/10.1115/1.4029937.
[58] Fish J, Wagner GJ, Keten S. Mesoscopic and multiscale modelling in materials. Nat Mater 2021;20(6):774–86. https://doi.org/10.1038/s41563-020-00913-0.
[59] Ewen JP, Fernández ER, Smith ER, Dini D. Nonequilibrium molecular dynamics simulations of tribological systems. In: Modeling and simulation of Tribological problems in technology. Cham, Switzerland: Springer; 2019. p. 95–130. https://doi.org/10.1007/978-3-030-20377-1_3.
[60] Alber M, Buganza Tepole A, Cannon WR, De S, Dura-Bernal S, Garikipati K, et al. Integrating machine learning and multiscale modeling—perspectives, challenges, and opportunities in the biological, biomedical, and behavioral sciences. npj Digital Med 2019;2(115):1–11. https://doi.org/10.1038/s41746-019-0193-y.
[61] Peng GCY, Alber M, Buganza Tepole A, Cannon WR, De S, Dura-Bernal S, et al. Multiscale modeling meets machine learning: what can we learn? Arch Comput Methods Eng 2021;28(3):1017–37. https://doi.org/10.1007/s11831-020-09405-5.
[62] Keith JA, Vassilev-Galindo V, Cheng B, Chmiela S, Gastegger M, Müller K-R, et al. Combining machine learning and computational chemistry for predictive insights into chemical systems. Chem Rev 2021;121(16):9816–72. https://doi.org/10.1021/acs.chemrev.1c00107.
[63] Rosenkranz A, Marian M, Profito FJ, Aragon N, Shah R. The use of artificial intelligence in tribology—a perspective. Lubricants 2020;9(1):2. https://doi.org/10.3390/lubricants9010002.
[64] Sose AT, Joshi SY, Kunche LK, Wang F, Deshmukh SA. A review of recent advances and applications of machine learning in tribology. Phys Chem Chem Phys 2023;25(6):4408–43. https://doi.org/10.1039/D2CP03692D.
[65] Paturi UMR, Palakurthy ST, Reddy NS. The role of machine learning in tribology: a systematic review. Arch Comput Methods Eng 2023;30(2):1345–97. https://doi.org/10.1007/s11831-022-09841-5.
[66] Zhu D, Mixed EHL. Encyclopedia of tribology. Boston, MA, Boston, MA, USA: Springer; 2013. p. 2266–76. https://doi.org/10.1007/978-0-387-92897-5_659.
[67] Zhu D, Wang J. Interfacial mechanics: Theories and methods for contact and lubrication. Boca Raton, FL, USA: CRC Press; 2019.
[68] Spikes HA. Mixed lubrication — an overview. Lubr Sci 1997;9(3):221–53. https://doi.org/10.1002/ls.3010090302.
[69] Dobrica MB, Fillon M. Mixed lubrication. In: Encyclopedia of tribology. Boston, MA, Boston, MA, USA: Springer; 2013. p. 2284–91. https://doi.org/10.1007/978-0-387-92897-5_27.
[70] Gohar R. Elastohydrodynamics. London, England, UK: World Scientific; 2001.
[71] Johnson KL. Regimes of elastohydrodynamic lubrication. J Mech Eng Sci 1970;12 (1):9–16. https://doi.org/10.1243/JMES_JOUR_1970_012_004_02.
[72] Dowson D. Elastohydrodynamic and micro-elastohydrodynamic lubrication. Wear 1995;190(2):125–38. https://doi.org/10.1016/0043-1648(95)06660-8.
[73] Spikes H. Basics of ehl for practical application. Lubr Sci 2015;27(1):45–67. https://doi.org/10.1002/ls.1271.
[74] Habchi W, Sperka P, Bair S. Is elastohydrodynamic minimum film thickness truly governed by inlet rheology? Tribol Lett 2023;71(3):96–9. https://doi.org/10.1007/s11249-023-01771-y.
[75] Bair S, Habchi W. Quantitative elastohydrodynamic lubrication—seventeen years in. J Tribol 2024;146(8). https://doi.org/10.1115/1.4065299.
[76] Habchi W, Bair S. Quantifying the inlet pressure and shear stress of elastohydrodynamic lubrication. Tribol Int 2023;182:108351. https://doi.org/10.1016/j.triboint.2023.108351.
[77] Putignano C, Dini D. Soft Matter Lubrication: Does Solid Viscoelasticity Matter? ACS Appl Mat Interfaces 2017;9(48):42287–95. https://doi.org/10.1021/acsami.7b09381.
[78] Putignano C. Soft lubrication: a generalized numerical methodology. J Mech Phys Solids 2020;134:103748. https://doi.org/10.1016/j.jmps.2019.103748.
[79] Moukalled F, Mangani L, Darwish M. The finite volume method in computational fluid dynamics. Cham, Switzerland: Springer International Publishing; 2016.
[80] Ferziger JH, Perić M. Computational methods for fluid dynamics. 4th ed. Switzerland: Springer Cham; 2020.
[81] Pinkus O, Sternlicht B. Theory of hydrodynamic lubrication. Maidenhead, England, UK: McGraw-Hill; 1961.
[82] Peterson W, Singh K, Sadeghi F. Fluid–solid interaction modeling of elastohydrodynamic lubrication point contacts. J Tribol 2022;144(11). https://doi.org/10.1115/1.4054589.
[83] Dowson D. A generalised Reynolds equation for fluid-film lubrication. Int J Mech Sci 1962;4(2):159–70. https://doi.org/10.1016/S0020-7403(62)80038-1.
[84] Berthe D, Godet M. A more general form of Reynolds equation–application to rough surfaces. Wear 1974;27(3):345–57. https://doi.org/10.1016/0043-1648(74)90119-7.
[85] Peiran Y, Shizhu W. A generalised Reynolds equation for non-newtonian thermal elastohydrodynamic lubrication. J Tribol 1990;112(4):631–6. https://doi.org/10.1115/1.2920308.
[86] Peiran Y, Shizhu W. A generalised Reynolds equation based on non-newtonian flow in lubrication mechanics. Acta Mech Sin 1990;6(4):289–95. https://doi.org/10.1007/BF02486885.
[87] Najji B, Bou-Said B, Berthe D. New formulation for lubrication with non-newtonian fluids. J Tribol 1989;111(1):29–34. https://doi.org/10.1115/1.3261875.
[88] Almqvist A, Burtseva E, Rajagopal K, Wall P. On lower-dimensional models in lubrication, part a: common misinterpretations and incorrect usage of the Reynolds equation. Proc Inst Mech Eng J J Eng Tribol 2020;235(8):1692–702. https://doi.org/10.1177/1350650120973792.
[89] Almqvist A, Burtseva E, Rajagopal K, Wall P. On lower-dimensional models in lubrication, part b: derivation of a Reynolds type of equation for incompressible piezo-viscous fluids. Proc Inst Mech Eng J J Eng Tribol 2020;235(8):1703–18. https://doi.org/10.1177/1350650120973800.
[90] Almqvist A, Burtseva E, Rajagopal K, Wall P. On lower-dimensional models of thin film flow, part c: derivation of a Reynolds type of equation for fluids with temperature and pressure dependent viscosity. Proc Inst Mech Eng J J Eng Tribol 2022;237(3):514–26. https://doi.org/10.1177/13506501221135269.
[91] Franc J-P, Michel J-M. Fundamentals of cavitation: 76 (fluid mechanics and its applications, 76). New York, NY, USA: Springer; 2004.

[92] Prosperetti A. Bubbles. Phys Fluids 2004;16(6):1852–65. https://doi.org/10.1063/1.1695308.
[93] Dowson D, Taylor CM. Cavitation in bearings. Annu Rev Fluid Mech 1979;11:35–65. https://doi.org/10.1146/annurev.fl.11.010179.000343.
[94] Brennen CE. Cavitation and bubble dynamics. Cambridge, England, UK: Cambridge University Press; 2013. https://doi.org/10.1017/CBO9781107338760.
[95] Braun MJ, Hannon WM. Cavitation formation and modelling for fluid film bearings: a review. Proc Inst Mech Eng J J Eng Tribol 2010;224(9):839–63. https://doi.org/10.1243/13506501JET772.
[96] Kim K-H, Chahine G, Franc J-P, Karimi A. Advanced experimental and numerical techniques for cavitation Erosion prediction: 106 (fluid mechanics and its applications, 106). Dordrecht, The Netherlands: Springer; 2014.
[97] Delale CF. Bubble dynamics and shock waves: 8 (shock wave science and technology reference library, 8). Berlin, Germany: Springer; 2012.
[98] Benjamin B, Ellis A. A discussion on deformation of solids by the impact of liquids, and its relation to rain damage in aircraft and missiles, to blade erosion in steam turbines, and to cavitation erosion - the collapse of cavitation bubbles and the pressures thereby produced against solid boundaries. Philos Transact R Soc Lond Ser A Math Phys Sci 1966;260(1110):221–40. https://doi.org/10.1098/rsta.1966.0046.
[99] Spurk JH, Aksel N. Fluid mechanics. Berlin, Germany: Springer; 2021.
[100] Snyder TA, Braun MJ, Pierson KC. Two-way coupled Reynolds and rayleigh–plesset equations for a fully transient, multiphysics cavitation model with pseudo-cavitation. Tribol Int 2016;93:429–45. https://doi.org/10.1016/j.triboint.2015.08.040.
[101] San Andrés L, Diaz S. Flow visualization and forces from a squeeze film damper operating with natural air entrainment. J Tribol Transact Asme 2003;125. https://doi.org/10.1115/1.1510878.
[102] Fowell M, Olver AV, Gosman AD, Spikes HA, Pegg I. Entrainment and inlet suction: two mechanisms of hydrodynamic lubrication in textured bearings. J Tribol 2007;129(2):336–47. https://doi.org/10.1115/1.2540089.
[103] Sommerfeld A. Zur hydrodynamischen theorie der schmiermittlereibung. Zeit Angew Math u Physik 1904;50:97–155.
[104] Gümbel L. Über geschmierte arbeitsräder. Z f d ges Turbinenwes 1916;13:357.
[105] Swift H. The stability of lubricating films in journal bearings. Proc Inst Civil Eng (Lond) 1932;233:267–88.
[106] Stieber W. Das Schwimmlager: Hydrodynamische Theorie des Gleitlagersvol. 233. Berlin: V.D.I. Verlag GMBH; 1933.
[107] Qiu Y, Khonsari MM. On the prediction of cavitation in dimples using a mass-conservative algorithm. J Tribol 2009;131(4). https://doi.org/10.1115/1.3176994.
[108] Ausas RF, Jai M, Buscaglia GC. A mass-conserving algorithm for dynamical lubrication problems with cavitation. J Tribol 2009;131(3). https://doi.org/10.1115/1.3142903.
[109] Jakobsson B. The finite journal bearing considering vaporization, Transvol. 190. Sweden: Chalmers Univ. of Tech; 1965.
[110] Floberg L. On hydrodynamic lubricationwith special reference to sub-cavity pressures and number of streamers in cavitation regions. Acta Polytechnica Scandinavica Mech Eng Series 1965;19.
[111] Floberg L. On the tensile strength of liquids. Lund, Sweden, Lund Technical University: Transactions of Machine Elements Division / Lund Technical University; 1973.
[112] Elrod HG, Adams ML. A computer program for cavitation and starvation problems, in: Cavitation and related phenomena in lubrication: Proceedings of the 1st Leeds-Lyon symposium on tribology. Department of Mechanical Engineering: The University of Leeds, England; 1974. p. 37–41.
[113] Elrod HG. A general theory for laminar lubrication with Reynolds roughness. J Lubrication Technol 1979;101(1):8–14.
[114] Elrod HG. A cavitation algorithm. J Lubrication Technol 1981;103(3):350–4.
[115] Ardah S, Profito FJ, Reddyhoff T, Dini D. Advanced modeling of lubricated interfaces in general curvilinear grids. arXiv 2023. https://doi.org/10.48550/arXiv.2304.04510. arXiv:2304.04510.
[116] Brewe DE. Theoretical modeling of the vapor cavitation in dynamically loaded journal bearings. J Tribol 1986;108(4):628–37. https://doi.org/10.1115/1.3261288.
[117] Ausas R, Ragot P, Leiva J, Jai M, Bayada G, Buscaglia GC. The impact of the cavitation model in the analysis of microtextured lubricated journal bearings. J Tribol 2007;129(4):868–75. https://doi.org/10.1115/1.2768088.
[118] Bonneau D, Guines D, Frene J Xn, Toplosky J. Ehd analysis, including structural inertia effects and a mass-conserving cavitation model. J Tribol 1995;117(3):540–7. https://doi.org/10.1115/1.2831288.
[119] Kumar A, Booker JF. A finite element cavitation algorithm. J Tribol 1991;113(2):276–84. https://doi.org/10.1115/1.2920617.
[120] Yu Q, Keith Jr TG. A boundary element cavitation algorithm. Trans: Tribol; 1994.
[121] Vijayaraghavan D, Jr TGK. Development and evaluation of a cavitation algorithm. Tribol Transact 1989;32(2):225–33. https://doi.org/10.1080/10402008908981882.
[122] Vijayaraghavan D, Keith TG. An efficient, robust, and time accurate numerical scheme applied to a cavitation algorithm. J Tribol 1990;112(1):44–51. https://doi.org/10.1115/1.2920229.
[123] Sahlin F, Almqvist A, Larsson R, Glavatskih S. A cavitation algorithm for arbitrary lubricant compressibility. Tribol Int 2007;40(8):1294–300. https://doi.org/10.1016/j.triboint.2007.02.009.
[124] Bayada G, Martin S, Vázquez C. Two-scale homogenization of a hydrodynamic elrod–Adams model. Asymptot Anal 2005;44(1–2):75–110.
[125] Giacopini M, Fowell MT, Dini D, Strozzi A. A mass-conserving complementarity formulation to study lubricant. J Tribol 2010;132(4). https://doi.org/10.1115/1.4002215.
[126] Almqvist A, Fabricius J, Larsson R, Wall P. A new approach for studying cavitation in lubrication. J Tribol 2014;136(1). https://doi.org/10.1115/1.4025875.
[127] Cottle RW, Pang J-S, Stone RE. The linear complementarity problem, Society for Industrial and Applied Mathematics (SIAM, 3600 market street, floor 6, pHiladelphia, PA 19104). pHiladelphia: PA, USA; 1992.
[128] Guy B. From a compressible fluid model to new mass conserving cavitation algorithms. Tribol Int 2014;71:38–49. https://doi.org/10.1016/j.triboint.2013.10.014.
[129] Woloszynski T, Podsiadlo P, Stachowiak GW. Efficient solution to the cavitation problem in hydrodynamic lubrication. Tribol Lett 2015;58(1):11–8. https://doi.org/10.1007/s11249-015-0487-4.
[130] Brunetière N. A general model for liquid and gas lubrication, including cavitation. J Tribol 2017;140(2):021702. https://doi.org/10.1115/1.4037355.
[131] Ransegnola T, Sadeghi F, Vacca A. An efficient cavitation model for compressible fluid film bearings. Tribol Transact 2021;64(3):434–53. https://doi.org/10.1080/10402004.2020.1853864.
[132] Hertz H. Ueber die berührung fester elastischer körper. De Gruyter 1882;1882(92):156–71. https://doi.org/10.1515/crll.1882.92.156.
[133] Popov VL. Contact mechanics and friction: Physical principles and applications. Berlin, Germany: Springer; 2010.
[134] Timoshenko S, Goodier JN. Theory of elasticity. Maidenhead, England, UK: McGraw-Hill; 1951.
[135] Boussinesq J. Application des potentiels à l'étude de l'équilibre et du mouvement des solides élastiques: principalement au calcul des deformations et des pressions que produisent, dans ces solides, des efforts quelconques exercés sur und petite partie de leur surface ou de leur intérieur; memoire suivi de notes étendues sur divers points de physique mathématique et d'analyse. Paris, France: Gauthier-Villars; 1885.
[136] Flamant A. Sur la re'partition des pressions dans un solide rectangulaire charge´ transversalement. C R Acad Sci Parisction 1892;114:1465–8.
[137] Mindlin RD. Force at a point in the interior of a semi-infinite solid. Physics 1936;7(5):195–202. https://doi.org/10.1063/1.1745385.
[138] Thomson W. Note on the integration of the equations of equilibrium of an elastic solid. In: Mathematical and physical papers. Cambridge, England, UK: Cambridge University Press; 2011. p. 97–9. https://doi.org/10.1017/CBO9780511996009.038.
[139] Papkovich P. The representation of the general integral of the fundamental equations of elasticity theory in terms of harmonic functions. Izv Akad Nauk SSSR, Phys-Math Ser 1932;10(1425):90.
[140] O'Sullivan TC, King RB. Sliding contact stress field due to a spherical indenter on a layered elastic half-space. J Tribol 1988;110(2):235–40. https://doi.org/10.1115/1.3261591.
[141] Peng W, Bhushan B. Sliding contact analysis of layered elastic/plastic solids with rough surfaces. J Tribol 2002;124(1):46–61. https://doi.org/10.1115/1.1401018.
[142] Wang W, Wang H, Liu Y, Hu Y, Zhu D. A comparative study of the methods for calculation of surface elastic deformation. Proc Inst Mech Eng J J Eng Tribol 2003;217:145–54. https://doi.org/10.1243/13506500360603570.
[143] Love A. The stress produced in a semi-infinite solid by pressure on part of the boundary. Philos Transact R Soc A 1929;228:377–420. https://doi.org/10.1098/RSTA.1929.0009.
[144] Dowson D, Hamrock BJ. Numerical evaluation of the surface deformation of elastic solids subjected to a hertzian contact stress. A S L E Transactions 1976;19(4):279–86. https://doi.org/10.1080/05698197608982804.
[145] Biswas S, Snidle RW. Calculation of surface deformation in point contact ehd. J Lubr Technol 1977;99(3):313–7. https://doi.org/10.1115/1.3453208.
[146] Ai X. Numerical analyses of elastohydrodynamically lubricated line and point contacts with rough surfaces by using semi-system and multigrid methods. Ph.D. thesis,. Evanston, IL: Northwestern University; 1993.
[147] Lubrecht T, Venner CH. Multi-level methods in lubrication. Amsterdam, The Netherlands: Elsevier; 2000.
[148] Evans HP, Hughes TG. Evaluation of deflection in semi-infinite bodies by a differential method. Proc Inst Mech Eng C J Mech Eng Sci 2000;214(4):563–84. https://doi.org/10.1243/0954406001523911.
[149] Hughes TG, Elcoate CD, Evans HP. Coupled solution of the elastohydrodynamic line contact problem using a differential deflection method. Proc Inst Mech Eng C J Mech Eng Sci 2000;214(4):585–98. https://doi.org/10.1243/0954406001523920.
[150] Ren N, Lee SC. Contact simulation of three-dimensional rough surfaces using moving grid method. J Tribol 1993;115(4):597–601. https://doi.org/10.1115/1.2921681.
[151] Nogi T, Kato T. Influence of a hard surface layer on the limit of elastic contact—part i: analysis using a real surface model. J Tribol 1997;119(3):493–500. https://doi.org/10.1115/1.2833525.
[152] Polonsky IA, Keer LM. A numerical method for solving rough contact problems based on the multi-level multi-summation and conjugate gradient techniques. Wear 1999;231(2):206–19. https://doi.org/10.1016/S0043-1648(99)00113-1.
[153] Ju Y, Farris TN. Spectral analysis of two-dimensional contact problems. J Tribol 1996;118(2):320–8. https://doi.org/10.1115/1.2831303.
[154] Liu S, Wang QJ, Liu G. A versatile method of discrete convolution and fft (dc-fft) for contact analyses. Wear 2000;243:101–11.

[155] Liu S, Hua D, Chen WW, Wang QJ. Tribological modeling: application of fast fourier transform. Tribol Int 2007;40(8):1284–93. https://doi.org/10.1016/j.triboint.2007.02.004.

[156] Chen WW, Liu S, Wang QJ. Fast fourier transform based numerical methods for elasto-plastic contacts of nominally flat surfaces. J Appl Mech 2008;75(1). https://doi.org/10.1115/1.2755158.

[157] Liu S, Hua DY. Three-dimensional semiperiodic line contact–periodic in contact length direction. J Tribol 2009;131(2). https://doi.org/10.1115/1.3084237.

[158] Wang QJ, Sun L, Zhang X, Liu S, Zhu D. Fft-based methods for computational contact mechanics. Front Mech Eng 2020;6. https://doi.org/10.3389/fmech.2020.00061.

[159] Sun L, Wang QJ, Zhang M, Zhao N, Keer LM, Liu S, et al. Discrete convolution and fft method with summation of influence coefficients (dcs–fft) for three-dimensional contact of inhomogeneous materials. Comput Mech 2020;65(6):1509–29. https://doi.org/10.1007/s00466-020-01832-2.

[160] Reddy JN. Introduction to the finite element method 4E (MECHANICAL ENGINEERING). Maidenhead, England, UK: McGraw Hill; 2018.

[161] Bathe KJ. Finite Element Procedures. Klaus-Jurgen Bathe; 2007.

[162] Zienkiewicz OC, Taylor RL, Zhu JZ. The finite element method: its basis and fundamentals, Butterworth-Heinemann, Oxford, England. UK 2013. https://doi.org/10.1016/C2009-0-24909-9.

[163] Profito F. On the development of advanced techniques for Mixed-EHL modelling of journal and sliding bearing systems. Ph.D. thesis,. Brazil: Polytechnic School of the University of São Paulo; 2015.

[164] Offner G. Modelling of condensed flexible bodies considering non-linear inertia effects resulting from gross motions. Proc Inst Mech Eng K J Multi-body Dynamics 2011;225(3):204–19. https://doi.org/10.1177/1464419311416553.

[165] Krinner A, Rixen DJ. Interface reduction methods for mechanical systems with elastohydrodynamic lubricated revolute joints. Multibody SysDyn 2018;42(1):79–96. https://doi.org/10.1007/s11044-017-9575-6.

[166] Kim S, Choi J, Kim J-G, Hatakeyama R, Kuribara H, Choi JH. Coupled simulation of elastohydrodynamics and multi-flexible body dynamics in piston-lubrication system. Adv Mech Eng 2019;11(12). https://doi.org/10.1177/1687814019895855. 1687814019895855.

[167] Wen S, Huang P. Principles of tribology. Hoboken, NJ, USA: Wiley; 2011.

[168] Jacobson BO. Rheology and Elastohydrodynamic lubrication. Walthm, MA, USA: Elsevier Science; 2012.

[169] White FM. Viscous fluid flow. Maidenhead, England, UK: McGraw-Hill; 2006.

[170] Perelman TL. On conjugated problems of heat transfer. Int J Heat Mass Transfer 1961;3(4):293–303. https://doi.org/10.1016/0017-9310(61)90044-8.

[171] Abram DS. Conjugate problems in convective heat transfer. Boca Raton, FL, USA: CRC Press; 2018.

[172] John B, Senthilkumar P, Sadasivan S. Applied and theoretical aspects of conjugate heat transfer analysis: a review. Arch Comput Methods Eng 2019;26(2):475–89. https://doi.org/10.1007/s11831-018-9252-9.

[173] Guo F, Yang P, Qu S. On the theory of thermal elastohydrodynamic lubrication at high slide-roll ratios—circular glass-steel contact solution at opposite sliding. J Tribol 2001;123(4):816–21. https://doi.org/10.1115/1.1330739.

[174] Wang J, Yang P. A numerical analysis for tehl of eccentric-tappet pair subjected to transient load. J Tribol 2003;125(4):770–9. https://doi.org/10.1115/1.1576425.

[175] Verstraete T, Scholl S. Stability analysis of partitioned methods for predicting conjugate heat transfer. Int J Heat Mass Transfer 2016;101:852–69. https://doi.org/10.1016/j.ijheatmasstransfer.2016.05.041.

[176] Giles MB. Stability analysis of numerical interface conditions in fluid–structure thermal analysis. Int J Numer Methods Fluids 1997;25(4):421–36. https://doi.org/10.1002/(SICI)1097-0363(19970830)25:4<421::AID-FLD557>3.0.CO;2-J.

[177] Jaeger JC. Moving sources of heat and the temperature at sliding contacts. J Proc R Soc New South Wales 1943;76(3):203–24. https://doi.org/10.5962/p.360338.

[178] Carslaw H, Jaeger J. Conduction of heat in solids. Oxford, UK: Oxford University Press; 1959.

[179] Kim HJ, Ehret P, Dowson D, Taylor CM. Thermal elastohydrodynamic analysis of circular contacts part 1: Newtonian model. Proc Inst Mech Eng J J Eng Tribol 2001;215(4):339–52. https://doi.org/10.1243/1350650011543583.

[180] Tian X, Kennedy FE. Maximum and average flash temperatures in sliding contacts. J Tribol 1994;116(1):167–74. https://doi.org/10.1115/1.2927035.

[181] Bos J, Moes H. Frictional heating of tribological contacts. J Tribol 1995;117(1):171–7. https://doi.org/10.1115/1.2830596.

[182] Liu S, Rodgers MJ, Wang Q, Keer LM. A fast and effective method for transient thermoelastic displacement analyses. J Tribol 2000;123(3):479–85. https://doi.org/10.1115/1.1308010.

[183] Liu Y-C, Wang H, Wang W-Z, Hu Y-Z, Zhu D. Methods comparison in computation of temperature rise on frictional interfaces. Tribol Int 2002;35(8):549–60. https://doi.org/10.1016/S0301-679X(02)00062-2.

[184] Müller M, Fan J, Spikes H. Influence of polymethacrylate viscosity index improvers on friction and wear of lubricant formulations. SAE Transact 2007;116:580–8.

[185] Okrent EH. The effect of lubricant viscosity and composition on engine friction and bearing wear. A S L E Transactions 1961;4(1):97–108. https://doi.org/10.1080/05698196108972423.

[186] Okrent EH. The effect of lubricant viscosity and composition on engine friction and bearing wear. Ii, a S L E. Transactions 1961;4(2):257–62. https://doi.org/10.1080/05698196108972437.

[187] Evans CR, Johnson KL. The rheological properties of elastohydrodynamic lubricants. Proc Inst Mech Eng C J Mech Eng Sci 1986;200(5):303–12. https://doi.org/10.1243/PIME_PROC_1986_200_134_02.

[188] Spikes H, Jie Z. History, origins and prediction of elastohydrodynamic friction. Tribol Lett 2014;56(1):1–25. https://doi.org/10.1007/s11249-014-0396-y.

[189] Jadhao V, Robbins MO. Rheological properties of liquids under conditions of elastohydrodynamic lubrication. Tribol Lett 2019;67(3):1–20. https://doi.org/10.1007/s11249-019-1178-3.

[190] Dowson D, Higginson GR. Elasto-hydrodynamic lubrication. Oxford, England, UK: Pergamon Press; 1966.

[191] Hamrock BJ, Dowson D. Ball bearing lubrication: The Elastohydrodynamics of elliptical contacts. Chichester, England, UK: Wiley; 1981.

[192] Barus C. Isothermals, isopiestics and isometrics relative to viscosity. Am J Sci 1893;s3-45 (266):87–96. https://doi.org/10.2475/ajs.s3-45.266.87.

[193] Spikes HA. Sixty years of ehl. Lubr Sci 2006;18(4):265–91. https://doi.org/10.1002/ls.23.

[194] Vergne P, Bair S. Classical ehl *versus* quantitative ehl: a perspective part i—real viscosity-pressure dependence and the viscosity-pressure coefficient for predicting film thickness. Tribol Lett 2014;54(1):1–12. https://doi.org/10.1007/s11249-014-0302-7.

[195] Bair S, Martinie L, Vergne P. Classical ehl *versus* quantitative ehl: a perspective part ii—super-arrhenius piezoviscosity, an essential component of elastohydrodynamic friction missing from classical ehl. Tribol Lett 2016;63(3):10–37. https://doi.org/10.1007/s11249-016-0725-4.

[196] Bair S. The rheological assumptions of classical ehl: what went wrong? Tribol Int 2019;131:45–50. https://doi.org/10.1016/j.triboint.2018.10.020.

[197] Bair S, Vergne P, Kumar P, Poll G, Krupka I, Hartl M, et al. Comment on "history, origins and prediction of elastohydrodynamic friction" by spikes and jie. Tribol Lett 2015;58(1):16–8. https://doi.org/10.1007/s11249-015-0481-x.

[198] Angell CA. Relaxation in liquids, polymers and plastic crystals — strong/fragile patterns and problems. J Non Cryst Solids 1991;131-133:13–31. https://doi.org/10.1016/0022-3093(91)90266-9.

[199] Mauro JC, Yue Y, Ellison AJ, Gupta PK, Allan DC. Viscosity of glass-forming liquids. Proc Natl Acad Sci U S A 2009;106(47):19780–4. https://doi.org/10.1073/pnas.0911705106.

[200] Bair S. The viscosity at the glass transition of a liquid lubricant. Friction 2019;7(1):86–91. https://doi.org/10.1007/s40544-018-0210-1.

[201] Voigtmann T. Nonlinear glassy rheology. Curr Opin Colloid Interface Sci 2014;19(6):549–60. https://doi.org/10.1016/j.cocis.2014.11.001.

[202] Habchi W, Sperka P, Bair S. The role of the glass transition for ehl minimum film thickness. Tribol Int 2023;190:109061. https://doi.org/10.1016/j.triboint.2023.109061.

[203] Godey F, Fleury A, Soldera A. Local dynamics within the glass transition domain. Sci Rep 2019;9(9638):1–9. https://doi.org/10.1038/s41598-019-45933-2.

[204] Angell CA. Formation of glasses from liquids and biopolymers. Science 1995;267(5206):1924–35. https://doi.org/10.1126/science.267.5206.1924. URL, https://www.science.org/doi/abs/10.1126/science.267.5206.1924.

[205] Martini A, Bair S. The role of fragility in ehl entrapment. Tribol Int 2010;43(1):277–82. https://doi.org/10.1016/j.triboint.2009.06.006.

[206] Bair S, Roland CM, Casalini R. Fragility and the dynamic crossover in lubricants. Proc Inst Mech Eng J J Eng Tribol 2007;221(7):801–11. https://doi.org/10.1243/13506501JET278.

[207] Bair S, Habchi W. The role of fragility in thermal elastohydrodynamics. Tribol Lett 2023;71(1):24–9. https://doi.org/10.1007/s11249-023-01696-6.

[208] Brunton SL, Kutz JN. Data-driven science and engineering: Machine learning, dynamical systems, and control. Cambridge, England, UK: Cambridge University Press; 2019. https://doi.org/10.1017/9781108380690.

[209] Marian M, Tremmel S. Current trends and applications of machine learning in tribology—a review. Lubricants 2021;9(9):86. https://doi.org/10.3390/lubricants9090086.

[210] Baghoolizadeh M, Nasajpour-Esfahani N, Pirmoradian M, Toghraie D. Using different machine learning algorithms to predict the rheological behavior of oil sae40-based nano-lubricant in the presence of mwcnt and mgo nanoparticles. Tribol Int 2023;187:108759. https://doi.org/10.1016/j.triboint.2023.108759.

[211] Zhou R, Ma R, Bao L, Cai M, Zhou F, Li W, et al. "Lubrication brain" — a machine learning framework of lubrication oil molecule design. Tribol Int 2023;183:108381. https://doi.org/10.1016/j.triboint.2023.108381.

[212] Rohde M, Oh K. A unified treatment of thick and thin film elastohydrodynamic problems by using higher order element methods. Proceedings of the Royal Society of London. A. Mathematical and Physical Sciences 1975;343(1634):315–31. https://doi.org/10.1098/rspa.1975.0068.

[213] Rohde M, Oh P. Numerical solution of the point contact problem using the finite element method. Int J Numer Methods Eng 1977;11(10):1507–18. https://doi.org/10.1002/nme.1620111003.

[214] Okamura H. A contribution to the numerical analysis of isothermal elastohydrodynamic lubrication. In: Proc. 9th Leeds-Lyon Symp. On tribology, Leeds; 1982. p. 313–20.

[215] Houpert LG, Hamrock BJ. Fast approach for calculating film thicknesses and pressures in elastohydrodynamically lubricated contacts at high loads. J Tribol 1986;108(3):411–9. https://doi.org/10.1115/1.3261220.

[216] Degroote J, Bathe K-J, Vierendeels J. Performance of a new partitioned procedure *versus* a monolithic procedure in fluid–structure interaction. Comput Struct 2009;87(11):793–801. https://doi.org/10.1016/j.compstruc.2008.11.013.

[217] Degroote J. Partitioned simulation of fluid-structure interaction. Arch Comput Methods Eng 2013;20(3):185–238. https://doi.org/10.1007/s11831-013-9085-5.

[218] Profito FJ, Zachariadis DC, Dini D. Partitioned fluid-structure interaction techniques applied to the mixed-elastohydrodynamic solution of dynamically loaded connecting-rod big-end bearings. Tribol Int 2019;140:105767. https://doi.org/10.1016/j.triboint.2019.05.007.

[219] Degroote J, Haelterman R, Annerel S, Bruggeman P, Vierendeels J. Performance of partitioned procedures in fluid–structure interaction. Comput Struct 2010;88 (7):446–57. https://doi.org/10.1016/j.compstruc.2009.12.006.
[220] Hamrock BJ, Dowson D. Isothermal elastohydrodynamic lubrication of point contacts: part 1—theoretical formulation. J Lubr Technol 1976;98(2):223–8. https://doi.org/10.1115/1.3452801.
[221] Evans HP, Snidle RW. Inverse solution of Reynolds' equation of lubrication under point-contact elastohydrodynamic conditions. J Lubr Technol 1981;103(4): 539–46. https://doi.org/10.1115/1.3251733.
[222] Hughes TG, Elcoate CD, Evans HP. A novel method for integrating first- and second-order differential equations in elastohydrodynamic lubrication for the solution of smooth isothermal, line contact problems. Int J Numer Methods Eng 1999;44(8):1099–113. https://doi.org/10.1002/(SICI)1097-0207(19990320)44:8<1099::AID-NME546>3.0.CO;2-7.
[223] Lubrecht AA, Napel WET, Bosma R. Multigrid, an alternative method for calculating film thickness and pressure profiles in elastohydrodynamically lubricated line contacts. J Tribol 1986;108(4):551–6. https://doi.org/10.1115/1.3261260.
[224] Venner CH, Lubrecht AA. Multigrid techniques: a fast and efficient method for the numerical simulation of elastohydrodynamically lubricated point contact problems. Proc Inst Mech Eng J J Eng Tribol 2000;214(1):43–62. https://doi.org/10.1243/1350650001543007.
[225] Zhu D. On some aspects of numerical solutions of thin-film and mixed elastohydrodynamic lubrication. Proc Inst Mech Eng J J Eng Tribol 2007;221(5): 561–79. https://doi.org/10.1243/13506501JET259.
[226] Habchi W, Eyheramendy D, Vergne P, Morales-Espejel G. A full-system approach of the elastohydrodynamic line/point contact problem. J Tribol 2008;130(2). https://doi.org/10.1115/1.2842246.
[227] Nurgat E, Berzins M, Scales L. Solving ehl problems using iterative, multigrid, and homotopy methods. J Tribol 1999;121(1):28–33. https://doi.org/10.1115/1.2833805.
[228] Wang W-Z, Li S, Shen D, Zhang S, Hu Y-Z. A mixed lubrication model with consideration of starvation and interasperity cavitations. Proc Inst Mech Eng J J Eng Tribol 2012;226(12):1023–38. https://doi.org/10.1177/1350650112460830.
[229] Beheshti A, Khonsari MM. Asperity micro-contact models as applied to the deformation of rough line contact. Tribol Int 2012;52:61–74. https://doi.org/10.1016/j.triboint.2012.02.026.
[230] Liu G, Wang Q, Lin C. A survey of current models for simulating the contact between rough surfaces. Tribol Trans 1999;42(3):581–91. https://doi.org/10.1080/10402009908982257.
[231] Maaboudallah F, Najah M, Atalla N. A review on the contact mechanics modeling of rough surfaces in the elastic regime: Fundamentals, theories, and numerical implementations. In: Pintaude G, Cousseau T, Rudawska A, editors. Tribology of machine elements. vol. Ch. 3. Rijeka: IntechOpen; 2022. https://doi.org/10.5772/intechopen.102358.
[232] Taylor RI. Rough surface contact modelling—a review. Lubricants 2022;10(5):98. https://doi.org/10.3390/lubricants10050098.
[233] Patel R, Khan Z, Saeed A, Bakolas V. A review of mixed lubrication modelling and simulation. Tribol Industry 2021;12. https://doi.org/10.24874/ti.1186.09.21.11.
[234] Spikes HA, Olver AV. Basics of mixed lubrication. Lubr Sci 2003;16(1):1–28. https://doi.org/10.1002/ls.3010160102.
[235] Morales-Espejel GE. Surface roughness effects in elastohydrodynamic lubrication: a review with contributions. Proc Inst Mech Eng J J Eng Tribol 2013;228(11): 1217–42. https://doi.org/10.1177/1350650113513572.
[236] Grützmacher PG, Profito FJ, Rosenkranz A. Multi-scale surface texturing in tribology—current knowledge and future perspectives. Lubricants 2019;7(11):95. https://doi.org/10.3390/lubricants7110095.
[237] Costa HL, Profito FJ, Zhang X, Thole KA. Optimizing the surface of manufactured components for friction, adhesion, and convective heat transfer. MRS Bull 2022; 47(12):1247–59. https://doi.org/10.1557/s43577-022-00467-3.
[238] Archard F. Elastic deformation and the laws of friction. Proc R Soc Lond A Math Phys Sci 1957;243(1233):190–205. https://doi.org/10.1098/rspa.1957.0214.
[239] Greenwood A, Williamson JB. Contact of nominally flat surfaces. Proc. R. Soc. London A - Math. Phys. Sci. 1966;295(1442):300–19. https://doi.org/10.1098/rspa.1966.0242.
[240] Tzeng ST, Saibel E. Surface roughness effect on slider bearing lubrication. A S L E Transactions 1967;10(3):334–48. https://doi.org/10.1080/05698196708972191.
[241] Christensen H. Stochastic models for hydrodynamic lubrication of rough surfaces. Proc Inst Mech Eng 1969;184(1):1013–26. https://doi.org/10.1243/PIME_PROC_1969_184_074_02.
[242] Christensen H. Some aspects of the functional influence of surface roughness in lubrication. Wear 1971;17(2):149–62. https://doi.org/10.1016/0043-1648(71)90025-1.
[243] Christensen H. A theory of mixed lubrication. Proc Inst Mech Eng 1972;186(1): 421–30. https://doi.org/10.1177/002034837218600126.
[244] Greenwood JA, Tripp JH. The contact of two nominally flat rough surfaces. Proc Inst Mech Eng 1970;185(1):625–33. https://doi.org/10.1243/PIME_PROC_1970_185_069_02.
[245] Whitehouse David J, Archard F. The properties of random surfaces of significance in their contact. Proc R Soc Lond A 1970;316(1524):97–121. https://doi.org/10.1098/rspa.1970.0068.
[246] Nayak PR. Random process model of rough surfaces. J Lubr Technol 1971;93(3): 398–407. https://doi.org/10.1115/1.3451608.
[247] Onions RA, Archard JF. The contact of surfaces having a random structure. J Phys D Appl Phys 1973;6(3):289. https://doi.org/10.1088/0022-3727/6/3/302.
[248] Bush AW, Gibson RD, Thomas TR. The elastic contact of a rough surface. Wear 1975;35(1):87–111. https://doi.org/10.1016/0043-1648(75)90145-3.
[249] Fuller G, David T. The effect of surface roughness on the adhesion of elastic solids. Proc R Soc Lond A 1975;345(1642):327–42. https://doi.org/10.1098/rspa.1975.0138.
[250] Chang WR, Etsion I, Bogy DB. An elastic-plastic model for the contact of rough surfaces. J Tribol 1987;109(2):257–63. https://doi.org/10.1115/1.3261348.
[251] Bayada G, Chambat M. New models in the theory of the hydrodynamic lubrication of rough surfaces. J Tribol 1988;110(3):402–7. https://doi.org/10.1115/1.3261642.
[252] Bayada G, Faure JB. A double scale analysis approach of the Reynolds roughness comments and application to the journal bearing. J Tribol 1989;111(2):323–30. https://doi.org/10.1115/1.3261917.
[253] Majumdar A, Bhushan B. Role of fractal geometry in roughness characterization and contact mechanics of surfaces. J Tribol 1990;112(2):205–16. https://doi.org/10.1115/1.2920243.
[254] Majumdar A, Bhushan B. Fractal model of elastic-plastic contact between rough surfaces. J Tribol 1991;113(1):1–11. https://doi.org/10.1115/1.2920588.
[255] Jai M. Homogenization and two-scale convergence of the compressible reynolds lubrication equation modelling the flying characteristics of a rough magnetic head over a rough rigid-disk surface. M2AN - Modélisation mathématique et analyse numérique 1995;29(2):199–233.
[256] Lee SC, Ren N. Behavior of elastic-plastic rough surface contacts as affected by surface topography, load, and material hardness. Tribol Transact 1996;39(1): 67–74. https://doi.org/10.1080/10402009608983503.
[257] Zhao Y, Maietta DM, Chang L. An asperity microcontact model incorporating the transition from elastic deformation to fully plastic flow. J Tribol 2000;122(1): 86–93. https://doi.org/10.1115/1.555332.
[258] Persson BNJ. Theory of rubber friction and contact mechanics. J Chem Phys 2001; 115(8):3840–61. https://doi.org/10.1063/1.1388626.
[259] Persson BNJ. Elastoplastic contact between randomly rough surfaces. Phys Rev Lett 2001;87(11):116101. https://doi.org/10.1103/PhysRevLett.87.116101.
[260] Persson BNJ, Bucher F, Chiaia B. Elastic contact between randomly rough surfaces: comparison of theory with numerical results. Phys Rev B 2002;65(18): 184106. https://doi.org/10.1103/PhysRevB.65.184106.
[261] Buscaglia G, Ciuperca I, Jai M. Homogenization of the transient Reynolds equation. Asymptotic Analysis 2002;32.
[262] Buscaglia G, Jai M. A new numerical scheme for non uniform homogenized problems: application to the non linear Reynolds compressible equation. Math Probl Eng 2001;7. https://doi.org/10.1155/S1024123X01001685.
[263] Buscaglia GC, Jai M. Homogenization of the generalised Reynolds equation for ultra-thin gas films and its resolution by FEM. J Tribol 2004;126(3):547–52. https://doi.org/10.1115/1.1739410.
[264] Harp SR, Salant RF. An average flow model of rough surface lubrication with inter-asperity cavitation. J Tribol 2001;123(1):134–43. https://doi.org/10.1115/1.1332397.
[265] Harp SR, Salant RF. Inter-asperity cavitation and global cavitation in seals: an average flow analysis. Tribol Int 2002;35(2):113–21. https://doi.org/10.1016/S0301-679X(01)00103-7.
[266] Kogut L, Etsion I. Elastic-plastic contact analysis of a sphere and a rigid flat. J Appl Mech 2002;69(5):657–62. https://doi.org/10.1115/1.1490373.
[267] Kogut L, Etsion I. A finite element based elastic-plastic model for the contact of rough surfaces. Tribol Trans 2003;46:383–90. https://doi.org/10.1080/10402000308982641.
[268] Jackson RL, Green I. A finite element study of elasto-plastic hemispherical contact against a rigid flat. J Tribol 2005;127(2):343–54. https://doi.org/10.1115/1.1866166.
[269] Jackson RL, Green I. A statistical model of elasto-plastic asperity contact between rough surfaces. Tribol Int 2006;39(9):906–14. https://doi.org/10.1016/j.triboint.2005.09.001.
[270] Ciavarella M, Delfine V, Demelio G. A "re-vitalized" greenwood and Williamson model of elastic contact between fractal surfaces. J Mech Phys Solids 2006;54 (12):2569–91. https://doi.org/10.1016/j.jmps.2006.05.006.
[271] Ciavarella M, Greenwood JA, Paggi M. Inclusion of "interaction" in the greenwood and Williamson contact theory. Wear 2008;265(5):729–34. https://doi.org/10.1016/j.wear.2008.01.019.
[272] Almqvist A, Essel EK, Persson L-E, Wall P. Homogenization of the unstationary incompressible Reynolds equation. Tribol Int 2007;40(9):1344–50. https://doi.org/10.1016/j.triboint.2007.02.021.
[273] Almqvist A, Essel EK, Fabricius J, Wall P. Reiterated homogenization applied in hydrodynamic lubrication. Proc Inst Mech Eng J J Eng Tribol 2008;222(7): 827–41. https://doi.org/10.1243/13506501JET426.
[274] Almqvist A. Homogenization of the Reynolds equation governing hydrodynamic flow in a rotating device. J Tribol 2011;133(2). https://doi.org/10.1115/1.4003650.
[275] Kim TW, Cho YJ. The flow factors considering the elastic deformation for the rough surface with a non-gaussian height distribution. Tribol Transact 2008;51 (2):213–20. https://doi.org/10.1080/10402000701730502.
[276] Fatu A, Bonneau D, Fatu R. Computing hydrodynamic pressure in mixed lubrication by modified Reynolds equation. Proc Inst Mech Eng J J Eng Tribol 2012;226(12):1074–94. https://doi.org/10.1177/1350650112461866.
[277] Hu J, Wei C. Research on the friction behaviors of two rough surfaces covered with boundary film. Tribol Lett 2014;53(2):487–96. https://doi.org/10.1007/s11249-013-0288-6.

[278] Yuan W, Long J, Ding Y, Wang G. Statistical contact model of rough surfaces: the role of surface tension. Int J Solids Struct 2018;138:217–23. https://doi.org/10.1016/j.ijsolstr.2018.01.014.
[279] Fourt E, Arghir M. Comparison between the homogenization and the multiscale methods for the analysis of very thin compressible flow between rough surfaces. Tribol Int 2022;165:107251. https://doi.org/10.1016/j.triboint.2021.107251.
[280] Hansen E, Vaitkunaite G, Schneider J, Gumbsch P, Frohnapfel B. Establishment and calibration of a digital twin to replicate the friction behaviour of a pin-on-disk tribometer. Lubricants 2023;11(2):75. https://doi.org/10.3390/lubricants11020075.
[281] Andersson T, Allan-Persson BG. The boundary element method applied to two-dimensional contact problems. In: Progress in boundary element methods. Vol. 2. New York, NY, New York, NY, USA: Springer; 1983. p. 136–57. https://doi.org/10.1007/978-1-4757-6300-3_5.
[282] Francis HA. The accuracy of plane strain models for the elastic contact of three-dimensional rough surfaces. Wear 1983;85(2):239–56. https://doi.org/10.1016/0043-1648(83)90067-4.
[283] Goglia PR, Conry TF, Cusano C. The effects of surface irregularities on the elastohydrodynamic lubrication of sliding line contacts. Part i—single irregularities. J Tribol 1984;106(1):104–12. https://doi.org/10.1115/1.3260845.
[284] Brandt A, Lubrecht AA. Multilevel matrix multiplication and fast solution of integral equations. J Comput Phys 1990;90(2):348–70. https://doi.org/10.1016/0021-9991(90)90171-V.
[285] Tian X, Bhushan B. A numerical three-dimensional model for the contact of rough surfaces. J Tribol 1996;118(1):33–42. https://doi.org/10.1115/1.2837089.
[286] Zhu D, Hu YZ. The study of transition from full film elastohydrodynamic to mixed and boundary lubrication. In: STLE/ASME H. S. Cheng tribology surveillance, STLE, the advancing frontier of engineering tribology, Park Ridge, IL; 1999. p. 150–6.
[287] Hu Y-Z, Zhu D. A full numerical solution to the mixed lubrication in point contacts. J Tribol 2000;122(1):1–9. https://doi.org/10.1115/1.555322.
[288] Zhu D, Hu Y-Z. A computer program package for the prediction of ehl and mixed lubrication characteristics, friction, subsurface stresses and flash temperatures based on measured 3-d surface roughness. Tribol Transact 2001;44(3):383–90. https://doi.org/10.1080/10402000108982471.
[289] Jiang X, Hua DY, Cheng HS, Ai X, Lee SC. A mixed elastohydrodynamic lubrication model with asperity contact. J Tribol 1999;121(3):481–91. https://doi.org/10.1115/1.2834093.
[290] Campañá C, Müser MH. Practical green's function approach to the simulation of elastic semi-infinite solids. Phys Rev B 2006;74(7):075420. https://doi.org/10.1103/PhysRevB.74.075420.
[291] Chen WW, Wang QJ, Liu Y, Chen W, Cao J, Xia C, et al. Analysis and convenient formulas for elasto-plastic contacts of nominally flat surfaces: average gap, contact area ratio, and plastically deformed volume. Tribol Lett 2007;28(1):27–38. https://doi.org/10.1007/s11249-007-9244-7.
[292] Chen H, Li Y, Tian T. A novel approach to model the lubrication and friction between the twin-land oil control ring and liner with consideration of micro structure of the liner surface finish in internal combustion engines. SAE Int 2008. https://doi.org/10.4271/2008-01-1613.
[293] Li Y, Chen H, Tian T, Li Y, Chen H, Tian T. A deterministic model for lubricant transport within complex geometry under sliding contact and its application in the interaction between the oil control ring and rough liner in internal combustion engines. SAE Int 2008. https://doi.org/10.4271/2008-01-1615.
[294] Putignano C, Afferrante L, Carbone G, Demelio G. A new efficient numerical method for contact mechanics of rough surfaces. Int J Solids Struct 2012;49(2):338–43. https://doi.org/10.1016/j.ijsolstr.2011.10.009.
[295] Profito FJ, Tomanik E, Zachariadis DC. Effect of cylinder liner wear on the mixed lubrication regime of tlocrs. Tribol Int 2016;93:723–32. https://doi.org/10.1016/j.triboint.2015.01.004.
[296] Brunetière N, Francisco A. Lubrication mechanisms between parallel rough surfaces. Tribol Lett 2019;67(4):114–6. https://doi.org/10.1007/s11249-019-1228-x.
[297] Ghanbarzadeh A, Faraji M, Neville A. Deterministic normal contact of rough surfaces with adhesion using a surface integral method. Proc R Soc A 2020;476(2242). https://doi.org/10.1098/rspa.2020.0281.
[298] Geng Y, Zhu K, Qi S, Liu Y, Zhao Y, Yu R, et al. A deterministic mixed lubrication model for parallel rough surfaces considering wear evolution. Tribol Int 2024;194:109443. https://doi.org/10.1016/j.triboint.2024.109443.
[299] Tzeng ST, Saibel E. Surface roughness effect on slider bearing lubrication. ASLE TRANSACTIONS 1967;10(3):334–48.
[300] Chow LSH, Cheng HS. The effect of surface roughness on the average film thickness between lubricated rollers. J Lubr Technol 1976;98(1):117–24. https://doi.org/10.1115/1.3452743.
[301] Tripp JH. Surface roughness effects in hydrodynamic lubrication: the flow factor method. J Lubr Technol 1983;105(3):458–63. https://doi.org/10.1115/1.3254641.
[302] Prat M, Plouraboué F, Letalleur N. Averaged Reynolds equation for flows between rough surfaces in sliding motion. Transp Porous Media 2002;48(3):291–313. https://doi.org/10.1023/A:1015772525610.
[303] Wilson WRD, Marsault N. Partial hydrodynamic lubrication with large fractional contact areas. J Tribol 1998;120(1):16–20. https://doi.org/10.1115/1.2834180.
[304] Wu C, Zheng L. An average Reynolds equation for partial film lubrication with a contact factor. J Tribol 1989;111(1):188–91. https://doi.org/10.1115/1.3261872.
[305] Meng FM, Cen SQ, Hu YZ, Wang H. On elastic deformation, inter-asperity cavitation and lubricant thermal effects on flow factors. Tribol Int 2009;42(2):260–74. https://doi.org/10.1016/j.triboint.2008.06.009.
[306] Bayada G, Martin S, Vázquez C. An average flow model of the Reynolds roughness including a mass-flow preserving cavitation model. J Tribol 2005;127(4):793–802. https://doi.org/10.1115/1.2005307.
[307] Almqvist A, Fabricius J, Wall P. Homogenization of a Reynolds equation describing compressible flow. J Math Anal Appl 2012;390(2):456–71. https://doi.org/10.1016/j.jmaa.2012.02.005.
[308] Cioranescu D, Donato P. An introduction to homogenization. Oxford University Press 1999. https://doi.org/10.1093/oso/9780198565543.001.0001. https://doi.org/10.1093/oso/9780198565543.001.0001.
[309] Almqvist A, Fabricius J, Spencer A, Wall P. Similarities and differences between the flow factor method by patir and cheng and homogenization. J Tribol 2011;133(3). https://doi.org/10.1115/1.4004078.
[310] Rom M, König F, Müller S, Jacobs G. Why homogenization should be the averaging method of choice in hydrodynamic lubrication. Appl Eng Sci 2021;7:100055. https://doi.org/10.1016/j.apples.2021.100055.
[311] Martin S. Influence of multiscale roughness patterns in cavitated flows: applications to journal bearings. Math Probl Eng 2008;2008(1):439319. https://doi.org/10.1155/2008/439319.
[312] Persson BNJ, Scaraggi M. Lubricated sliding dynamics: Flow factors and Stribeck curve. Eur. Phys. J. E 2011;34:113. https://doi.org/10.1140/epje/i2011-11113-9.
[313] Scaraggi M, Carbone G, Persson BNJ, Dini D. Lubrication in soft rough contacts: A novel homogenized approach Part I - Theory. Soft Matt 2011;7:10395. https://doi.org/10.1039/c1sm05128h.
[314] Hou TY, Wu X-H. A multiscale finite element method for elliptic problems in composite materials and porous media. J Comput Phys 1997;134(1):169–89. https://doi.org/10.1006/jcph.1997.5682.
[315] Jenny P, Lee SH, Tchelepi HA. Multi-scale finite-volume method for elliptic problems in subsurface flow simulation. J Comput Phys 2003;187(1):47–67. https://doi.org/10.1016/S0021-9991(03)00075-5.
[316] Pattnayak MR, Arghir M. Homogenization coefficients for modeling the partial and full-film lubrication regimes. Tribol Int 2024;197:109801. https://doi.org/10.1016/j.triboint.2024.109801.
[317] Garcia N, Stoll E. Monte carlo calculation for electromagnetic-wave scattering from random rough surfaces. Phys Rev Lett 1984;52(20):1798–801. https://doi.org/10.1103/PhysRevLett.52.1798.
[318] Pérez-Ràfols F, Almqvist A. Generating randomly rough surfaces with given height probability distribution and power spectrum. Tribol Int 2019;131:591–604. https://doi.org/10.1016/j.triboint.2018.11.020.
[319] Bush AW, Gibson RD, Keogh GP. Strongly anisotropic rough surfaces. J Lubr Technol 1979;101(1):15–20. https://doi.org/10.1115/1.3453271.
[320] Whitehouse David J, Phillips J. Discrete properties of random surfaces. Philos Transact R Soc Lond Ser A Math Phys Sci 1978;290(1369):267–98. https://doi.org/10.1098/rsta.1978.0084.
[321] Whitehouse David J, Phillips J. Two-dimensional properties of random surfaces. Philos Transact R Soc Lond Ser A Math Phys Sci 1982;305(1490):441–68. https://doi.org/10.1098/rsta.1982.0043.
[322] Pugliese G, Tavares SMO, Ciulli E, Ferreira LA. Rough contacts between actual engineering surfaces: part ii. Contact mechanics. Wear 2008;264(11):1116–28. https://doi.org/10.1016/j.wear.2007.08.027.
[323] Ghaednia H, Wang X, Saha S, Xu Y, Sharma A, Jackson RL. A review of elastic–plastic contact mechanics. Appl Mech Rev 2017;69(6). https://doi.org/10.1115/1.4038187.
[324] Ai X, Cheng HS, Zheng L. A transient model for micro-elastohydrodynamic lubrication with three-dimensional irregularities. J Tribol 1993;115(1):102–10. https://doi.org/10.1115/1.2920961.
[325] Chang L, Cusano C, Conry TF. Effects of lubricant rheology and kinematic conditions on micro-elastohydrodynamic lubrication. J Tribol 1989;111(2):344–51. https://doi.org/10.1115/1.3261920.
[326] Chang L, Webster MN, Jackson A. A line-contact micro-ehl model with three-dimensional surface topography. J Tribol 1994;116(1):21–8. https://doi.org/10.1115/1.2927040.
[327] Kweh CC, Evans HP, Snidle RW. Micro-elastohydrodynamic lubrication of an elliptical contact with transverse and three-dimensional sinusoidal roughness. J Tribol 1989;111(4):577–84. https://doi.org/10.1115/1.3261980.
[328] Lubrecht AA, Ten Napel WE, Bosma R. The influence of longitudinal and transverse roughness on the elastohydrodynamic lubrication of circular contacts. J Tribol 1988;110(3):421–6. https://doi.org/10.1115/1.3261645.
[329] Kweh CC, Patching MJ, Evans HP, Snidle RW. Simulation of elastohydrodynamic contacts between rough surfaces. J Tribol 1992;114(3):412–9. https://doi.org/10.1115/1.2920900.
[330] Xu G, Sadeghi F. Thermal ehl analysis of circular contacts with measured surface. J Tribol 1996;118(3):473–82. https://doi.org/10.1115/1.2831560.
[331] Liu Y, Wang QJ, Wang W, Hu Y, Zhu D. Effects of differential scheme and mesh density on ehl film thickness in point contacts. J Tribol 2006;128(3):641–53. https://doi.org/10.1115/1.2194916.
[332] Pu W, Wang J, Zhu D. Progressive mesh densification method for numerical solution of mixed elastohydrodynamic lubrication. J Tribol 2016;138(2). https://doi.org/10.1115/1.4031495.
[333] Wang Y, Azam A, Zhang G, Dorgham A, Liu Y, Wilson MCT, et al. Understanding the mechanism of load-carrying capacity between parallel rough surfaces through a deterministic mixed lubrication model. Lubricants 2022;10(1):12. https://doi.org/10.3390/lubricants10010012.

[334] Wang QJ, Shi F, Lee SC. A mixed-lubrication study of journal bearing conformal contacts. J Tribol 1997;119(3):456–61. https://doi.org/10.1115/1.2833519.
[335] Shi F, Wang QJ. A mixed-tehd model for journal-bearing conformal contacts—part i: model formulation and approximation of heat transfer considering asperity contact. J Tribol 1998;120(2):198–205. https://doi.org/10.1115/1.2834410.
[336] Wang QJ, Shi F, Lee SC. A mixed-tehd model for journal-bearing conformal contact—part ii: contact, film thickness, and performance analyses. J Tribol 1998;120(2):206–13. https://doi.org/10.1115/1.2834411.
[337] Xu Y, Jackson RL. Boundary element method (bem) applied to the rough surface contact *vs.* bem in computational mechanics. Friction 2019;7(4):359–71. https://doi.org/10.1007/s40544-018-0229-3.
[338] Tripp J, van Kuilenburg J, Morales-Espejel G, Lugt P. Frequency response functions and rough surface stress analysis. Tribol Trans 2003;46(3):376–82.
[339] Westergaard H. Bearing pressures and cracks. J Appl Mech 1939;6:A49–53.
[340] Lai WT, Cheng HS. Computer simulation of elastic rough contacts. A S L E Transactions 1985;28(2):172–80. https://doi.org/10.1080/05698198508981609.
[341] Webster MN, Sayles RS. A numerical model for the elastic frictionless contact of real rough surfaces. J Tribol 1986;108(3):314–20. https://doi.org/10.1115/1.3261185.
[342] Banerjee PK, Butterfield R. Boundary element methods in engineering science. US: McGraw-Hill Inc.; 1981.
[343] Bemporad A, Paggi M. Optimization algorithms for the solution of the frictionless normal contact between rough surfaces. Int J Solids Struct 2015;69-70:94–105. https://doi.org/10.1016/j.ijsolstr.2015.06.005.
[344] Jackson RL, Xu Y, Saha S, Schulze KD. Elastic rough surface contact and the root mean square slope of measured surfaces over multiple scales. Fractal Fract 2021;5(2):44. https://doi.org/10.3390/fractalfract5020044.
[345] Putignano C, Afferrante L, Carbone G, Demelio G. The influence of the statistical properties of self-affine surfaces in elastic contacts: a numerical investigation. J Mech Phys Solids 2012;60(5):973–82. https://doi.org/10.1016/j.jmps.2012.01.006.
[346] Putignano C, Afferrante L, Carbone G, Demelio GP. A multiscale analysis of elastic contacts and percolation threshold for numerically generated and real rough surfaces. Tribol Int 2013;64:148–54. https://doi.org/10.1016/j.triboint.2013.03.010.
[347] Hyun S, Pei L, Molinari J-F, Robbins MO. Finite-element analysis of contact between elastic self-affine surfaces. Phys Rev E 2004;70(2):026117. https://doi.org/10.1103/PhysRevE.70.026117.
[348] Paggi M, Ciavarella M. The coefficient of proportionality κ between real contact area and load, with new asperity models. Wear 2010;268(7):1020–9. https://doi.org/10.1016/j.wear.2009.12.038.
[349] Zienkiewicz OC, Taylor RL. The finite element method: Solid mechanicsvol. 2. Butterworth-heinemann; 2000.
[350] Wriggers P. Computational contact mechanics. Berlin, Germany: Springer; 2006.
[351] Laursen TA. Computational contact and impact mechanics: Fundamentals of modeling interfacial phenomena in nonlinear finite element analysis. Springer Science & Business Media; 2013.
[352] Yastrebov VA. Numerical methods in contact mechanics. John Wiley & Sons; 2013.
[353] Wriggers P, Reinelt J. Multi-scale approach for frictional contact of elastomers on rough rigid surfaces. Comput Methods Appl Mech Eng 2009;198(21):1996–2008. https://doi.org/10.1016/j.cma.2008.12.021.
[354] Pei L, Hyun S, Molinari JF, Robbins MO. Finite element modeling of elasto-plastic contact between rough surfaces. J Mech Phys Solids 2005;53(11):2385–409. https://doi.org/10.1016/j.jmps.2005.06.008.
[355] Venugopalan SP, Müser MH, Nicola L. Green's function molecular dynamics meets discrete dislocation plasticity. Model Simul Mater Sci Eng 2017;25(6):065018. https://doi.org/10.1088/1361-651X/aa7e0e.
[356] Campañá C, Müser MH. Contact mechanics of real *vs.* randomly rough surfaces: a green's function molecular dynamics study. Europhys Lett 2007;77(3):38005. https://doi.org/10.1209/0295-5075/77/38005.
[357] Almqvist A, Campañá C, Prodanov N, Persson BNJ. Interfacial separation between elastic solids with randomly rough surfaces: comparison between theory and numerical techniques. J Mech Phys Solids 2011;59(11):2355–69. https://doi.org/10.1016/j.jmps.2011.08.004.
[358] Pastewka L, Prodanov N, Lorenz B, Müser MH, Robbins MO, Persson BNJ. Finite-size scaling in the interfacial stiffness of rough elastic contacts. Phys Rev E 2013;87(6):062809. https://doi.org/10.1103/PhysRevE.87.062809.
[359] Pohrt R, Popov VL. Contact stiffness of randomly rough surfaces. Sci Rep 2013;3. https://doi.org/10.1038/srep03293.
[360] Prodanov N, Dapp WB, Müser MH. On the contact area and mean gap of rough, elastic contacts: dimensional analysis, numerical corrections, and reference data. Tribol Lett 2014;53(2):433–48. https://doi.org/10.1007/s11249-013-0282-z.
[361] Yastrebov VA, Anciaux G, Molinari J-F. From infinitesimal to full contact between rough surfaces: evolution of the contact area. Int J Solids Struct 2015;52:83–102. https://doi.org/10.1016/j.ijsolstr.2014.09.019.
[362] Hyun S, Robbins MO. Elastic contact between rough surfaces: effect of roughness at large and small wavelengths. Tribol Int 2007;40(10):1413–22. https://doi.org/10.1016/j.triboint.2007.02.003.
[363] Bonari J, Paggi M. Viscoelastic effects during tangential contact analyzed by a novel finite element approach with embedded interface profiles. Lubricants 2020;8(12):107. https://doi.org/10.3390/lubricants8120107.
[364] Bonari J, Paggi M, Dini D. A new finite element paradigm to solve contact problems with roughness. Int J Solids Struct 2022;253:111643. https://doi.org/10.1016/j.ijsolstr.2022.111643.
[365] Churaev NV, Sobolev VD, Somov AN. Slippage of liquids over lyophobic solid surfaces. J Colloid Interface Sci 1984;97(2):574–81. https://doi.org/10.1016/0021-9797(84)90330-8.
[366] Vinogradova OI. Slippage of water over hydrophobic surfaces. Int J Miner Process 1999;56(1):31–60. https://doi.org/10.1016/S0301-7516(98)00041-6.
[367] Pit R, Hervet H, Léger L. Friction and slip of a simple liquid at a solid surface. Tribol Lett 1999;7(2):147–52. https://doi.org/10.1023/A:1019161101812.
[368] Neto C, Evans DR, Bonaccurso E, Butt H-J, Craig VSJ. Boundary slip in newtonian liquids: a review of experimental studies. Rep Prog Phys 2005;68(12):2859. https://doi.org/10.1088/0034-4885/68/12/R05.
[369] Thompson PA, Robbins MO. Origin of stick-slip motion in boundary lubrication. Science 1990;250(4982):792–4. https://doi.org/10.1126/science.250.4982.792.
[370] Rothstein JP. Slip on superhydrophobic surfaces. Annu Rev Fluid Mech 2010;42:89–109. https://doi.org/10.1146/annurev-fluid-121108-145558.
[371] Senatore A, Rao TVVLN. Partial slip texture slider and journal bearing lubricated with newtonian fluids: a review. J Tribol 2018;140(4). https://doi.org/10.1115/1.4039226.
[372] Cho J-HJ, Law BM, Rieutord F. Dipole-dependent slip of newtonian liquids at smooth solid hydrophobic surfaces. Phys Rev Lett 2004;92(16):166102. https://doi.org/10.1103/PhysRevLett.92.166102.
[373] Guo L, Wong PL, Guo F. Correlation of contact angle hysteresis and hydrodynamic lubrication. Tribol Lett 2015;58(3):45–9. https://doi.org/10.1007/s11249-015-0518-1.
[374] Huang DM, Sendner C, Horinek D, Netz RR, Bocquet L. Water slippage *versus* contact angle: a quasiuniversal relationship. Phys Rev Lett 2008;101(22):226101. https://doi.org/10.1103/PhysRevLett.101.226101.
[375] Navier C. Mémoire sur les lois du mouvement des fluides, éditeur inconnu. 1822.
[376] Salant RF, Fortier AE. Numerical analysis of a slider bearing with a heterogeneous slip/no-slip surface. Tribol Transact 2004;47(3):328–34. https://doi.org/10.1080/05698190490455348.
[377] Fortier AE, Salant RF. Numerical analysis of a journal bearing with a heterogeneous slip/no-slip surface. J Tribol 2005;127(4):820–5. https://doi.org/10.1115/1.2033897.
[378] Thompson PA, Troian SM. A general boundary condition for liquid flow at solid surfaces. Nature 1997;389(6649):360–2. https://doi.org/10.1038/38686.
[379] Niavarani A, Priezjev NV. Slip boundary conditions for shear flow of polymer melts past atomically flat surfaces. Phys Rev E 2008;77(4). https://doi.org/10.1103/PhysRevE.77.041606. Pt. arXiv:18517634.
[380] Ren W, Trinh PH, Weinan E. On the distinguished limits of the navier slip model of the moving contact line problem. J Fluid Mech 2015;772:107–26. https://doi.org/10.1017/jfm.2015.173.
[381] Çam MY, Giacopini M, Dini D, Biancofiore L. A numerical algorithm to model wall slip and cavitation in two-dimensional hydrodynamically lubricated contacts. Tribol Int 2023;184:108444. https://doi.org/10.1016/j.triboint.2023.108444.
[382] Spikes HA. The half-wetted bearing. Part 1: extended Reynolds equation. Proc Inst Mech Eng J J Eng Tribol 2003;217(1):1–14. https://doi.org/10.1243/135065003321164758.
[383] Spikes HA. The half-wetted bearing. Part 2: potential application in low load contacts. Proc Inst Mech Eng J J Eng Tribol 2003;217(1):15–26. https://doi.org/10.1243/135065003321164776.
[384] Sofonea M, Matei A. Mathematical models in contact mechanics. Cambridge University Press; 2012.
[385] Bayada MEATG, Hilal M. Existence and uniqueness results for compressible Reynolds equation with slip boundary conditions. Applicable Analysis 2019;100(2):302–21. https://doi.org/10.1080/00036811.2019.1602725.
[386] Spikes H, Granick S. Equation for slip of simple liquids at smooth solid surfaces. Langmuir 2003;19(12):5065–71. https://doi.org/10.1021/la034123j.
[387] Bayada G. A fast algorithm for boundary slippage including mass flow conserving cavitation model. Tribol Int 2018;118:71–88. https://doi.org/10.1016/j.triboint.2017.09.008.
[388] Alder BJ, Wainwright TE. Phase transition for a hard sphere system. J Chem Phys 1957;27(5):1208–9. https://doi.org/10.1063/1.1743957.
[389] Alder BJ, Wainwright TE. Studies in molecular dynamics. i. General method. J Chem Phys 1959;31(2):459–66. https://doi.org/10.1063/1.1730376.
[390] Metropolis N, Rosenbluth AW, Rosenbluth MN, Teller AH, Teller E. Equation of state calculations by fast computing machines. J Chem Phys 1953;21(6):1087–92. https://doi.org/10.1063/1.1699114.
[391] Ewen JP, Heyes DM, Dini D. Advances in nonequilibrium molecular dynamics simulations of lubricants and additives. Friction 2018;6(4):349–86. https://doi.org/10.1007/s40544-018-0207-9.
[392] Harrison JA, Schall JD, Maskey S, Mikulski PT, Knippenberg MT, Morrow BH. Review of force fields and intermolecular potentials used in atomistic computational materials research. Appl Phys Rev 2018;5(3):031104. https://doi.org/10.1063/1.5020808.
[393] Yong X, Zhang LT. Thermostats and thermostat strategies for molecular dynamics simulations of nanofluidics. J Chem Phys 2013;138(8):084503. https://doi.org/10.1063/1.4792202.
[394] Frenkel D, Smit B. Understanding molecular simulation, Elsevier. Academic Press 2002. https://doi.org/10.1016/B978-0-12-267351-1.X5000-7.
[395] Evans DJ, Morriss GP. Statistical mechanics of nonequilibrium liquids, Elsevier. Academic Press 1990. https://doi.org/10.1016/C2013-0-10633-2.

[396] Todd BD, Daivis PJ. Nonequilibrium molecular dynamics: Theory, algorithms and applications. Cambridge, England, UK: Cambridge University Press; 2017. https://doi.org/10.1017/9781139017848.
[397] Müser MH. Shear thinning in the prandtl model and its relation to generalised newtonian fluids. Lubricants 2020;8(4):38. https://doi.org/10.3390/lubricants8040038.
[398] Spikes H, Zhang J. Reply to the comment by Scott bair, philippe vergne, punit kumar, gerhard poll, ivan krupka, martin hartl, wassim habchi, Roland larson on "history, origins and prediction of elastohydrodynamic friction" by spikes and jie in tribology letters. Tribol Lett 2015;58(1):6–17. https://doi.org/10.1007/s11249-015-0483-8.
[399] McCabe C, Cui S, Cummings PT, Gordon PA, Saeger RB. Examining the rheology of 9-octylheptadecane to giga-pascal pressures. J Chem Phys 2001;114(4):1887–91. https://doi.org/10.1063/1.1334676.
[400] Liu P, Yu H, Ren N, Lockwood FE, Wang QJ. Pressure–viscosity coefficient of hydrocarbon base oil through molecular dynamics simulations. Tribol Lett 2015;60(3):34–9. https://doi.org/10.1007/s11249-015-0610-6.
[401] Ewen JP, Gattinoni C, Thakkar FM, Morgan N, Spikes HA, Dini D. A comparison of classical force-fields for molecular dynamics simulations of lubricants. Materials (Basel) 2016;9(8):651. arXiv:28773773, https://doi.org/10.3390/ma9080651.
[402] Bair S, Kottke P. Pressure-viscosity relationships for elastohydrodynamics. Tribol Transact 2003;46(3):289–95. https://doi.org/10.1080/10402000308982628.
[403] Eyring H. Viscosity, plasticity, and diffusion as examples of absolute reaction rates. J Chem Phys 1936;4(4):283–91. https://doi.org/10.1063/1.1749836.
[404] Carreau PJ. Rheological equations from molecular network theories. Transact Soc Rheol 1972;16(1):99–127. https://doi.org/10.1122/1.549276.
[405] Bair S, McCabe C, Cummings PT. Calculation of viscous EHL traction for squalane using molecular simulation and rheometry. Tribol Lett 2002;13(4):251–4. https://doi.org/10.1023/A:1021011225316.
[406] Jadhao V, Robbins MO. Probing large viscosities in glass-formers with nonequilibrium simulations. Proc Natl Acad Sci U S A 2017;114(30):7952–7. https://doi.org/10.1073/pnas.1705978114.
[407] Heyes DM, Dini D, Smith ER. Incremental viscosity by non-equilibrium molecular dynamics and the eyring model. J Chem Phys 2018;148(19):194506. arXiv:30307245, https://doi.org/10.1063/1.5027681.
[408] Thompson PA, Robbins MO. Shear flow near solids: epitaxial order and flow boundary conditions. Phys Rev A 1990;41(12):6830–7. https://doi.org/10.1103/PhysRevA.41.6830.
[409] Robbins MO, Smith ED. Connecting molecular-scale and macroscopic tribology. Langmuir 1996;12(19):4543–7. https://doi.org/10.1021/la9505576.
[410] Plint MA. Third paper: traction in elastohydrodynamic contacts. Proc Inst Mech Eng 1967;182(1):300–6. https://doi.org/10.1243/PIME_PROC_1967_182_028_02.
[411] Ehret P, Dowson D, Taylor CM. On lubricant transport conditions in elastohydrodynamic conjuctions. Proc R Soc Lond A 1998;454(1971):763–87. https://doi.org/10.1098/rspa.1998.0185.
[412] Heyes DM, Smith ER, Dini D, Spikes HA, Zaki TA. Pressure dependence of confined liquid behavior subjected to boundary-driven shear. J Chem Phys 2012;136(13). https://doi.org/10.1063/1.3698601.
[413] Gattinoni C, Heyes DM, Lorenz CD, Dini D. Traction and nonequilibrium phase behavior of confined sheared liquids at high pressure. Phys Rev E 2013;88(5):052406. https://doi.org/10.1103/PhysRevE.88.052406.
[414] Maćkowiak S, Heyes DM, Dini D, Brańka AC. Non-equilibrium phase behavior and friction of confined molecular films under shear: a non-equilibrium molecular dynamics study. J Chem Phys 2016;145(16):164704. arXiv:27802615, https://doi.org/10.1063/1.4965829.
[415] Ewen JP, Gattinoni C, Zhang J, Heyes DM, Spikes HA, Dini D. On the effect of confined fluid molecular structure on nonequilibrium phase behaviour and friction. Phys Chem Chem Phys 2017;19(27):17883–94. https://doi.org/10.1039/C7CP01895A.
[416] Washizu H, Ohmori T, Suzuki A. Molecular origin of limiting shear stress of elastohydrodynamic lubrication oil film studied by molecular dynamics. Chem Phys Lett 2017;678:1–4. https://doi.org/10.1016/j.cplett.2017.04.020.
[417] Porras-Vazquez A, Martinie L, Vergne P, Fillot N. Independence between friction and velocity distribution in fluids subjected to severe shearing and confinement. Phys Chem Chem Phys 2018;20(43):27280–93. https://doi.org/10.1039/C8CP04620D.
[418] Zhang J, Tan A, Spikes H. Effect of base oil structure on elastohydrodynamic friction. Tribol Lett 2016;65(1):13–24. https://doi.org/10.1007/s11249-016-0791-7.
[419] He J, Tang H, Wang C. Advances of molecular dynamics simulation in tribochemistry and lubrication investigations: a review. J Ind Eng Chem 2023;126:1–19. https://doi.org/10.1016/j.jiec.2023.06.002.
[420] Molinari J-F, Aghababaei R, Brink T, Frérot L, Milanese E. Adhesive wear mechanisms uncovered by atomistic simulations. Friction 2018;6(3):245–59. https://doi.org/10.1007/s40544-018-0234-6.
[421] Pastewka L, Robbins MO. Contact between rough surfaces and a criterion for macroscopic adhesion. Proc Natl Acad Sci U S A 2014;111(9):3298–303. https://doi.org/10.1073/pnas.1320846111.
[422] Mo Y, Turner KT, Szlufarska I. Friction laws at the nanoscale. Nature 2009;457(7233):1116–9. https://doi.org/10.1038/nature07748.
[423] Aghababaei R, Warner DH, Molinari J-F. Critical length scale controls adhesive wear mechanisms. Nat Commun 2016;7(11,816):1–8. https://doi.org/10.1038/ncomms11816.
[424] Eder SJ, Rodríguez Ripoll M, Cihak-Bayr U, Dini D, Gachot C. Unraveling and mapping the mechanisms for near-surface microstructure evolution in cuni alloys under sliding. ACS Appl Mater Interfaces 2020;12(28):32197–208. https://doi.org/10.1021/acsami.0c09302.
[425] Eder SJ, Grützmacher PG, Rodríguez Ripoll M, Gachot C, Dini D. Does speed kill or make friction better?—designing materials for high velocity sliding. Appl Mater Today 2022;29:101588. https://doi.org/10.1016/j.apmt.2022.101588.
[426] Sha Z-D, Sorkin V, Branicio PS, Pei Q-X, Zhang Y-W, Srolovitz DJ. Large-scale molecular dynamics simulations of wear in diamond-like carbon at the nanoscale. Appl Phys Lett 2013;103(7):073118. https://doi.org/10.1063/1.4818713.
[427] Tafrishi H, Sadeghzadeh S, Ahmadi R. Molecular dynamics simulations of phase change materials for thermal energy storage: a review. RSC Adv 2022;12(23):14776–807. https://doi.org/10.1039/D2RA02183H.
[428] Vandenhaute S, Rogge SMJ, Van Speybroeck V. Large-scale molecular dynamics simulations reveal new insights into the phase transition mechanisms in mil-53 (al). Front Chem 2021;9:718920. https://doi.org/10.3389/fchem.2021.718920.
[429] Srivastava I, Kotia A, Ghosh SK, Ali MKA. Recent advances of molecular dynamics simulations in nanotribology. J Mol Liq 2021;335:116154. https://doi.org/10.1016/j.molliq.2021.116154.
[430] Qiu F, Song H, Feng W, Yang Z, Lu Z, Hu X. Atomic-scale insights into graphene/fullerene tribological mechanisms and machine learning prediction of properties. J Tribol 2024;146(6). https://doi.org/10.1115/1.4064402.
[431] Berman D, Deshmukh SA, Sankaranarayanan SKRS, Erdemir A, Sumant AV. Macroscale superlubricity enabled by graphene nanoscroll formation. Science 2015;348(6239):1118–22. https://doi.org/10.1126/science.1262024.
[432] Li C, Tang W, Tang X-Z, Yang L, Bai L. A molecular dynamics study on the synergistic lubrication mechanisms of graphene/water-based lubricant systems. Tribol Int 2022;167:107356. https://doi.org/10.1016/j.triboint.2021.107356.
[433] Codrignani A, Peeters S, Holey H, Stief F, Savio D, Pastewka L, et al. Toward a continuum description of lubrication in highly pressurized nanometer-wide constrictions: the importance of accurate slip laws. Sci Adv 2023;9(48). https://doi.org/10.1126/sciadv.adi2649.
[434] Wang Z, Li L, Yang M. Molecular dynamics simulation of the wetting characteristics of a nanofluid droplet on rough substrate. J Mol Liq 2020;319:114204. https://doi.org/10.1016/j.molliq.2020.114204.
[435] Zheng X, Su L, Deng G. Influence of nanoparticles in lubricant on sliding contact of atomic rough surfaces—a molecular dynamics study. Lubricants 2024;12(5):160. https://doi.org/10.3390/lubricants12050160.
[436] Galli G, Pasquarello A. First-principles molecular dynamics. In: Computer simulation in chemical physics. Dordrecht, The Netherlands: Springer; 1993. p. 261–313. https://doi.org/10.1007/978-94-011-1679-4_8.
[437] Mouvet F, Villard J, Bolnykh V, Rothlisberger U. Recent advances in first-principles based molecular dynamics. Acc Chem Res 2022;55(3):221–30. https://doi.org/10.1021/acs.accounts.1c00503.
[438] Loehlé S, Righi MC. *Ab initio* molecular dynamics simulation of tribochemical reactions involving phosphorus additives at sliding iron interfaces. Lubricants 2018;6(2):31. https://doi.org/10.3390/lubricants6020031.
[439] Hu C, Bai M, Lv J, Li X. Molecular dynamics simulation of mechanism of nanoparticle in improving load-carrying capacity of lubricant film. Comput Mater Sci 2015;109:97–103. https://doi.org/10.1016/j.commatsci.2015.07.028.
[440] Spikes H. Friction modifier additives. Tribol Lett 2015;60(1):5–26. https://doi.org/10.1007/s11249-015-0589-z.
[441] Wu J. Classical density functional theory for molecular systems. In: Variational methods in molecular modeling. Singapore: Springer; 2016. p. 65–99. https://doi.org/10.1007/978-981-10-2502-0_3.
[442] Zhang X, Li T, Guan M, Li R, Liu J, Wang Y, et al. Dft insights into the migration of effective electrons towards o2 for oh formation over electron-rich sites on biobr (001) surface. Appl Surf Sci 2021;567:150828. https://doi.org/10.1016/j.apsusc.2021.150828.
[443] Wei B, Kong N, Zhang J, Li H, Hong Z, Zhu H, et al. A molecular dynamics study on the tribological behavior of molybdenum disulfide with grain boundary defects during scratching processes. Friction 2021;9(5):1198–212. https://doi.org/10.1007/s40544-020-0459-z.
[444] Ingram GD, Cameron IT, Hangos KM. Classification and analysis of integrating frameworks in multiscale modelling. Chem Eng Sci 2004;59(11):2171–87. https://doi.org/10.1016/j.ces.2004.02.010.
[445] O'Connell ST, Thompson PA. Molecular dynamics–continuum hybrid computations: a tool for studying complex fluid flows. Phys Rev E 1995;52(6):R5792–R5795(R). https://doi.org/10.1103/PhysRevE.52.R5792.
[446] Hadjiconstantinou NG, Patera AT. Heterogeneous atomistic-continuum representations for dense fluid systems. Int J Mod Phys C 1997;08(04):967–76. https://doi.org/10.1142/S0129183197000837.
[447] Tang Y-H, Kudo S, Bian X, Li Z, Karniadakis GE. Multiscale universal interface: a concurrent framework for coupling heterogeneous solvers. J Comput Phys 2015;297:13–31. https://doi.org/10.1016/j.jcp.2015.05.004.
[448] Weinan E. Principles of multiscale modeling. Cambridge, England, UK: Cambridge University Press; 2011.
[449] Nie XB, Chen SY, Robbins MO. A continuum and molecular dynamics hybrid method for micro- and nano-fluid flow. J Fluid Mech 2004;500:55–64. https://doi.org/10.1017/S0022112003007225.
[450] Nie X, Robbins MO, Chen S. Resolving singular forces in cavity flow: multiscale modeling from atomic to millimeter scales. Phys Rev Lett 2006;96(13):134501. https://doi.org/10.1103/PhysRevLett.96.134501.
[451] Liu J, Chen S, Nie X, Robbins MO. A continuum–atomistic simulation of heat transfer in micro- and nano-flows. J Comput Phys 2007;227(1):279–91. https://doi.org/10.1016/j.jcp.2007.07.014.

[452] Miller RE, Tadmor EB. A unified framework and performance benchmark of fourteen multiscale atomistic/continuum coupling methods. Model Simul Mater Sci Eng 2009;17(5):053001. https://doi.org/10.1088/0965-0393/17/5/053001.
[453] Smith ER, Heyes DM, Dini D, Zaki TA. A localised momentum constraint for non-equilibrium molecular dynamics simulations. J Chem Phys 2015;142(7):074110. https://doi.org/10.1063/1.4907880.
[454] Smith ER, Trevelyan DJ, Ramos-Fernandez E, Sufian A, O'Sullivan C, Dini D. Cpl library — a minimal framework for coupled particle and continuum simulation. Comput Phys Commun 2020;250:107068. https://doi.org/10.1016/j.cpc.2019.107068.
[455] Tong Z-X, He Y-L, Tao W-Q. A review of current progress in multiscale simulations for fluid flow and heat transfer problems: the frameworks, coupling techniques and future perspectives. Int J Heat Mass Transfer 2019;137:1263–89. https://doi.org/10.1016/j.ijheatmasstransfer.2019.04.004.
[456] Mohamed KM, Mohamad AA. A review of the development of hybrid atomistic–continuum methods for dense fluids. Microfluid Nanofluid 2010;8(3):283–302. https://doi.org/10.1007/s10404-009-0529-z.
[457] Kalweit M, Drikakis D. Multiscale simulation strategies and mesoscale modelling of gas and liquid flows. IMA J Appl Math 2011;76(5):661–71. https://doi.org/10.1093/imamat/hxr048.
[458] Tadmor EB, Phillips R, Ortiz M. Hierarchical modeling in the mechanics of materials. Int J Solids Struct 2000;37(1):379–89. https://doi.org/10.1016/S0020-7683(99)00095-5.
[459] Tak M, Park D, Park T. Computational coupled method for multiscale and phase analysis. J Eng Mater Technol 2013;135(2):0210131. https://doi.org/10.1115/1.4023776.
[460] Jordan MI, Mitchell TM. Machine learning: trends, perspectives, and prospects. Science 2015;349(6245):255–60. https://doi.org/10.1126/science.aaa8415.
[461] Butler KT, Davies DW, Cartwright H, Isayev O, Walsh A. Machine learning for molecular and materials science. Nature 2018;559(7715):547–55. https://doi.org/10.1038/s41586-018-0337-2.
[462] Shameer K, Johnson KW, Glicksberg BS, Dudley JT, Sengupta PP. Machine learning in cardiovascular medicine: are we there yet? Heart 2018;104(14):1156–64. arXiv:29352006, https://doi.org/10.1136/heartjnl-2017-311198.
[463] Ward L, Wolverton C. Atomistic calculations and materials informatics: a review. Curr Opin Solid State Mater Sci 2017;21(3):167–76. https://doi.org/10.1016/j.cossms.2016.07.002.
[464] Unke OT, Chmiela S, Sauceda HE, Gastegger M, Poltavsky I, Schütt KT, et al. Machine learning force fields. Chem Rev 2021;121(16):10142–86. https://doi.org/10.1021/acs.chemrev.0c01111.
[465] Won D-O, Müller K-R, S.-W.. Lee, an adaptive deep reinforcement learning framework enables curling robots with human-like performance in real-world conditions. Sci Rob 2020;5(46):eabb9764. https://doi.org/10.1126/scirobotics.abb9764.
[466] Sahana M, Areendran G, Sajjad H. Assessment of suitable habitat of mangrove species for prioritizing restoration in coastal ecosystem of sundarban biosphere reserve, India. Sci Rep 2022;12(20,997):1–20. https://doi.org/10.1038/s41598-022-24953-5.
[467] Pazzani M, Billsus D. Learning and revising user profiles: the identification of interesting web sites. Machine Learning 1997;27(3):313–31. https://doi.org/10.1023/A:1007369909943.
[468] Singh A, Thakur N, Sharma A. A review of supervised machine learning algorithms. In: In: 2016 3rd international conference on computing for sustainable global development (INDIACom). IEEE; 2016. p. 1310–5.
[469] Bengio Y, Courville A, Vincent P. Representation learning: A review and new perspectives. arXiv 2012. https://doi.org/10.48550/arXiv.1206.5538. arXiv:1206.5538.
[470] Zhu X, Goldberg AB. Introduction to semi-supervised learning. Cham, Switzerland: Springer International Publishing; 2009.
[471] Sutton RS, Barto AG. Reinforcement learning, second edition: An introduction (adaptive computation and machine learning series). Bradford Books; 2018.
[472] Jhaveri RH, Revathi A, Ramana K, Raut R, Dhanaraj RK. A review on machine learning strategies for real-world engineering applications. Mobile Information Syst 2022;2022. https://doi.org/10.1155/2022/1833507.
[473] Alzubaidi L, Zhang J, Humaidi AJ, Al-Dujaili A, Duan Y, Al-Shamma O, et al. Review of deep learning: concepts, cnn architectures, challenges, applications, future directions. J Big Data 2021;8(1):1–74. https://doi.org/10.1186/s40537-021-00444-8.
[474] Krogh A. What are artificial neural networks? Nat Biotechnol 2008;26(2):195–7. https://doi.org/10.1038/nbt1386.
[475] LeCun Y, Bengio Y, Hinton G. Deep learning. Nature 2015;521(7553):436–44. https://doi.org/10.1038/nature14539.
[476] Hassoun M. Fundamentals of artificial neural networks (a Bradford book). Cambridge, MA, USA: MIT Press; 2003.
[477] Argatov I. Artificial neural networks (anns) as a novel modeling technique in tribology. Front Mech Eng 2019;5. https://doi.org/10.3389/fmech.2019.00030.
[478] Paturi UMR, Cheruku S, Reddy NS. The role of artificial neural networks in prediction of mechanical and tribological properties of composites—a comprehensive review. Arch Comput Methods Eng 2022;29(5):3109–49. https://doi.org/10.1007/s11831-021-09691-7.
[479] Malekian A, Chitsaz N. Concepts, procedures, and applications of artificial neural network models in streamflow forecasting. In: Advances in streamflow forecasting. Walthm, MA, USA: Elsevier; 2021. p. 115–47. https://doi.org/10.1016/B978-0-12-820673-7.00003-2.
[480] Saikia P, Baruah RD, Singh SK, Chaudhuri PK. Artificial neural networks in the domain of reservoir characterization: a review from shallow to deep models. Comput Geosci 2020;135:104357. https://doi.org/10.1016/j.cageo.2019.104357.
[481] Raissi M, Perdikaris P, Karniadakis GE. Physics informed deep learning (part i): Data-driven solutions of nonlinear partial differential equations. arXiv 2017. https://doi.org/10.48550/arXiv.1711.10561. arXiv:1711.10561.
[482] Raissi M, Perdikaris P, Karniadakis GE. Physics informed deep learning (part ii): Data-driven discovery of nonlinear partial differential equations. arXiv 2017. https://doi.org/10.48550/arXiv.1711.10566. arXiv:1711.10566.
[483] Raissi M, Perdikaris P, Karniadakis GE. Physics-informed neural networks: a deep learning framework for solving forward and inverse problems involving nonlinear partial differential equations. J Comput Phys 2019;378:686–707. https://doi.org/10.1016/j.jcp.2018.10.045.
[484] Baydin AG, Pearlmutter BA, Radul AA, Siskind JM. Automatic differentiation in machine learning: a survey. J Mach Learn Res 2017;18(1):5595–637. https://doi.org/10.5555/3122009.3242010.
[485] Almqvist A. Fundamentals of physics-informed neural networks applied to solve the Reynolds boundary value problem. Lubricants 2021;9(8):82. https://doi.org/10.3390/lubricants9080082.
[486] Rom M. Physics-informed neural networks for the Reynolds equation with cavitation modeling. Tribol Int 2023;179:108141. https://doi.org/10.1016/j.triboint.2022.108141.
[487] Zhao Y, Guo L, Wong PPL. Application of physics-informed neural network in the analysis of hydrodynamic lubrication. Friction 2023;11(7):1253–64. https://doi.org/10.1007/s40544-022-0658-x.
[488] Marian M, Tremmel S. Physics-informed machine learning—an emerging trend in tribology. Lubricants 2023;11(11):463. https://doi.org/10.3390/lubricants11110463.
[489] Cai S, Mao Z, Wang Z, Yin M, Karniadakis GE. Physics-informed neural networks (pinns) for fluid mechanics: a review. Acta Mech Sin 2021;37(12):1727–38. https://doi.org/10.1007/s10409-021-01148-1.
[490] Hinton G, Deng L, Yu D, Dahl GE, Mohamed A-R, Jaitly N, et al. Deep neural networks for acoustic modeling in speech recognition: the shared views of four research groups. IEEE Signal Process Mag 2012;29(6):82–97. https://doi.org/10.1109/MSP.2012.2205597.
[491] Vapnik VN. An overview of statistical learning theory. IEEE Trans Neural Netw 1999;10(5):988–99. https://doi.org/10.1109/72.788640.
[492] Wu X, Kumar V, Ross Quinlan J, Ghosh J, Yang Q, Motoda H, et al. Top 10 algorithms in data mining. Knowl Inf Syst 2008;14(1):1–37. https://doi.org/10.1007/s10115-007-0114-2.
[493] Kajita S, Kinjo T, Nishi T. Autonomous molecular design by Monte-Carlo tree search and rapid evaluations using molecular dynamics simulations. Commun Phys 2020;3(77):1–11. https://doi.org/10.1038/s42005-020-0338-y.
[494] Prašnikar E, Ljubič M, Perdih A, Borišek J. Machine learning heralding a new development phase in molecular dynamics simulations. Artif Intell Rev 2024;57(4):102–36. https://doi.org/10.1007/s10462-024-10731-4.
[495] Noé F, Tkatchenko A, Müller K-R, Clementi C. Machine learning for molecular simulation. Annu Rev Phys Chem 2020;71(1):361–90. https://doi.org/10.1146/annurev-physchem-042018-052331.
[496] Bishara D, Xie Y, Liu WK, Li S. A state-of-the-art review on machine learning-based multiscale modeling, simulation, homogenization and design of materials. Arch Comput Methods Eng 2023;30(1):191–222. https://doi.org/10.1007/s11831-022-09795-8.
[497] Jia D, Duan H, Zhan S, Jin Y, Cheng B, Li J. Design and development of lubricating material database and research on performance prediction method of machine learning. Sci Rep 2019;9(20,277):1–11. https://doi.org/10.1038/s41598-019-56776-2.
[498] Lubbers N, Agarwal A, Chen Y, Son S, Mehana M, Kang Q, et al. Modeling and scale-bridging using machine learning: nanoconfinement effects in porous media. Sci Rep 2020;10(13,312):1–13. https://doi.org/10.1038/s41598-020-69661-0.
[499] Xiao S, Hu R, Li Z, Attarian S, Björk K-M, Lendasse A. A machine-learning-enhanced hierarchical multiscale method for bridging from molecular dynamics to continua. Neural Comput Applic 2020;32(18):14359–73. https://doi.org/10.1007/s00521-019-04480-7.
[500] McCammon JA. Computer-aided molecular design. Science 1987;238(4826):486–91. https://doi.org/10.1126/science.3310236.
[501] Tkatchenko A. Machine learning for chemical discovery. Nat Commun 2020;11(4125):1–4. https://doi.org/10.1038/s41467-020-17844-8.
[502] Dimitrov T, Kreisbeck C, Becker JS, Aspuru-Guzik A, Saikin SK. Autonomous molecular design: then and now. ACS Appl Mater Interfaces 2019;11(28):24825–36. https://doi.org/10.1021/acsami.9b01226.
[503] Silver D, Huang A, Maddison CJ, Guez A, Sifre L, van den Driessche G, et al. Mastering the game of go with deep neural networks and tree search. Nature 2016;529(7587):484–9. https://doi.org/10.1038/nature16961.
[504] Świechowski M, Godlewski K, Sawicki B, Mańdziuk J. Monte carlo tree search: a review of recent modifications and applications. Artif Intell Rev 2023;56(3):2497–562. https://doi.org/10.1007/s10462-022-10228-y.
[505] Zhang L, Lu B, Wu Y, Wang J, Zhang X, Wang L, et al. Molecular dynamics simulation and experimental study on the lubrication of graphene additive films. Proc Inst Mech Eng J J Eng Tribol 2020;234(12):1957–72. https://doi.org/10.1177/1350650119899213.
[506] Salahub DR. Multiscale molecular modelling: from electronic structure to dynamics of nanosystems and beyond. Phys Chem Chem Phys 2022;24(16):9051–81. https://doi.org/10.1039/D1CP05928A.

[507] Singh V, Patra S, Murugan NA, Toncu D-C, Tiwari A. Recent trends in computational tools and data-driven modeling for advanced materials. Mater Adv 2022;3(10):4069–87. https://doi.org/10.1039/D2MA00067A.
[508] Raccuglia P, Elbert KC, Adler PDF, Falk C, Wenny MB, Mollo A, et al. Machine-learning-assisted materials discovery using failed experiments. Nature 2016;533 (7601):73–6. https://doi.org/10.1038/nature17439.
[509] Segler MHS, Preuss M, Waller MP. Planning chemical syntheses with deep neural networks and symbolic ai. Nature 2018;555(7698):604–10. https://doi.org/10.1038/nature25978.